Programa de doctorado Matemáticas

PhD Dissertation

New Methods and Results in the Optimisation of Solar Power Tower Plants

---

Author

Thomas Ian Ashley

Supervisors

Prof. Dr. *Emilio Carrizosa Priego*

Prof. Dr. *Enrique Fernández-Cara*

A todos los que se han implicado en mi formación,
tanto profesional como personal, en los últimos tres años.
Espero devolver el mismo apoyo que me habéis demostrado.
Gracias.

Agradecimientos

A Thesis is a journey of self discovery that is completed by oneself, but also profoundly affected by the people with whom one is surrounded. For me, these people have been especially important, and here I will attempt to express my gratitude to a select few.

En primer lugar, me gustaría agradecer a mis directores Emilio y Enrique, quienes me han guiado tanto durante los últimos tres años. En vez de contratar a un estudiante conocido de la universidad, tomaron el riesgo de contratar a un inglés desconocido, y por eso siempre estaré agradecido. Me han enseñado no sólo a investigar, sino también la cultura española; hasta me he convertido en un nativo de Los Palacios.

Quiero agradecer a los trabajadores de la secretaría del IMUS, quienes me han ayudado mucho con los trámites complejos del doctorado, recibiéndome siempre con una sonrisa y sin quejarse nunca por mis dificultades con el español.

Llegando a Sevilla con una lengua y cultura nuevas era todo un reto. Tuve la inmensa suerte de ser bienvenido en un grupo de gente increíble en el IMUS, que ha aceptado las diferencias culturales y mi español mediocre, y todo ello me ha hecho sentir como en casa.

La Familia IMUS es el logro más importante de mi tiempo en Sevilla, y aunque sois demasiados para mencionaros individualmente a todos, espero que todos sepáis el gran impacto que habéis generado en mi vida; Asun, Víctor, Tana, Nati, Mónica, Sandra, Alba, Moisés, FJ, Vanesa, Marina, Elena, Carlos, Edu, Jose, Marithania, etc.

Gracias por los cafés, congresos, risas, fiestas, bodas (pronto tres) y momentos especiales. Aunque estoy cerrando esta etapa en el IMUS, yo sé que aun quedan muchas más historias memorables con vosotros, y con los próximos miembros de la Familia IMUS (bebé Rodrigo).

Por supuesto, quiero agradecer a Las Pueblecitas, Reme y Cristina, por siempre haber estado cuando las he necesitado, aunque hacer un resumen aquí no les haría justicia. Las dos me han apoyado al máximo durante estos tres años, tanto en el trabajo como enseñándome a ser de Posadas. Gracias a Reme por haber aguantado mis preguntas tontas constantes, y por ser la voz de la razón. Especialmente me gustaría dar las gracias a Cristina, ya que ella fue quien me recogió en el parking de la universidad mi primer día, y ha sido una de mis mejores amigas hasta mi último día en el IMUS.

Eres la luz de La Familia y una fuente de alegría e imaginación para todos. El IMUS no sería igual sin ti.

I must also thank my family, who have raised me to be the person I am today, and have always strived to provide me with the best opportunities to succeed. Although we now live in separate countries and are unable to meet as much as we would like, their continued love and support has helped me immensely over the years of this work.

También tengo que agredecer a la familia de Marta, mi nueva familia, que me ha ayudado mucho a acostumbrarme a vivir en España y por aceptarme sin dudas.

To Marta I must give the greatest thanks, and beg the most forgiveness. It is thanks to you that I came to Sevilla, and thanks to you that I complete this Thesis. You have supported me through the bad moments, and been there to enjoy all of the good ones. We have grown together, learned together, and ultimately married in this latest etapa of our lives. It is cliche, but true; this part of my life would not have been possible without you, and for that I thank you from the bottom of my heart.

Este trabajo ha sido financiado por:

- *Optimal Heliostat Fields for Solar Tower Power Plants (PCIN-2015-108). Ministerio de Economía y Competitividad, Spain.*
- *Mathematical Optimization for Data Visualization and Decision Making (MTM2015-65915-R). Ministerio de Economía y Competitividad, Spain.*
- *Optimización Global. Nuevos Algoritmos y Aplicaciones (P11-FQM-7603). Consejería de Innovación, Ciencia y Empresas. Junta de Andalucía.*
- *Optimización (FQM-329). Junta de Andalucía.*
- *Ecuaciones Diferenciales, Simulación Numérica y Desarrollo del Software (FQM - 131) Junta de Andalucía*
- *COST Action Mathematics for industry network MI-NET (TD1409). European Union.*
- *Research and Innovation Staff Exchange Network of European Data Scientists - NeEDS (H2020-EU RISE 822214). European Union.*

Resumen

La tecnología aplicada a la generación de energía renovable ha experimentado un gran avance en las últimas décadas, propiciando un mayor interés en la literatura. Plantas conocidas como Planta Solar de Torre Central (SPT, del inglés Solar Power Tower) son un tipo de tecnología termosolar de concentración (CSP, del inglés Concentrated Solar Power) que continúan en pleno desarrollo por todo el mundo, y consisten en subsistemas que están abiertos a su optimización.

Esta Tesis se enmarca en el desarrollo de nuevos métodos y resultados para la optimización de plantas SPT, con un interés particular en la optimización de las operaciones.

El Capítulo 1 ofrece información relevante sobre el sector energético actual y continúa con la descripción del diseño y la modelización de una planta SPT. En este capítulo también se describe la teoría óptica que determina la transferencia de radiación incidente en el sistema, y se presentan sus ecuaciones más relevantes.

En el Capítulo 2, las operaciones de limpieza del campo de heliostatos están optimizadas por un horario de duración fija, usando programación lineal entera binaria (BILP, del inglés Binary Integer Linear Programming). El problema dimensional se aborda con un algoritmo de agrupamiento, antes de encontrar una solución inicial para el problema de asignación. Por último, se presenta una búsqueda local novedosa mediante técnicas heurísticas que mide el "atractivo" de una ruta a través del uso de un procedimiento de optimización secuencial por pares que minimiza una medida ponderada de beneficio, mientras penaliza la pérdida de energía total.

En los Capítulos 3-5 se investiga la estrategia de enfoque adoptada para el campo de heliostatos cuando consideramos un perfil de la distribución del flujo deseado, además de incluir restricciones operacionales. En el Capítulo 3, se desarrolla un modelo BILP, donde se seleccionan unos puntos de enfoque predeterminados en el receptor. La función objetiva es lineal y se restringe por equivalencias lineales que se relacionan por una distribución suavizada (para proteger los componentes del receptor de cargas de flujo anormales) a través del uso de una penalización. En el Capítulo 4, se extiende este modelo considerando las variables continuas en el receptor en vez de fijadas en puntos de enfoque predeterminados. El resultado es un problema de optimización con una función objetiva no-lineal, no-convexa y con restricciones no-lineales. En este caso,

un algoritmo de ascenso de tipo gradiente es desarrollado utilizando una técnica de selección de paso no estándar. En el Capítulo 5, se amplía el modelo de optimización de la estrategia de enfoque al considerar un escenario dinámico. En este caso, la estrategia de enfoque durante un período de tiempo puede ser optimizada, teniendo en cuenta las limitaciones tecnológicas de las plantas SPT. Se han considerado dos algoritmos, Penalización y Lagrangiano Aumentado, y se presentan condiciones de optimalidad.

Por último, en el Capítulo 6, se incluyen efectos de inclemencias climáticas en el modelo de optimización presentado en el Capítulo 3. En este capítulo, se incorporan procesos estocásticos para determinar la estrategia óptima de enfoque en un instante temporal fijo cuando los datos climatológicos pudieran ser inciertos.

Toda la investigación presentada en esta Tesis Doctoral está ilustrada usando datos reales de una planta SPT, y conclusiones y recomendaciones para futuras investigaciones son presentados.

Abstract

Renewable energy technology has seen great advances in recent decades, combined with an ever increasing interest in the literature. Solar Power Tower (SPT) plants are a form of Concentrating Solar Power (CSP) technology which continue to be developed around the world, and are formed of subsystems that are open to optimisation.

This thesis is concerned with the development of new methods and results in the optimisation of SPT plants, with particular focus on operational optimisation.

Chapter 1 provides background information on the energy sector, before describing the design and modelling of an SPT plant. Here, the optical theory behind the transfer of incident radiation in the system is developed and the relevant equations presented.

In Chapter 2, the cleaning operations of the heliostat field are optimised for a fixed schedule length using Binary Integer Linear Programming (BILP). Problem dimensionality is addressed by a clustering algorithm, before an initial solution is found for the allocation problem. Finally, a novel local search heuristic is presented that treats the so-called route "attractiveness" through the use of a sequential pair-wise optimisation procedure that minimises a weighted attractiveness measure whilst penalising for overall energy loss.

Chapters 3-6 investigate the aiming strategy utilised by the heliostat field when considering a desired flux distribution profile and operational constraints. In Chapter 3, a BILP model was developed, where a pre-defined set of aiming points on the receiver surface was chosen. The linear objective function was constrained with linear equalities that related to distribution smoothing (to protect receiver components from abnormal flux loads) via the use of penalisation. Chapter 4 extended this model by instead considering continuous variables with no fixed grid of aiming points. This led to an optimisation problem with a non-linear, non-convex objective function, with non-linear constraints. In this case, a gradient ascent algorithm was developed, utilising a non-standard step-size selection technique. Chapter 5 further extended the aiming point optimisation topic to consider the dynamic case. In this sense, the aiming strategy across a period of time could be optimised, taking into account SPT plant technological limitations. Two algorithms were considered, Penalisation and Augmented Lagrangian, where theoretical properties for optimality and solution existence were presented. Fi-

nally Chapter 6 considered the effects of inclement weather on the optimisation model presented in Chapter 3. Stochastic processes were investigated to determine optimal aiming strategies at a fixed point in time when weather data could not be known for certain.

All research presented in this thesis is illustrated using real-world data for an SPT plant, and conclusions and recommendations for future work are presented.

Contents

Nomenclature

(u, v)	Coordinates on receiver surface
(u_i, v_i)	Test point i on receiver surface
α_{clu}	Clustering distance weighting constant
α_{ls}	Local search distance weighting constant
α_{sun}	Solar angle
$\bar{H}$	Set of primary heliostats
β_{clu}	Clustering energy weighting constant
β_{ls}	Local search energy weighting constant
β_{sun}	Solar angle
$\dot{\mathbf{p}}(t)$	Velocity of aim points at time t
ϵ	*Armijo's Rule* parameter
γ	Step size
γ_0	Initial step size
γ_k	Step size k
κ	Heliostat efficiency
$\mathcal{L}$	Lagrangian
$\mathbf{E}$	Euclidean space
$\mathbf{F}$	Euclidean space
$\mathbf{P}$	Hilbert space
$\mathbf{p}(t)$	Collection of aim points at time t

$\mathbf{V}_p$	Target velocity vector
$\mathcal{P}$	Projection function
μ	Penalisation constant
Ω	Receiver Surface
σ_1	Velocity constraint threshold
σ_2	Radiation constraint threshold
τ	Radiation distribution limit
$\tilde{K}$	Heliostat efficiency
$\vec{p}$	Receiver normal vector
$\vec{v}$	Solar vector
$\vec{w}$	Heliostat-Receiver vector
$\vec{w}_h$	Heliostat-Receiver vector for heliostat h
ξ	Receiver inclination
ζ	Degradation function
A	Weighting parameter
C	Set of periods in schedule
c	Convergence limit
C^*	Maximum energy constant
C_*	Minimum energy constant
c_e	Heliostat effective area
c_r	Heliostat reflectance
E^{tar}	Target distribution
$E^{tar}_{u,v}$	Target distribution at point (u, v)
$f(h, p)$	Total radiation on receiver for heliostat h aiming at p
f_{atm}	Atmospheric attenuation
f_{cos}	Cosine efficiency

f_{ref}	Heliostat reflectivity
f_{sp}	Spillage efficiency
$F_{u,v}(h,p)$	Gaussian distribution of heliostat h aiming at p
G	Balanced objective function
g	Objective function
H	Total number of heliostats in field
h	Heliostat h
I	Number of test points
i	Receiver test point
J	Combined objective function
K	Average heliostat efficiency
M_1	Velocity constraint operator
M_2	Radiation constraint operator
P	Number of heliostat clusters
p	Aiming point p
p_h	Aiming point for heliostat h
S	Size of heliostat clusters
s	Slack variable
S_h	Cardinality of cluster with primary heliostat h
s_i	Period i of schedule
T_h	Tower height
Tol	Simulation tolerance
V_p	Velocity constraint constant

Acronyms

BILP Binary Integer Linear Programming.

CSP Concentrated Solar Power.

DNI Direct Normal Irradiance.

HTF Heat Transfer Fluid.

NRES Non-Renewable Energy Sources.

PV Photovoltaic.

SPT Solar Power Tower.

TES Thermal Energy Storage.

UN United Nations.

VRP Vehicle Routing Problem.

Chapter 1

Introduction

Introduction

1.1 Energy Sources

Energy demand across the globe continues to rise with population growth [Jones and Warner, 2016], and in tandem with our ever-increasing dependence on technology [Sorrell, 2015].

To meet this demand, various natural resources are exploited, including:

- Crude Oil
- Coal
- Natural Gas
- Nuclear
- Biomass
- Solar
- Wind
- Hydroelectric

The current dominant resources used in the production of electricity are fossil fuels (Crude oil, coal, natural gas) [Martins et al., 2018]. In 2016, the authors in Jones and Warner [2016] noted that 91% of worldwide electricity was produced by non-renewable energy sources (NRES) and that 87% was from fossil fuel.

Research suggests that whilst there is a significant amount of crude oil remaining, more than two-thirds of production may need to be replaced by 2030 [Sorrell et al., 2010]. There is much discussion on the theoretical date when the world will reach *Peak Oil* [Chapman, 2014], that is when the crude oil easiest to extract has been depleted and costs begin to rise, and these uncertainties indicate the need to progress alternative resource adoption. However, the improvement of alternative fossil fuel extraction techniques (for example shale gas extraction [Soeder, 2018]) promises to extend potential supply for many years to come [Helm, 2016].

The environmental cost of fossil fuel use, for example land degradation and emissions (e.g. carbon dioxide and sulphur dioxide), has come to the forefront in the public domain in recent years and cast a negative light on their continued use. Specifically, the gradual warming of our planet and its consequent effects on the environment has become a global issue, where it is projected that surface warming increases nearly linearly with carbon emissions [Williams et al., 2017].

To reduce the negative environmental effects associated with continued fossil fuel use, governments across the globe are pushing renewable energy strategies [Mowery et al., 2010; Nejat et al., 2015] and in 2015 the *UN* ratified the *Paris Climate Agreement* [Christoff, 2016]. Although such efforts have seen the global use of renewable energy sources increase, the *UN* target of $< 2°C$ temperature increase by 2100 is becoming unachievable [Warner and Jones, 2017].

The change to renewable energy resources is progressing slowly, in part due to geographical and technical aspects required, as investigated by the authors in Moriarty and Honnery [2016]. The same authors discuss the transient nature of renewable energy sources, where a guaranteed and steady supply is not possible, and as such are not compatible with the current electricity network infrastructure. Limitations on locations of new renewable energy based power plants are imposed as they must be located in areas where the source is abundant, whereas non-renewable energy plants can be located worldwide, with necessary materials transported from the source. Another negative issue that may be slowing adoption can be seen in the comparatively low efficiency ratings in solar energy plants, as discussed in Kabir et al. [2018], and problems with renewable energy storage [Trainer, 2017].

It is clear that further research and development of renewable energy technologies is necessary in order to improve efficiencies and accelerate adoption. This has been demonstrated by governmental schemes that intend to promote the use of renewable energy resources by the public [Viardot, 2013], covering technologies such as solar panels or biomass heaters. An important factor for new technological advances comes from public opinion, where research has shown that new technology uptake may be affected by occupant age [Willis et al., 2011] and that certain barriers exist in the adoption of the technology [Viardot, 2013], for example cost, reliability, and lack of information.

Therefore, if renewable energy use is to increase and global temperature targets reached, it is imperative that investigation into the technology is continued and improvements made, as noted by the authors in [Jones and Warner, 2016].

1.2 Renewable Energy

The main types of renewable energy sources are wind, solar, hydroelectric and geothermal, whose development has seen rapid growth during recent decades [Jacobsson and Johnson, 2000; Kaldellis and Zafirakis, 2011]. However, primitive forms of these technologies have been in use for thousands of years, from treadmills, sailboats and windmills to waterwheels and concentrated solar fire starters [Sørensen, 1991].

In 2017, an estimated 23.7% of energy generated was from renewable energy sources, an increase from an estimated 20% in 2014 [Zarfl et al., 2014]. Of this, 16.6% was attributed to hydro, 1.2% to solar and 3.7% to wind [Hussain et al., 2017].

Wind energy is sourced through the use of wind turbines, which has seen a rapid growth in implementation and can currently provide between kilowatts to megawatts [Kumar et al., 2016]. Hydroelectricity relies on the movement of water to drive turbines (hydropower), normally within a dam. In 2014, the authors Zarfl et al. [2014] predicted that the global capacity of hydroelectricity was to increase by 74% to 1,700GW, due in part to the continued construction of hydroelectric dams.

Of the renewable energy sources, solar energy has proven to be of particular interest in recent decades, where the authors of the work Kabir et al. [2018] remark that nearly four million exajoules ($1EJ = 1018J$) of solar radiation reaches the earth annually, which is theoretically sufficient to fulfil the entire planet's energy needs. The same authors also report that with an energy conversion efficiency of as low as 8%, and the placement of key solar power plants, the primary energy demand of the planet could be fulfilled.

Due to the immense interest in the literature and potential for improvement, this Thesis focuses on the development of mathematical models to describe solar energy technology.

1.3 Solar Energy

The two main types of solar energy technology are Photovoltaic (PV) and Concentrated Solar Power (CSP), where a plant can typically comprise elements of one of these, or a combination of both.

PV plants use a direct conversion of energy from incident solar radiation into the electricity grid. These systems are scaleable, that is a PV system can easily be adapted for the space in which it is to be placed, thus lending them to use in large power plants and also personal homes [Parida et al., 2011]. The low-cost and scalability of this technology has led to it becoming one of the most adopted solar energy technologies, with research such as Breyer et al. [2018] indicating that PV will be a prime renewable energy source in the near future.

CSP plants use mirrors to concentrate the incident solar radiation onto a receiver, where the resultant thermal load is used to generate electricity. There are four main types of CSP plants; parabolic trough, fresnel, dish sterling and Solar Power Tower (SPT).

Parabolic trough plants consist of parabolic plate mirrors that reflect incident solar radiation onto a tube filled with a Heat Transfer Fluid (HTF). The receiver tube is fixed in place, whilst the parabolic mirror is able to rotate, in order to concentrate the incident radiation onto the receiver at all times of the day.

Fresnel reflectors utilise the same principles as parabolic trough plants, but with flat plate mirrors instead of parabolic. This form is much cheaper to produce, and

therefore reduces overall plant cost. Recent research into this technology includes novel optical optimisation models [Cheng et al., 2018] and experimental investigations into the efficiency of a linear fresnel system over a long period [Bellos et al., 2018].

SPT plants are one of the most researched and implemented types of solar energy technology, with over 100 articles published each year on a variety of topics [Islam et al., 2018]. The continued interest in the literature on SPT plants demonstrates that further advancements in this technology are of interest to the wider scientific community, and are the focus of this Thesis.

1.4 Description and operation of SPT plants

SPT plants are formed by a field of mirrors (known as heliostats) that concentrate incident solar radiation onto a centrally located receiver, which is mounted atop a tower. Typically, the resultant thermal energy on the receiver surface is transported to a traditional steam generator via a HTF.

The HTF used is dependent on the type of receiver, with examples ranging from molten salt in tube receivers [Turchi et al., 2018; Bonk et al., 2018] to sand in falling particle receivers [Calderón et al., 2018]. The transient property of solar energy as a resource brings concerns for inclusion in the network of these plants, and for this reason the ability to store the thermal energy generated is imperative. Thermal Energy Storage (TES) allows the energy captured in the HTF to be stored [El-Leathy et al., 2019], and converted into electricity for the grid at a later time, in such a way that the solar energy harvesting can be decoupled from the actual electricity production [Polimeni et al., 2018].

The two main types of SPT plant receivers are cavity and external, where external receivers are usually employed with a 360 degree heliostat field configuration, whereas cavity receivers may be limited to a directional field. Regardless of type, the transport of HTF through the receiver is critical for efficiency, where research has been conducted to improve current designs, such as Rodríguez-Sánchez et al. [2018] where the authors consider variable velocity in the HTF and improve upon plant efficiency.

The initial collection of incident solar radiation is a direct result of heliostat placement in the field, where the design and construction accounts for roughly 50% of the cost and 40% of energy loss in the system [Leonardi et al., 2019; Cruz et al., 2018a]. Part of this cost is associated to the rotating base that each heliostat is mounted on, allowing them to track the movement of the sun and maintain focus on the receiver surface.

SPT plant daily operation is driven by the principle objective of maximising profit for the operator, which requires monitoring not only the electrical output of the plant, but also the market value of electricity. This user demand defined quantity will influence

decisions for the plant operator, for example on whether to store energy or increase production at certain times.

It is therefore apparent, that both the design and operation of an SPT plant are crucial in determining the eventual efficiency and subsequent profits that it is able to produce. It has been demonstrated in the literature [Chesney et al., 2017] that Operations Research techniques can be employed in both of these regards in order to maximise the objective of higher efficiency/profits.

1.5 Design and optimisation of SPT plants

An SPT plant can be modelled using a mathematical description of the various subsystems in both the design and operation phase. Utilising known information on the radiation input from the sun, an optical model can be used to calculate the transfer of radiation through the system, and how this affects the production of electricity. With such a model, an SPT plant designer or operator is able to make decisions based upon predictable mathematical concepts that allow the optimisation of the efficiency in the system.

Optimisation techniques have been thoroughly studied in the literature, and have found immense popularity due to their applicability in real-life scenarios. In the case of solar energy technologies, there are many aspects of an SPT plant that may be optimised to improve performance, including:

- Number of heliostats
- Heliostat placement
- Heliostat cleaning
- Tower design
- Receiver design
- HTF
- Heliostat aiming strategy
- TES

The design and optimisation of an SPT plant has been investigated in the literature, with examples such as Carrizosa et al. [2015a], where the authors simultaneously optimise the heliostat field and tower properties utilising a greedy-based heuristic method, and Conroy et al. [2018], where the authors model the performance of various HTFs in a CSP system.

Multiple analysis and simulation tools have been developed to assist in the design and optimisation of heliostat fields for SPT plants, such as Wagner and Wendelin [2018] and Richter et al. [2018]. In these articles, the authors develop tools to simulate the performance of an SPT plant heliostat field using weather data and allow the user to reconfigure the heliostat locations. Simulation tools have also been developed for operational aspects of SPT plants that are already built, such as a model to evaluate

glare and avian-flux hazards [Sims et al., 2018].

A key mechanism in the SPT plant system is the transfer of thermal energy gathered from the concentrated solar radiation to the HTF via the receiver surface. The design and materials used in the receiver are important, as they must ensure efficient thermal transfer to the HTF whilst withstanding extreme heat flux over a prolonged period of time. Due to cost, the operational reliability of receiver components is an important factor in the design phase, and research has been conducted into the ageing of materials used in SPT plants under thermal loads [Reoyo-Prats et al., 2019; Lalau et al., 2019]. Such research permits designers the knowledge on how best to design receiver components in order to improve their performance.

For this reason, research into the materials used in receivers is abundant and ongoing, such as López-Herraiz et al. [2017], where the authors numerically investigate the impact of various receiver coatings on efficiency, and Larrouturou et al. [2016], where the authors study spectral selectivity and its effect on absorption of solar flux.

The thermal transfer of radiation on the receiver surface to the HTF is directly affected by the distribution of radiation reflected by the heliostats. This distribution is determined not only by the quantity of incident solar radiation reaching the field, but also by the choice of the points on the receiver at which the heliostats aim, known as the aiming strategy. It has been shown in the literature that this topic is important in both the design and operation phase of an SPT plant [Besarati et al., 2014; Binotti et al., 2016], and continues to be of interest.

As with all renewable energy sources, solar power can be negatively affected by local weather conditions, which can be unpredictable and severe. Usually, in regions of high solar irradiance, the input to the system can be predicted with good accuracy due to large amounts of historical data. However, cloud cover can not only reduce the quantity of solar energy reaching the receiver (as investigated by Crespi et al. [2018]), it can also provoke rapid thermal changes and cause permanent damage to receiver components [Salomé et al., 2013].

Regions with high solar irradiance are normally arid, and can suffer from dust particulates being deposited onto the heliostat surfaces. This reduces their efficiency [Roth and Pettit, 1980] and necessitates regular cleaning to be employed, where, coupled with water shortages in arid regions and potentially high labour costs, careful planning is required. A study of cleaning methods given by the authors in Fernández-García et al. [2013] identifies the effectiveness of various cleaning solutions through experimentation.

The problem of cleaning is compounded when the heliostat field size is large. For example, the heliostat field for PS10 and PS20 SPT plants in Seville, Spain [Abengoa, 2019] contain 624 and 1255 heliostats respectively, and cleaning operations are likely dictated by the concentric roads that separate rows of heliostats. The size of these fields is moderate, and careful planning may be sufficient to decide a cleaning strategy.

However, fields of larger size or a more chaotic placement scheme will benefit from an optimised approach to cleaning. The Ivanpah plant [BrightSource Energy, 2019] in the United States has almost 175,000 heliostats in its field, and their placement does not follow such a rigid concentric pattern as that of PS10. In such a case, the cleaning schedule utilised should be optimised using mathematical techniques to ensure maximum efficiency of the heliostats.

A variety of technologies exist for the cleaning of an SPT plant, each of which is tailored to specific plant designs or concentrator types. The authors in Pfahl et al. [2017] investigate various aspects of heliostat development, including cleaning technology. The authors identify methods that utilise robotics as a potential for the future [Hardt et al., 2011], and indicate that the most prevalant technology utilised now is a vehicle which drives past a heliostat and uses a brush and water to clean.

The technological and operational aspects of an SPT plant discussed in this section have direct impacts on efficiency, and are open to optimisation in both the design and operational phases. The work presented in this Thesis pertains to the mathematical description of radiation transfer in an SPT plant, and the development of new methods and results in the optimisation of the topics discussed above: heliostat aiming strategies and heliostat cleaning scheduling.

1.6 Contributions of this Thesis

The following sections present a summary of the contributions given in this Thesis.

1.6.1 Heliostat field cleaning scheduling for Solar Power Tower plants: A heuristic approach

Chapter 2 presents the work published in the article Ashley et al. [2019a], where optimisation techniques are utilised to find the optimal heliostat field cleaning strategy across a time period.

Cleaning operations typically depend on the structure of the heliostat field and available resources, which decide to some degree the route that a cleaning vehicle will take. In this work we consider heliostat location and potential radiation input to form an optimisation problem, where we look to maximise efficiency of the heliostats across a length of time.

The potential radiation input to the receiver is a measure of how important a particular heliostat is to the SPT plant, and has been calculated as the average reflected radiation for that heliostat across one day. This factor will influence the regularity of cleaning across the heliostat field: larger values indicate higher importance for cleaning over heliostats with smaller values.

The cleanliness of a heliostat decreases over time due to particulate deposition, and can be measured from historical data for a particular region and used to create an expected degradation function. In this work we assume a linear degradation function $\delta = \delta(t)$, but note that any other function can also be implemented into the model.

The optimisation model applied in this work considered a 3 stage heuristic approach to maximise the efficiency of heliostats across a fixed-length schedule: first, a clustering optimisation to reduce problem dimensionality is performed; then, the optimisation of the cleaning schedule to produce an initial solution; finally, this initial solution is improved upon through the use of a pair-wise local search heuristic, which takes into account route "attractiveness".

Heliostat clustering

This can be modelled as a p-median problem, where heliostats can be viewed as clients and p potential plants have to be selected, the primary heliostats, which are the central heliostats of the groups. The formulation corresponds to a binary integer linear programming (BILP) problem in which the overall dissimilarity between each heliostat and its associated primary heliostat is to be minimised.

The dissimilarity between two heliostats h and h' is measured as the difference of the generated potential energies E_h and $E_{h'}$, combined with the physical distance $Dist(h, h')$ between heliostats h and h' in a weighted objective function $\lambda_{hh'} = \alpha Dist(h, h') + \beta |E_h - E_{h'}|$ where α, $\beta > 0$. In this way, a user can define relative importance in the clustering phase between energy generation similarity, or proximity of heliostats in clusters.

Once the optimal clustering of heliostats has been found, the next stage of the algorithm looks to optimise the cleaning schedule.

Schedule optimisation

The scheduling optimisation problem is considered with a BILP technique, where the objective is the maximisation of total efficiency of the heliostat field across the schedule.

The objective function comprises a summation of integer variables for the allocation of clusters to periods, multiplied by the energy reflected by each cluster in the corresponding period, where the degradation function is taken into account. In order to consider the cumulative degradation of efficiency across periods, binary linear constraints are included, and are explained in detail in Chapter 2.

In addition, linear constraints impose limits on the number of clusters that may be cleaned per day, as well as assuring that each heliostat is cleaned at least once across the schedule.

The resulting optimal cleaning schedule for the heliostat field considers the radiation potential of each heliostat, its degradation of efficiency over time and its grouping. With

this information, the cleaning vehicle operator has a daily schedule of heliostats to clean, where the specific route taken between selected groups must also be considered.

Local Search

When applied to large heliostat fields, the presented approach may result in optimal cleaning schedules where physically distant groups are allocated to the same day, which may be unappealing to the SPT plant operator. Therefore, a route improvement heuristic is provided, whereby the optimal schedule found in the initial solution is altered whilst considering route attractiveness [Rossit et al., 2016].

The algorithm developed for this heuristic is a rolling optimisation procedure with a penalised integer linear objective function.

The objective function minimises the physical distance between the groups in a single period, by permitting swaps from adjacent periods, with a penalty function applied that minimises the loss of efficiency caused by swapping groups from the optimal schedule previously found. The solution is the optimal allocation of groups between the two adjacent periods considered, where the weighted energy/distance objective function has been minimised.

The optimisation procedure is then repeated over subsequent pairs of periods, until no overall increase in the objective function is found. This local search heuristic looks to improve the schedule in terms of route attractiveness, but does so at a cost to the overall efficiency of the cleaning schedule. Such optimisation is scalable to any heliostat field shape and size, and can be tailored according to specific local constraints (for example impassible terrain) set by the operator.

As a final step, a greedy algorithm is implemented to find the shortest path for the route taken by the cleaning vehicle for each period of the schedule.

The proposed optimisation algorithm is demonstrated on the SPT plant described in Section 1.6.6, producing a cleaning schedule for a 16 day period and highlighting model functionality.

1.6.2 A first approach to the optimisation of aiming strategies

In Chapter 3, the work based on Ashley et al. [2017] is presented, which considers the optimisation of aiming strategies for the heliostat fields in SPT plants. The aiming strategy utilised is known to be important in SPT plant operation [Relloso and García, 2015], and has been a topic of interest in the literature. In Berenguel et al. [2018], the authors approach heliostat aiming with a two-layered optimisation procedure, utilising a genetic algorithm. Further examples can be seen in Besarati et al. [2014] and Astolfi et al. [2017a].

Such methods often lack a full mathematical description of the problem, and utilise

heuristics for simplification. We look to thoroughly model the SPT plant system as an optimisation problem which can be extended to any size and shape plant, and find the optimal aiming strategy under local weather conditions.

Optimisation formulation

In this work, a BILP model is presented to optimise the aiming strategy of heliostats in the field to a set of fixed aiming points on the receiver surface. The objective function is formed from the optical model given in Section 1.7.4 that describes the reflection of incident solar radiation by the heliostats onto the receiver surface, and calculates the total energy depending upon the aiming strategy chosen. Accurate optical models are essential for simulation of SPT plants and have been analysed extensively, for example Igel and Hughes [1979]; Collado et al. [1986].

The overall objective of an SPT plant operator is to maximise output (and therefore profit), where considerations on storage and current market value of electricity are taken into consideration. Therefore, the aiming point for heliostat h must be chosen so that it maximises radiation reaching the receiver, calculated by the aforementioned optical model.

The summation of these individual radiation contributions for all h gives the total radiation reaching the receiver for the given aiming strategy.

However, maximisation of the thermal energy reaching the receiver surface does not directly correlate to maximising efficiency. Depending on the type of receiver used, higher efficiencies are obtained when a certain distribution of energy is held across the receiver [Yu et al., 2014]. This distribution is dynamic, in that it changes with time and conditions of the receiver, and therefore must be taken into consideration within an optimisation procedure.

Hence, a set of linear constraints are added to the optimisation model that homogenise the distribution of energy across the receiver surface, whilst the objective seeks the maximal amount of energy.

A binary integer linear program is developed with a penalised objective function that assigns heliostats to aiming points at a specific time point, and the Gurobi solver package [Gurobi Optimization Solver, 2019] is used to find the optimal solution.

Finally, an illustrative example is presented for multiple time points across a day utilising the SPT plant data presented in Section 1.6.6, where behaviour of results in relation to solar angles is discussed.

1.6.3 Continuous aiming strategies (I): the stationary case

Chapter 4, based upon the article Ashley et al. [2018], concerns the reformulation of the work presented in Chapter 3 to consider the aiming points as continuous variables

across the feasible region Ω.

In this work, the objective again considers both the maximisation of energy reaching the receiver, and the minimisation of deviation from a specific target distribution, where the variables are now continuous across the receiver surface Ω. No pre-defined set of aiming points is used. Instead, each heliostats' aiming point is represented as an individual continuous variable in Ω. In this way, the solution found is more representative of the real-world case, but comes at the cost of higher problem complexity and dimensionality.

Optimisation model

Due to the use of continuous variables, a BILP technique can no longer be applied, and instead continuous optimisation techniques must be considered. In the case of optimisation of aiming strategies, our objective function is large dimensional, non-linear, non-convex and is subject to convex constraints on the aiming points $p_h \in \Omega$ for all h in the set H of heliostats in the field.

The objective function, given in Equation (1.6.1) and explained in Chapter 4, is differentiable across Ω, which permits the use of gradient based optimisation techniques.

$$A \sum_{h \in H} f(h, p_h) - (1 - A) \int \left[\sum_{h \in H} F_{u,v}(h, p_h) - E_{u,v}^{tar} \right]^2 d\Omega. \tag{1.6.1}$$

The relative weighting parameter A is added to both parts of the objective function, so that an analysis into the relative importance of each may be conducted and the *Pareto Front* approximated.

To solve the optimisation problem, a gradient ascent algorithm is developed that maximises the objective function by computing its gradient. To accomplish this, rapid numerical calculations of the partial derivatives of a non-linear and non-convex function must be performed, for each heliostat in the field.

Considering the aiming points p_h to be continuous across Ω introduces integrals across the domain, which for numerical purposes are replaced by finite dimensional approximations in space.

Computational time is tackled in the algorithm by the development of a non-standard step size selection routine, where each variable of the optimisation problem (aiming point) receives independent treatment.

The algorithm is written in Python and rapidly calculates the gradient for all heliostats in the field, and subsequently optimises the objective function. Due to the multi-modal nature of the considered function, it is necessary to incorporate techniques ensuring that the global solution is found, rather than a local maximum. In this work, a multi-start procedure from randomised starting positions is applied. The analysis shows

that, for this function, with a relatively low number of multi-starts, a suitable solution is found. To demonstrate the functionality of this algorithm, a numerical illustration is given with realistic SPT plant data defined in Section 1.6.6, where the weighting parameter is varied across multiple runs to generate an approximation to the *Pareto Front*. Finally, conclusions are drawn and further work is discussed.

1.6.4 Continuous aiming strategies (II): the dynamic case

In Chapter 5, the work in Chapter 4 is further extended to a dynamic formulation, where the optimal aiming strategy for a SPT plant is calculated across a time period. In dynamic optimisation, the objective function must be integrated over continuous time, where the unknown is a time-dependent function that indicates the points in Ω aimed at by the heliostats and a discretisation must be implemented to split the problem into manageable subsections of discrete time.

The work presented in this chapter, based upon the paper Ashley et al. [2019b], considers a theoretical investigation into various aspects of this dynamic problem. Specifically, the existence of a solution is proven, and the optimality conditions of the problem are presented. When applied to the SPT plant framework, the existence of a solution and optimality conditions are again confirmed.

In the case of SPT plants, the change to a dynamic problem allows the user to better simulate the physical behaviour of the system. One of the main concerns is the ever-changing meteorological conditions over the heliostat field, where incident radiation changes due to solar angle shift cause the optimal aiming strategy to change. If local weather conditions are known, and the future radiation figures for the field can be estimated (from forecasting or historical data analysis), then an optimisation procedure can be applied to optimise future aiming strategies.

Physical limitations on the rotational speed of the heliostats restrict the possible movement speed of aiming points that can be allowed. Without limitation, large oscillations could be found in aiming point position over time, which would negatively affect the simulation. Therefore, a constraint is added to the optimisation problem that limits the movement speed of aiming points to a prescribed constant.

On the other hand, thermal fluctuations across the receiver surface can provoke permanent damage if left unchecked [Relloso and García, 2015]. The optimisation problem looks to minimise the difference from a desired target distribution over time, where rapid changes may be encountered due to local weather conditions and radiation input. Therefore, it is necessary to include a constraint on the change in radiation on the receiver surface. This is achieved by the discretisation of the receiver into a large quantity of test points, where the change in radiation over time at any point may not be above a certain constant.

In this work, two algorithms are presented; in the first one, we incorporate the

dynamic constraints on the speed of rotation of the aim points and thermal fluctuations as penalty terms in the objective function; in the second one, we apply an Augmented Lagrangian technique.

In the penalisation algorithm, a similar approach to that applied in Chapter 4 is utilised. The partial derivatives of the penalised objective function are computed analytically over a time period, and a gradient ascent algorithm is applied to find the optimal solution. Once the optimal solution to the initial time step is found, it is used as an initial guess for the second time step and the constraints are updated with the new radiation information.

As in Chapter 4, the objective function considered here is non-linear, non-convex and formed of continuous variables across the feasible domain Ω. The extension to the dynamic case expands the problem dimensionality, and a second numerical approximation in the time variable is performed.

In the Augmented Lagrangian algorithm, the constraints are considered together with the objective function in a duality-penalty method. As before, a gradient ascent approach is used, where the gradient is calculated analytically. Again, a discretised time period is considered, and a recurring optimisation procedure is implemented to calculate the global optima across all time steps.

Both algorithms are implemented in Python and are demonstrated with an illustrative example utilising realistic SPT plant data from Section 1.6.6, with radiation information for the duration of a day. Finally, conclusions on the algorithms presented are drawn, and intentions of future work are discussed.

1.6.5 Inclement weather effects on optimal aiming strategies

Chapter 6 investigates in more depth the aiming point strategy of a heliostat field, considering the effects of inclement weather. Transient clouds not only have a profound impact on the efficiency of an SPT plant, but also pose a threat to the integrity of the receiver components, as rapid thermal fluctuations can cause permanent damage [Martínez-Chico et al., 2011].

A cloud may be modelled according to the location of its shadow on the heliostat field, with information on its approximate shape and size. The loss of efficiency associated with cloud cover on a heliostat is proportional to the density of the cloud, and is dependent on weather conditions.

When considering the aiming strategy of an SPT plant across a day, the varying solar radiation input is taken into account, and the strategy adjusted accordingly. If information on local cloud cover is available (see [Lopez-Martinez and Rubio, 2002; Martínez-Chico et al., 2011] for related research), from observation or forecasting, then the optimisation of aiming strategies can be updated to include efficiency losses due to cloud cover.

In this work, a BILP problem was developed that optimised the aiming strategy for a heliostat field at a given time point, when cloud information was known. With this model, the aiming strategy was optimised in order to approach a target distribution of energy on the receiver, whilst also preventing large thermal gradients between test points.

Due to the uncertainty of cloud cover, a stochastic linear integer programming technique was applied, where the cloud characteristics (location, size and density) were considered to be stochastic in nature. A variability percentage was allowed for these characteristics over a set of scenarios, and the optimisation problem updated to account for the uncertainty. The resulting optimal aiming strategy then describes the best solution when considering cloud characteristic uncertainty.

This methodology is illustrated with an example utilising realistic SPT plant data from Section 1.6.6, and assumed cloud characteristic parameters.

1.6.6 An illustrative example

The work presented in Chapters 2-6 of this Thesis develops optimisation models for various aspects related to SPT plant operation and design. In each chapter, the functionality and performance of the designed algorithms are presented using an illustrative example, where realistic data for a particular SPT plant is used.

In this section we summarise the SPT plant chosen (PS10 in Seville, Spain [Abengoa, 2019]) and the imposed assumptions. This was the first operational commercial SPT plant and therefore has an abundance of data available, and is frequently used in the literature.

The general specifications for the PS10 SPT plant are given in Table 1.1, and the layout of the 624 heliostats in the field is shown in Figure 1.1.

In Figure 1.2 the reflected radiation reaching the receiver for each heliostat, averaged across the design point day, is given. This averaged value is utilised in Chapter 2 in the optimisation of cleaning schedules, where the contribution across time of a heliostat must be considered. This averaged assumption is a sensible simplification for the purposes of optimisation model design, but would benefit from further investigation at a later date.

The incident radiation on the heliostat field is assumed equal for all heliostats, which is a common assumption in the literature due to almost negligible changes across short distances. The radiation profile for the design point day, noted in Table 1.1, is given in Figure 1.3.

It is worth noting that Figure 1.2 shows a distinct difference in the contribution to the system across heliostats, which demonstrates the need for optimisation of heliostat management.

The receiver of the PS10 SPT has been modelled as a circular flat plate in this Thesis, as a convenient simplification for the model. However, it should be noted that

all models developed in this work are directly applicable to any other receiver shape or size.

Attribute	Value	Note
General		
Cost	€35m	
Capacity	11MW	
Solar hours per day	$9-15$	320 days per year
Location	$37°26'32''N$ $06°15'15''W$	Latitude/Longitude
Design point day	21st March	To calculate incident radiation
Direct normal irradiance (DNI)	$823.9W/m^2$	Approximated at midday
Tower/Receiver		
Tower Height	115m	
Receiver Height	6m	Approximated
Receiver Width	6m	Approximated
Receiver Type	Cavity	
Receiver Inclination	$12.5°C$	Approximated
HTF	Water	
Storage	Yes	1 hour
Heliostat		
Number of Heliostats	624	
Heliostat size	$120m^2$	

Table 1.1: PS10 data

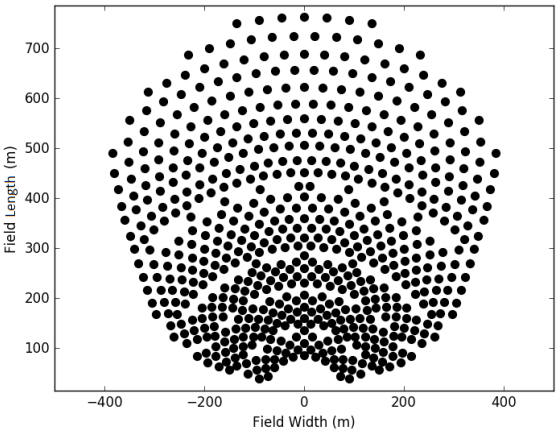

Figure 1.1: PS10 Heliostat Locations

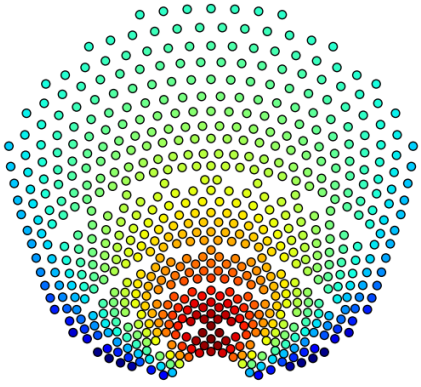

Figure 1.2: Average reflected radiation per heliostat

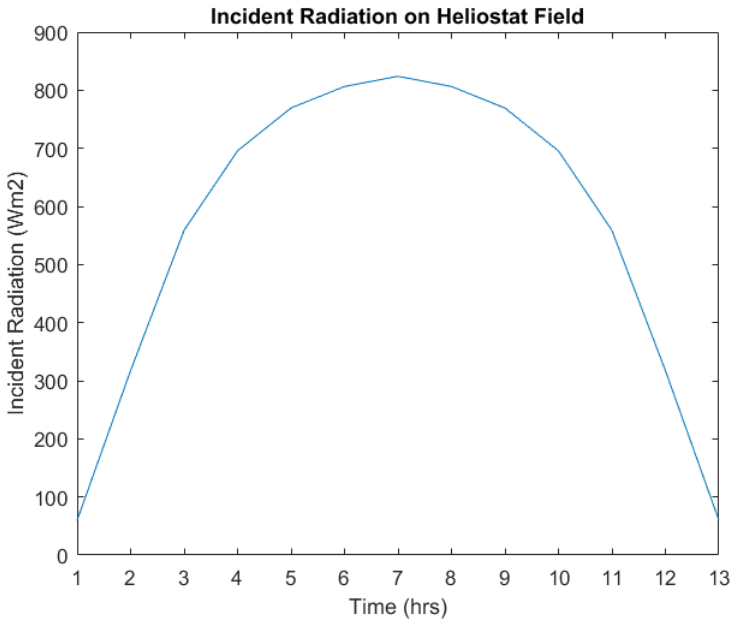

Figure 1.3: Design point radiation profile

1.7 Technical Background

In this section, we present a technological background of SPT plant subsystems and relevant radiation modelling information.

As introduced previously, an SPT plant is formed of a field of reflective surfaces, known as heliostats, which concentrate incident solar radiation onto a centrally located receiver, mounted atop a tower. The thermal energy generated by this process is transported by a HTF to a generator, whereby electricity is produced.

As demonstrated in Section 1.5, there are various subsystems of an SPT plant design that can be improved upon by mathematical optimisation, and what follows is a brief summary of the properties and equations that are important in an optimisation model of these subsystems.

1.7.1 Tower

In an SPT plant, the tower is usually the central focus of the plant, which supports the receiver at a designated height T_h. The gathered heat from the receiver is transported by the HTF via a system of tubes in the tower to the next stage of the cycle (either directly to the generator or to storage).

The height of the tower, T_h, influences the angle to which the heliostats must orientate themselves in order to maintain solar focus on the receiver, and also influences the optimal design of the heliostat field.

Tower design has been researched in terms of optimisation [Carrizosa et al., 2015a], but for the purposes of this Thesis, has been assumed prescribed.

1.7.2 Receiver

The receiver constitutes one of the most important elements of an SPT plant, and its design influences the type of heliostat field that will be employed. For the purposes of the work in this Thesis, a flat-plate circular receiver has been assumed. However, as previously mentioned, it should be noted that this was chosen for convenience, and the work presented is directly extendible to other receiver shapes and sizes.

For a flat plate receiver (and by extension any shape or size receiver) important properties include its dimensions, which directly influence the amount of radiation captured and spillage incurred.

The feasible region for the optimisation problems developed in this Thesis, Ω, is defined as the continuous region contained within the circle $r^2 = u^2 + v^2$ centered at the origin of the (u, v) plane on the receiver surface. Here, r is the given value of the radius of the circular receiver, where $r = \frac{1}{2}RecW$ and $RecW$ is the receiver width.

The inclination of the receiver, ξ, affects the distribution of radiation on the receiver surface. This is assumed constant in this work, however it is noted that in a coupled optimisation of aiming strategies and receiver design, this parameter will be of importance.

The materials and internal design of the receiver influence the transport of thermal energy from the surface to the HTF in the interior. Aside from maximising durability of the receiver (high thermal flux causes rapid deterioration [Relloso and García, 2015; Sánchez-González et al., 2015]), this also has implications on the required optimal radiation distribution.

1.7.3 Heliostat Field

The shape of the heliostat field largely depends upon the local topography, and the type of receiver employed. However, in almost all cases in existing SPT plants, a pattern-based approach has been used to form the layout of the heliostats. Examples of this approach include radially staggered, sunflower and spiral [Mutuberria et al., 2015].

Pattern-based fields are the easiest to develop and construct, but are not optimal in the sense of maximising efficiency. Non-pattern-based heliostat fields have been shown to improve overall efficiency of an SPT plant [Carrizosa et al., 2015a], and on a case-by-case basis could be used in the design of future plants.

For the purposes of this Thesis, we assume the concentric circle pattern utilised in the PS10 SPT plant, as described in Section 1.6.6.

In a South facing field (with a North facing receiver) the heliostats are defined with

cartesian coordinates (x, y, z), where the x-axis represents the West-East direction, the y-axis the North-South and z represents the height of each heliostat. In this work we consider $z = z_0$ to be constant across the field, or in other words that the heliostat field does not vary in height, therefore the heliostat coordinates are of the form (x, y, z_0), where $(x, y) \in D$ and $D \subset \mathbb{R}^2$.

Heliostat design has a direct impact on various efficiency factors within an SPT plant, and multiple types have been proposed (see [Domínguez-Bravo et al., 2016; Carrizosa et al., 2017] for information). In this Thesis we assume standard rectangular faceted heliostats, as shown in Figure 1.4.

Figure 1.4: Standard heliostat design [Abengoa, 2019]

The rectangular faceted design leads to small gaps between adjacent panels in the heliostat surface, which must be taken into account in efficiency calculations. The *effective area* of a heliostat is the proportion of the surface which reflects radiation, and is calculated as follows:

$$A_e(h) = c_e(h) \cdot A(h), \tag{1.7.1}$$

where $c_e(h)$ is a constant which accounts for the gaps between facets, and $A(h)$ is the physical area, for heliostat h. In this work, all heliostats are assumed to have the same effective area and $A_e(h)$ is therefore constant for all $h \in H$.

1.7.4 Radiation Modelling

Determined by the design of all elements of an SPT plant, as well as the time of day and year, the distribution of radiation on the receiver ultimately drives potential output. For this reason, accurate modelling of changes in this distribution due to varying inputs is key in the optimisation of SPT plants. The following sections define the inputs to the radiation distribution model used in this Thesis.

Incident Solar Radiation

The incident solar radiation input to the model is time dependent, and directly proportional to the quantity of radiation that reaches the receiver. The values used in this work consider clear skies for simplicity and are approximately symmetrical between the central solar hour of a day (See Figure 1.3), as well as months of the year.

The solar vector $\vec{v}$ is calculated using Spencer's formula (see the discussion in [Blanco-Muriel et al., 2001] for more information and other methods), where the inputs are the solar angles α_{sun} and β_{sun}. For a particular time point t, the solar vector $\vec{v}(t)$ is given by:

$$\vec{v}(t) = (-\cos\beta_{sun}(t)\cos\alpha_{sun}(t), \cos\beta_{sun}(t)\sin\beta_{sun}(t), \sin\beta_{sun}(t)). \tag{1.7.2}$$

Each heliostat in the field reflects incident solar radiation towards a selected aiming point on the receiver along the vector $\vec{w}$, as shown in Figure 1.5.

An aiming point can be defined in the heliostat field (x, y, z) coordinate system by $(R_x, u_y, T_h + v_z)$, where (u_y, v_z) are the receiver coordinates and the center is the origin. Here, R_x is a fixed offset from the x-axis of the angled receiver surface. This value will vary slightly when changing aiming point, depending on the angle of the receiver, but for simplicity has been assumed constant in this work.

Therefore, the heliostat-receiver vector $\vec{w}$ for heliostat h can be given by:

$$\vec{w} = (R_x - x, u_y - y, T_h + v_z - z_0) \tag{1.7.3}$$

The normal vector to the receiver is given by:

$$\vec{p} = (-\cos\xi, 0, \sin\xi) \tag{1.7.4}$$

The solar vector $\vec{v}$ is assumed constant across the heliostat field.

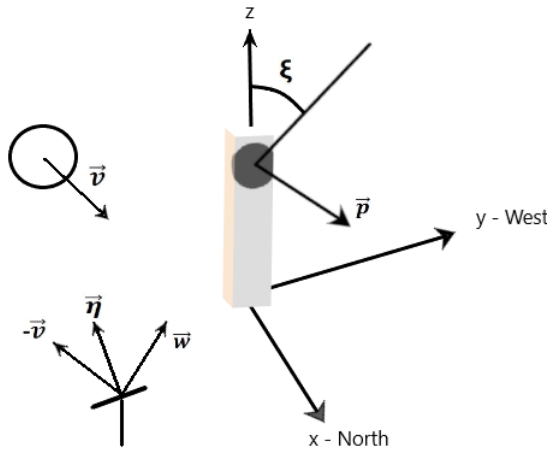

Figure 1.5: Directional Vectors

Cosine efficiency

The shape of the radiation distribution reaching the receiver is highly sensitive to the angle formed by the solar vector $\vec{v}$ and the heliostat-receiver vector $\vec{w}$. The cosine efficiency is the cosine of this angle, and is a measure of the effective reflective area of the heliostat.

The cosine efficiency can be calculated as:

$$f_{cos} = \sqrt{\frac{1}{2} + \frac{\vec{w} \cdot \vec{v}}{2||\vec{w}||}}. \tag{1.7.5}$$

A depiction of the cosine efficiency of two heliostats is given in Figure 1.6, where the maximal value $f_{cos} = 1$ is achieved when $\vec{v}$ and $\vec{w}$ are parallel.

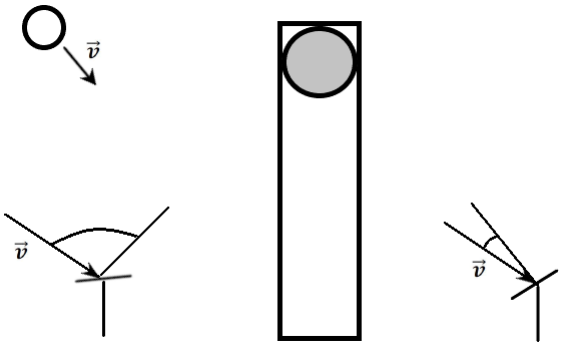

Figure 1.6: Cosine angles

Atmospheric attenuation

Transmission of radiation through air incurs losses which are directly proportional to the distance travelled. Therefore the length of the vector $\vec{w_h}$, or the distance between

heliostat h and the receiver, causes losses to the radiation received.

The atmospheric attenuation for a heliostat h is given by:

$$f_{atm} = \alpha_1 - \alpha_2||\vec{w}_h|| + \alpha_3||\vec{w}_h||^2, \tag{1.7.6}$$

where $||\cdot||$ denotes the Euclidean norm in $\mathbb{R}^3$ and α_i for $i = 1, 2, 3$ are fixed coefficients whose values are calculated empirically, where more information can be found in [Biggs and Vittitoe, 1979; Collado and Turégano, 1989; Collado and Guallar, 2012].

Heliostat reflectivity

Heliostat reflectivity is a measure of the ability ability to reflect incident radiation, and is determined by physical properties and temporal effects (dirt accumulation), giving an efficiency value between 0 and 1. Heliostat reflectivity, f_{ref}, is calculated as the product of reflectance and effective area.

The reflectance of the heliostat surface, c_r, concerns the efficiency of the reflective surface used in the heliostat, whilst the effective area c_e is a measure of heliostat size. The heliostat reflectivity is therefore given by:

$$f_{ref} = c_r \cdot c_e. \tag{1.7.7}$$

Cleanliness of a heliostat can be included in the reflectance coefficient $c_r \in (0, 1)$, where a value of $f_{ref} = 1$ represents a clean heliostat. A degradation of efficiency can be applied in order to model loss of reflectivity with accumulation of detritus. This degradation function is time dependent (and affected by local weather conditions), and for the purposes of this study a linear degradation function is assumed, as shown in Figure 1.7.

Shadowing and blocking

Heliostat placement in an SPT plant field has been a topic of interest in optimisation for many years [Barberena et al., 2016]. Close proximity of heliostats to one another causes efficiency losses known as shadowing and blocking, which are time dependent and involve interactions between large groups of neighbouring heliostats.

Shadowing is caused when the incident solar radiation on the vector $\vec{v}$ does not reach a heliostat surface, because another heliostat has intercepted it. Blocking occurs when reflected radiation from a heliostat on vector $\vec{w}$ strikes the rear of a neighbouring heliostat, and therefore does not reach the receiver.

However, it should be noted that these losses reduce the total proportion of radiation reflected to the receiver and should be recalculated for each time instant in an optimisation problem, due to changing solar angle. Shadowing and blocking will also

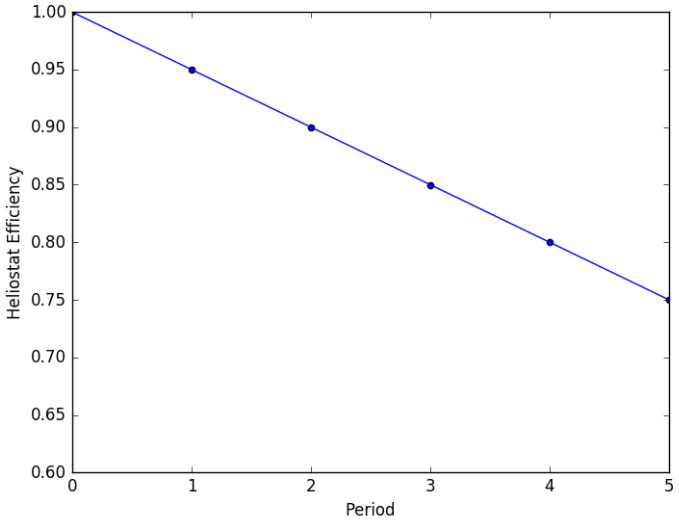

Figure 1.7: Linear degradation function

be affected by any change of aiming point which alters the $\vec{w}$ heliostat-receiver vector, and therefore should be included in future research for a more representative SPT plant model.

Radiation distribution

The radiation reflected by heliostats onto the receiver surface is modelled using a Gaussian distribution, where the heliostat coordinates are defined in the (x, y) plane and the receiver surface heliostat aiming coordinates in the (u, v) plane.

The formulation of the distribution equations given below assumes an aiming point in the (u, v) plane equal to $(0, 0)$. The extension to a non-centrally focused aiming point is given in Chapter 3.

The distribution is given by:

$$f_1(x, y) \exp\left(\frac{-f_2(u, v, x, y)}{2f_3^2(t, x, y)}\right), \tag{1.7.8}$$

where the f_i with $i = 1, 2, 3$ are as follows:

$$f_1(x, y) = \frac{f_4}{2\pi f_3^2(t, x, y)\,||\vec{w}||^2}, \tag{1.7.9}$$

$$f_2(u, v, x, y) = \frac{u^2 + v^2}{2\,||\vec{w}||^2}\left[(1 + f_4^2) + \frac{|u|}{\sqrt{u^2 + v^2}}(1 - f_4^2)\right], \tag{1.7.10}$$

$$f_3(t,x,y) = \Big[\mu_1^2 + \Big(\frac{\mu_2(1-f_{cos})}{4\,||\vec{w}||}\Big)^2\Big]^{1/2} \tag{1.7.11}$$

and, finally,

$$f_4(x,y) = \begin{cases} 0 & \text{if } \cos\beta \leq 0, \\ \frac{\vec{w}\cdot\vec{p}}{||\vec{w}||} & \text{otherwise,} \end{cases} \tag{1.7.12}$$

where f_4 is equal to $cos\beta$, and β is the angle between $\vec{w}$ and the vector normal to the receiver.

Spillage efficiency

The spillage efficiency of a heliostat is a time dependent function, which describes the amount of reflected radiation which falls onto the receiver surface (that is, the proportion that does not miss the receiver). This value, between 0 and 1, is calculated as the integration of the distribution given in Equation (1.7.8) across the receiver domain Ω.

$$f_{sp}(x,y) = f_1(x,y) \iint_{\Omega} exp\Big(\frac{-f_2(u,v,x,y)}{2f_3^2(x,y)}\Big)\,du\,dv. \tag{1.7.13}$$

Converting this to polar coordinates with $u = \rho\cos\phi$ and $v = \rho\sin\phi$, gives:

$$f_{sp}(x,y) = f_1(x,y) \int_0^{2\pi} \int_0^r exp\Big(\frac{-\tilde{f}_2(\rho,\phi,x,y)}{2f_3^2(x,y)}\Big)\rho\,d\rho\,d\phi\ , \tag{1.7.14}$$

where r is the radius of the circular receiver and $\tilde{f}_2(\rho,\phi,x,y) \equiv f_2(\rho\cos\phi, \rho\sin\phi, x, y)$.

The spillage efficiency, $f_{sp}(x,y)$, is thus found by means of an exact integral over ρ and then a numerical approximation over ϕ where $\phi_i = (i - \frac{1}{2})\pi/10$:

$$f_{sp}(t,x,y) \approx \frac{2\pi}{10} f_1(t,x,y) f_3^2(t,x,y) \sum_{i=1}^{10} \frac{1}{f_5(\phi_i,x,y)} \Big(1 - exp\Big(-\frac{r^2 f_5(\phi_i,x,y)}{2f_3^2(t,x,y)}\Big)\Big)\ , \tag{1.7.15}$$

where

$$f_5(\phi_i, x, y) = \frac{(1 + f_4^2(x, y)) + \cos\phi_i(1 - f_4^2(x, y))}{2\,||\vec{w}||^2}. \tag{1.7.16}$$

see [Collado et al., 1986; Collado, 2008] for more information.

The total radiation captured by the receiver for heliostat $h \in H$ at a specific time can then be calculated by the product of efficiency losses and radiation distribution:

$$f(h) = Rad \cdot f_{sp}(h) \cdot f_{atm}(h) \cdot f_{ref}(h) \cdot f_{sb}(h) \cdot f_{cos}(h), \tag{1.7.17}$$

where Rad is the level of incident solar radiation on the heliostat field.

Chapter 2

Heliostat field cleaning scheduling for Solar Power Tower plants: A heuristic approach

Heliostat field cleaning scheduling for Solar Power Tower plants: A heuristic approach

2.1 Introduction

Accessibility is a driving factor in the use of standard structured heliostat field designs, such as the radially staggered pattern [Sánchez and Romero, 2006]. Structured designs allow easy access to all heliostats for maintenance, and also partially pre-determine the way in which the heliostat field will be cleaned by their structure of rows of heliostats. On the other hand, utilising a pattern-free field design is shown to increase the efficiency of the heliostat field [Carrizosa et al., 2015a; Cruz et al., 2018b], but complicates the accessibility of heliostats within the field for both maintenance and cleaning.

Heliostats are required to be cleaned regularly, as accumulation of dust and foreign debris will lower the reflectivity of the mirror and therefore lower the efficiency of the solar plant [Roth and Pettit, 1980; Sarver et al., 2013].

Various strategies have been developed for cleaning heliostat fields [Fernández-García et al., 2013]. However, the most widely implemented method is the use of a vehicle with a cleaning arm, which cleans heliostats with a mixture of water and brushing. Cleaning all heliostats daily is impractical due to the number within the field and water scarcity is common in regions with high solar radiation. The frequency of cleaning for each heliostat is partially determined by its physical location within the field, as the energy generated by the heliostat is strongly dependent on its location, see Figure 1 in Carrizosa et al. [2017], and heliostats that provide more energy are of more importance to be kept clean. Moreover, the proximity between heliostats and to structures will cause shielding from wind, which can affect dust deposition [Singh et al., 2015].

The vehicle used for the cleaning activities in a CSP plant has a limited water carrying capacity, and will need to return to the water depot once empty. This limited water capacity, and length of time taken to clean each individual heliostat, will determine a maximum number of heliostats able to be cleaned in a certain cleaning period.

Therefore in order to clean an entire field of heliostats, a cleaning schedule is desired, where the objective is to maximise the overall amount of incident energy reflected onto the receiver, under constraints on the number of heliostats cleaned per time period.

The goal of this chapter is to optimise the cleaning schedule for CSP plants with any size and shape heliostat field. To do this, we will consider the optical efficiency of the heliostats in the field, and also the subsequent routing problems for each period in the schedule.

Whilst this study is applicable to heliostat fields in any general solar power plant, the case of most interest is in an SPT plant. In this type of solar plant, the heliostat field layout generally has a more complex geometry and larger size, causing the optimal scheduling of cleaning activities to be complicated.

The global cleaning strategy combines an allocation problem, whereby heliostats are allocated to particular cleaning periods, with a routing problem for each period. These problems are not independent, as the route taken by a cleaning vehicle in a particular period will affect the heliostats allocated across the cleaning schedule.

The main innovative contribution of this work, summarised in the pseudocode in Figure 2.1, is precisely the way this complex scheduling-routing problem is addressed: we first perform a clustering analysis to divide the field into homogeneous groups, then we determine the optimal cleaning schedule, and finally a local search is performed to improve this sequential solution.

Algorithm 1 Cleaning Optimisation

```
procedure CLUSTERING
    P ← Number of Groups Int
    S ← Size of Groups Int
    nhel ← Number of Heliostats Int
    for i = 1 to nhel do
        for j = 1 to nhel do
            Distance(i,j) ← Euclidean Distance between (i,j) float
            Energy(i,j) ← Energy difference between (i,j) float
    Min αEnergy + βDistance;
    Groups ← Clustering Result
procedure OPTIMISE SCHEDULE
    Max Schedule Energy ;
    Schedule Init ← Initial cleaning schedule result
while EDiff > Sensitivity do
    procedure LOCAL SEARCH
        for d = 1 to Num Days - 1 do
            Min Routing problem(d,d+1)
            EDiff ← Energy Difference float
        Next;
end;
```

Figure 2.1: Clustering Pseudocode

The structure of this chapter is as follows. In Section 2.2, degradation in optical

efficiency due to soiling is investigated; a grouping optimisation problem is presented, followed by an optimisation procedure to find the cleaning schedule. A subsequent local search heuristic is then applied to improve the obtained solution. Section 2.3 illustrates the presented approach with real SPT data given in Section 1.6.6. Finally, conclusions are given in Section 2.4.

2.2 Modelling

In this section, the effect of heliostat soiling on efficiency of energy transfer is detailed and the optimisation problem described. The incident solar radiation reflected by each heliostat h at any given time instant t, labelled $f(h,t)$, is calculated and stored in a preprocessing step. The method used to model the movement of incident radiation within the system is detailed in Section 1.7.

2.2.1 Efficiency Degradation

If heliostat soiling is not considered, the energy reflected by heliostat h at time t is $f(h,t)$ and thus the energy generated in a period of length T, $[0,T]$ is $\int_0^T f(h,t)dt$. In order to consider heliostat soiling, a degradation function $\zeta_h(t)$ for heliostat h at time t must be defined, where the optical efficiency and therefore the energy generated by a heliostat will be reduced over time, unless cleaning operations are performed. The degradation function chosen directly models the effect of soiling on the optical efficiency of a given heliostat and is dependent on local weather conditions. In this study, the degradation function is assumed to be linear in time.

Due to both routing and environmental costs, not all heliostats should be cleaned every day. If the analysis is performed for a single heliostat within the field, which is to be cleaned r times during a cleaning schedule, one can determine the optimal periods to perform cleaning operations in order to maximise optical efficiency of the heliostat. Ignoring routing issues, the solution is simple: the cleaning operations should be done periodically. Indeed, if we denote the efficiency of a fixed heliostat by $\kappa\big(s\big)$, where s is the allocated cleaning period, we can define the total efficiency across time as:

$$K\big(s\big) := \int_0^s \kappa\big(t\big)dt, \tag{2.2.1}$$

where $K' \equiv \kappa\big(x\big)$ is decreasing and K is therefore a concave function.

We can find the total efficiency of a heliostat, across a cleaning schedule with multiple cleaning instants, by calculating:

$$\tilde{K}\big(s_1,...,s_r\big) = \int_0^{s_1} \kappa\big(t\big)dt + \int_0^{s_2} \kappa\big(t\big)dt + ... + \int_0^{s_r} \kappa\big(t\big)dt, \tag{2.2.2}$$

Our aim is to maximise the efficiency of the heliostats across the cleaning schedule:

$$\text{Maximise } \tilde{K}\big(s_1, ..., s_r\big), \tag{2.2.3}$$

subject to:

$$s_1, ..., s_r \geq 0, \tag{2.2.4}$$

$$\sum_{i=1}^{r} s_i = T. \tag{2.2.5}$$

Since E is a concave function $\frac{1}{r}\tilde{K}\big(s_1, ..., s_r\big) = \frac{1}{r}\sum_{i=1}^{r} K(s_i) \leq K(\frac{T}{r})$ which implies $\tilde{K}\big(s_1, ..., s_r\big) \leq rK(\frac{T}{r}) = \tilde{K}\big(\frac{T}{r}, \frac{T}{r}, ..., \frac{T}{r}\big)$. Therefore, the best strategy is to perform periodic cleaning operations.

While the previous analysis shows that the optimal cleaning strategy for one single heliostat is given by a periodic schedule, the problem to be addressed involves many heliostats.

In the next section, we formulate the clustering procedure as an optimisation problem for the allocation of heliostats to groups.

2.2.2 Clustering heliostats

Addressing the scheduling problem and subsequent routing problems may be unmanageable, since the considered heliostat field may contain thousands of units. For this reason it is worthwhile applying a clustering strategy [Grotschel and Wakabayashi, 1989; Hansen and Jaumard, 1997] before the optimisation of a cleaning schedule, reducing problem size and complexity.

We look to cluster the heliostats in the field into distinct groups. Groups should not be geographically disperse, since this would increase routing costs. Moreover, since the cleaning schedule will be identical for heliostats in the same group, such heliostats should generate a similar amount of energy. For this analysis, the energy $f(h,t)$ generated by a heliostat h is averaged along one day and labelled E_h, as shown in Figure 2.2 for the PS10 SPT plant in Sanlúcar la Mayor, Seville [Abengoa, 2019].

A dissimilarity function is then introduced: for any pair of heliostats, h, h', let $\lambda_{hh'}$ denote the dissimilarity between h and h', given by $\lambda_{hh'} = \alpha_{clu} Dist(h,h') + \beta_{clu}|E_h - E_{h'}|$, where $\alpha_{clu}, \beta_{clu} > 0$ are given constants and $Dist(h,h')$ is the physical distance between the heliostats h and h'.

The choice of constants α_{clu} and β_{clu} determines the importance of distance and energy in the clustering optimisation. These values are chosen according to the plant being modelled and the interest of the user in maximising energy or minimising distance.

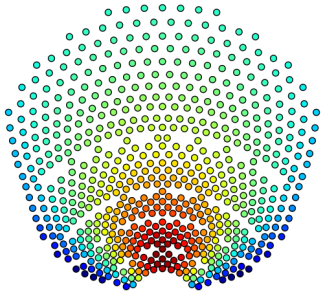

Figure 2.2: Average reflected radiation per heliostat

This clustering can be expressed as a p-median problem, as in Avella et al. [2007]; Daskin and Maass [2015]; Mladenović et al. [2007]. Heliostats can be viewed as clients and p potential plants have to be selected, the primary heliostats, which are the central heliostats of the groups. This is modelled as a binary linear problem in which the overall dissimilarity between each heliostat and its associated primary heliostat is to be minimised. More precisely, let us denote by H the set of heliostats in the SPT field. For any heliostat $h \in H$, let us set

$$y_h = \begin{cases} 1, & \text{if } h \text{ is a primary heliostat} \\ 0, & \text{otherwise.} \end{cases} \tag{2.2.6}$$

For heliostats h and $h' \in H$, let us set

$$a_{hh'} = \begin{cases} 1, & \text{if } h^{'} \text{ is allocated to group with primary heliostat } h \\ 0, & \text{otherwise.} \end{cases} \tag{2.2.7}$$

We then constrain the optimisation problem by requiring that each heliostat h may only be allocated to one group, with primary heliostat h:

$$\sum_{h \in H} a_{hh'} = 1 \quad \forall h^{'} \in H. \tag{2.2.8}$$

We also limit the number of clusters to a constant value P:

$$\sum_{h \in H} y_h = P. \tag{2.2.9}$$

Finally, we set a limit, S, on the number of heliostats allocated to each group.

$$\sum_{h' \in H} a_{hh'} \leq S y_h \quad \forall h \in H. \tag{2.2.10}$$

Finally, the objective function can be written in the form

$$\sum_{h' \in H} \sum_{h \in H} \lambda_{hh'} a_{hh'} \ , \tag{2.2.11}$$

which is to be minimised.

2.2.3 Schedule Optimisation

Once heliostats have been clustered into groups, as detailed in Section 2.2.2, we allocate those groups to cleaning periods in order to optimise the overall cleaning schedule. The objective of the optimisation procedure is to maximise the total energy generated over the schedule duration, whilst considering the allocation of heliostat groups to cleaning periods and the subsequent degradation of efficiency of each heliostat.

Using the reflected energy from each heliostat in the field (which is calculated in a preprocessing step) and the assumed degradation function, we maximise the total energy reflected by all heliostats across the cleaning period. In what follows we show how to address the scheduling problem by using Mathematical Optimisation.

We denote by C the set of periods and $\bar{H}$ the set of primary heliostats, obtained by solving the p-median problem described in Section 2.2.2. Moreover, we define the binary variable x_{hc}, where:

$$x_{hc} = \begin{cases} 1, & \text{if group with primary heliostat } h \text{ is cleaned in period } c \\ 0, & \text{otherwise.} \end{cases} \tag{2.2.12}$$

for any $h \in \bar{H}$ and $c = 1, ..., C$.

In order to determine the loss of efficiency for a specific period, it is necessary to also define the binary variable z_{hcr}, which accounts for whether a heliostat group has been cleaned in the previous periods with relation to the current period. Thus, for any $h \in \bar{H}$, $c \in C$ and $r = 0, ..., c$, we set:

$$z_{hcr} = \begin{cases} 1, & \text{if group with primary heliostat } h \text{ was cleaned } r \text{ periods before period } c \\ 0, & \text{otherwise.} \end{cases} \tag{2.2.13}$$

For instance, if we are considering whether or not to clean heliostat group 3 during a schedule of length 2, we would include the variables z_{310}, z_{311}, z_{320}, z_{321} and z_{322}.

By considering the energy generated by a heliostat with full optical efficiency, subtracting the amount of energy lost per period it is not cleaned, E_{hcr}, and summing for all heliostats over all periods, one can calculate the overall energy generated by the field. Using the binary variables z_{hcr}, our objective is then

$$\sum_{h\in\bar{H}}\sum_{c\in C}\sum_{r} E_{hcr} z_{hcr}, \tag{2.2.14}$$

to be maximised.

We constrain this objective function by requiring that each heliostat group must be cleaned at least once across all periods:

$$\sum_{c\in C} x_{hc} \geq 1 \quad \forall\ h \in \bar{H}. \tag{2.2.15}$$

This constraint is applied, as it is assumed that all groups of heliostats in the field provide significant energy to the system, and must all be maintained in the long term. In the case where a heliostat field has not been optimised, it may be of interest to not enforce this constraint, and investigate whether or not some heliostats are never cleaned and therefore may not be of significant value to the overall system.

We also assume that each cleaning route may clean at most τ heliostats:

$$\sum_{h\in\bar{H}} S_h \cdot x_{hc} \leq \tau \quad \forall\ c \in C, \tag{2.2.16}$$

where S_h denotes the cardinality of the group with primary heliostat h.

This constraint models the water carrying capacity of the cleaning vehicle, as well as the time taken to complete a cleaning period, and it may be changed according to each particular SPT plant specification.

We also introduce the following constraints:

$$z_{hcc} \leq 1 - x_{hi} \quad \forall i = 1, ..., c,\ \forall c = 1, ..., C,\ \forall h \in \bar{H}, \tag{2.2.17}$$

where z_{hcc} will be zero if heliostat group with primary heliostat h is cleaned in any period;

$$z_{hcr} \leq x_{h(c-r)} \quad \forall r = 0, ..., c-1,\ \ \forall c = 1, ..., C,\ \forall h \in \bar{H}, \tag{2.2.18}$$

where z_{hcr} will be zero if heliostat group with primary heliostat h is not cleaned r periods before period c;

$$z_{hcr} \leq 1 - x_{h(c-r+1)} \quad \forall r = 1, ..., c-1,\ \forall c = 1, ..., C,\ \forall h \in \bar{H}, \tag{2.2.19}$$

where z_{hcr} will be zero if heliostat group with primary heliostat h is cleaned in the

period r, before period c.

Finally, we include a constraint to remove the degradation penalty for a heliostat group cleaned in a particular period:

$$x_{hc} + \sum_{r=1}^{c} z_{hcr} = 1 \quad \forall c \in C,\ \forall h \in \bar{H}. \tag{2.2.20}$$

With the objective function (2.2.14) and the constraints (2.2.15) - (2.2.20), we now have a constrained binary integer linear program for the variables $x_{hc} \in \{0,1\}$, $z_{hcr} \in \{0,1\}$, with $h \in \bar{H}$, $c \in C$ and $r = 1, ..., c$.

2.2.4 Cluster Scheduling. Local Search

The cleaning schedule found using the method discussed in Section 2.2.3 produces a set of subsequent routing problems, where the groups assigned to each period form the clients within the local routing problem, as in Barreto et al. [2007]; Vidal et al. [2015]. When considering each routing problem, the objective is to minimise the route length whilst visiting all groups, however the operational ease of use for the cleaning vehicle should be seen as a factor of importance, as in Rossit et al. [2016]. In order to reduce operational costs, it may be of benefit to use heuristics to alter the cleaning schedule found, at a cost of total schedule energy.

We consider local search heuristics to produce routing refinement options, which may be used to improve the routes across the schedule, at a cost to the overall energy produced. The initial schedule designed in Section 2.2.3 can be refined by means of a 2-opt local search technique, by considering the optimisation of two routing problems at once, for two adjacent periods in the schedule, where groups can be swapped between the periods. This technique is then iterated across each pair of periods, and the sequence repeated until no further improvement to the solution is found. Observe that each iteration of the 2-opt local search amounts to solving an optimisation problem. Such an optimisation problem is much smaller in size than an overall optimisation procedure, since only the clusters in two consecutive periods are considered for reallocation. The formulation developed in this section is an adaptation of the Vehicle Routing Problem (VRP), see Hoogeboom et al. [2016]; Prodhon and Prins [2014], where we minimise the route of the cleaning vehicle for each period, whilst considering energy loss as a penalty factor.

Let us denote by P the number of groups and set

$$x_{ijp} = \begin{cases} 1, & \text{if group } i \text{ is allocated to period } j \text{ in route position } p \\ 0, & \text{otherwise,} \end{cases} \tag{2.2.21}$$

for any $i = 1, ..., P$, any $j = 1, 2$ and any $p = 1, ..., P-1$.

Let $l_{hh'}$ be the distance between primary heliostats h and $h^{'}$, and let D_i be the energy difference caused if group i swaps periods. Using the binary variables x_{ijp} and the distances between groups $l_{hh'}$, we minimise the overall route length for the two periods considered, whilst adding an energy based penalty D_i if a group has swapped period.

We therefore look to address the optimisation problem

$$\text{Minimise} \sum_{i \neq i'} \sum_{p=1}^{P-1} x_{i,j,p} x_{i',j,p+1} \cdot \alpha_{ls} l_{i,i'} + \beta_{ls} D_i \quad \forall j \tag{2.2.22}$$

We constrain this problem by permitting each group to be allocated to one day and in only one position:

$$\sum_{j=1}^{2} \sum_{p=1}^{P-1} x_{i,j,p} = 1 \quad \forall i = 1, ..., P. \tag{2.2.23}$$

We also ensure that each position in the route on each day may only have one group in total:

$$\sum_{i=1}^{P} x_{i,j,p} = 1 \quad \forall j = 1, 2, \ \forall p = 1, ..., P-1. \tag{2.2.24}$$

And, finally,

$$\sum_{i=1}^{P} x_{i,j,p} \in \{0, 1\} \quad \forall j = 1, 2, \ \forall p = 1, ..., P-1. \tag{2.2.25}$$

The objective function contains the product of two binary variables, and can be linearised using a Fortet scheme as follows.

Let us set

$$y^{j}_{ii'p} = x_{i,j,p} x_{i',j,p+1}. \tag{2.2.26}$$

The objective function then becomes:

$$\sum_{i \neq i'} \sum_{p=1}^{P-1} y^{j}_{ii'p} \cdot \alpha_{ls} l_{i,i'} + \beta_{ls} D_i \quad \forall j \tag{2.2.27}$$

to be minimised.

In the next section, we illustrate the developed optimisation procedure by producing a cleaning strategy for a sample SPT plant and solve the subsequent routing problems.

2.3 Results

2.3.1 Problem Description

The optimisation problem developed in this chapter is applied to the PS10 plant in Sanlúcar la Mayor, Seville [Abengoa, 2019], as described in Section 1.6.6. The parameters used are given in Table 2.1 and the heliostat field layout in Figure 2.3.

First, heliostats are clustered as described in Section 2.2.2, considering 52 groups of 12 heliostats ($P = 52, S = 12$) and the optimisation procedure developed in Section 2.2.3.

For the purposes of this study, where we are considering discrete time instants, we will assume a linear degradation function. This implies that, for each period that the heliostat is not cleaned, the efficiency decreases by a constant quantity ζ. This quantity will vary with the SPT plant location and heliostat construction, and will be assumed to be between 5% loss per period.

The initial cleanliness of the heliostat field is variable, and will have a distinct effect on the result of the optimisation procedure. For the purposes of this study, we will assume an initial random efficiency loss between 0 and 10% for each heliostat in the field.

The program was written using the Python programming language and utilised the Gurobi optimisation package [Gurobi Optimization Solver, 2019] on a computer with specifications: Intel®Core™ i7-7700HQ CPU @ 2.80 GHz. In the clustering analysis, as detailed in Section 2.2.2, the α_{clu} and β_{clu} weighting constants were chosen as 0.4 and 0.6 respectively, causing the difference in energy generation between heliostats to be slightly more important than the distance between them.

For simplicity, the incident radiation on the heliostat field is assumed to be identical for each period considered, and the maximum possible reflected radiation for each heliostat, shown in Figure 2.4, is averaged over one period. The data point chosen was midday with clear skies from the data point given in Section 1.6.6.

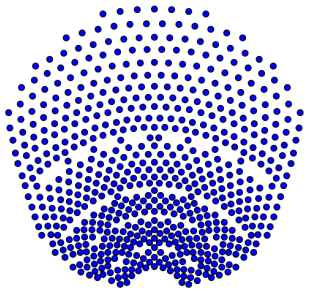

Figure 2.3: PS10 Heliostat field layout

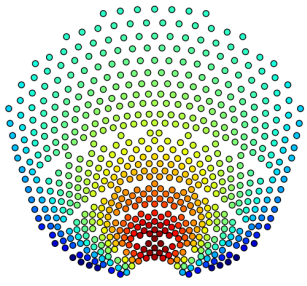

Figure 2.4: Average reflected radiation

Parameter	Value	Summary
P	52	Number of groups in clustering optimisation.
S	12	Number of heliostats in each group for clustering optimisation.
H	624	Number of heliostats in field.
α_{clu}	0.4	Importance of distance in clustering optimisation.
β_{clu}	0.6	Importance of energy in clustering optimisation.
α_{ls}	0.6	Importance of distance in local search heuristic.
β_{ls}	0.4	Importance of energy in local search heuristic.
τ	50	Maximum number of heliostats in a route.
ζ	5%	Efficiency degradation per period.
ζ_0	0-10%	Initial heliostat degradation.

Table 2.1: Cleaning optimisation parameter values

2.3.2 Schedule Optimisation

We first optimise the clustering of heliostats in the field, using the method described in Section 2.2.2. Figure 2.5 shows four of the optimised groups, which can be seen as black shaded heliostats. From this image, it can be seen that the groups are relatively compact, and there are few isolated heliostats in the same group. Considering the energy profile from Figure 2.4, it can be seen that the groups have also been clustered using similar energy profiles, which is an obvious consequence due to the choice of α_{clu} and β_{clu} in the objective function for the p-median problem used in building the clusters.

We then look to optimise the cleaning schedule problem, using the grouping already obtained, considering a schedule of 16 days. Figure 2.6 shows the computed cleaning schedule, where at each period, the cleaned heliostats are marked with white points. Figure 2.7 shows the resultant energy production of each heliostat in the field. From these figures, we can see the evolution of energy production over the schedule due to cluster allocation, and check that, as expected, the heliostats in the centre of the field are kept cleaner than the rest, due to their higher energy efficiency.

From these results, it can be seen that whilst a sub-optimal cleaning schedule with grouping has been found in terms of energy reflected onto the receiver, in certain periods disjoint subtours can be found (for example Period 4 in Figure 2.6), which are not desired by SPT plant operators and should therefore be removed in a local search phase.

2.3.3 Local Search Heuristic

The cleaning schedule shown in Figure 2.6 is taken as the initial solution in the swapping algorithm described in Section 2.2.4. We then obtain the results depicted in Figure 2.8. This solution was obtained within two iterations through the pairwise rolling optimisa-

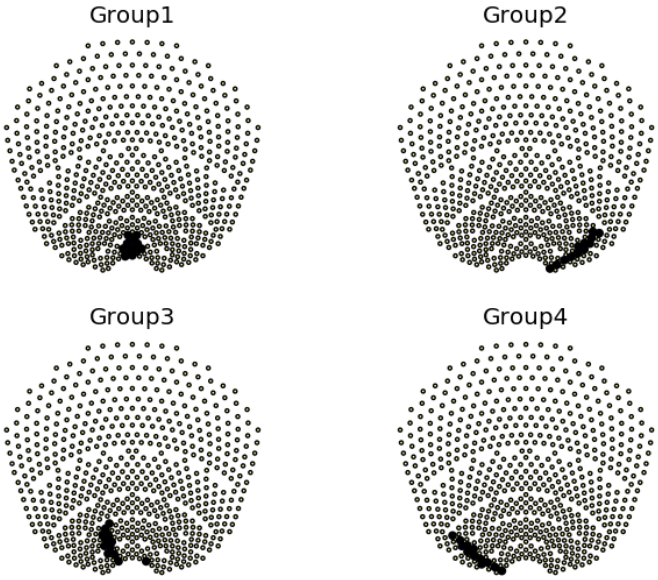

Figure 2.5: Optimised Heliostat Grouping (groups 1-4)

Figure 2.6: Optimal Cleaning Schedule Allocation

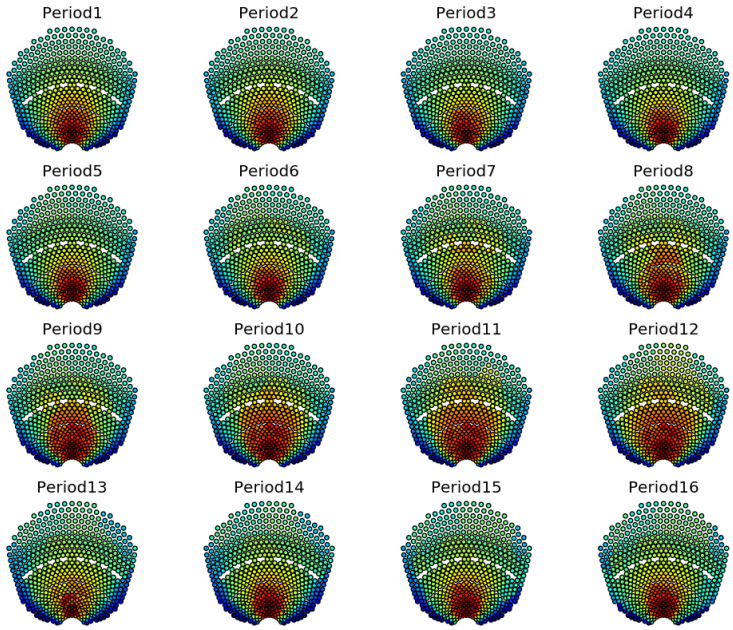

Figure 2.7: Optimal Cleaning Schedule Energy Profile

tion procedure, where an iteration is comprised of $N-1$ pairwise swaps. Comparing Figures 2.6 and 2.8, it can be seen that groups have swapped between periods where the loss in energy was outweighed by the benefit in having less disperse heliostat clusters in the same time periods.

With the cleaning schedule obtained in Figure 2.8, a standard Travelling Salesman Problem (TSP) is then solved for each period in the schedule. For example, Figure 2.9 shows the optimal route for the allocation of period 2 that can be seen in Figure 2.8. This route has been found using a Greedy Algorithm implemented in Python.

The local search heuristic alters the initial solution, yielding better routes for the final solution at the cost of overall collected energy. In this example, the value of total energy collected over the schedule reduces by 2.7% due to the application of the local search heuristic.

2.4 Conclusions

In this chapter a procedure has been developed to optimise the cleaning schedule for a SPT plant. This includes a novel heuristic approach to refine the solution, to account for route attractiveness. The procedure has been illustrated in a real SPT plant using

Figure 2.8: Optimised Cleaning Schedule

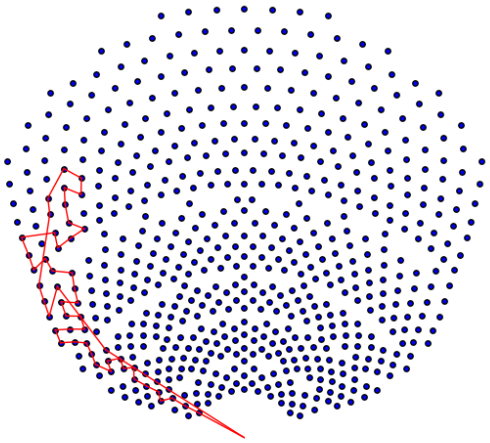

Figure 2.9: Calculated Route Period 2

typical cleaning technology and assumptions on the efficiency degradation of heliostats due to soiling mechanisms. The presented method provides an increase of nearly 5% in total energy of the schedule, when compared to an assumed cleaning schedule which followed the rows of the heliostats in the plant. Whilst an increase in total energy was found, the real benefit for the method would be found in the design phase of an SPT plant, where the location of heliostats and their access roads could take into account the optimal cleaning schedule.

A p-median type linear integer program was developed to perform a clustering analysis, reducing large problem spaces by finding the optimal grouping strategy of the heliostats, considering a weighted objective function of physical distance and energy profile between heliostats in the field. The heliostat grouping is then used to obtain an initial cleaning schedule of the heliostat groups over a period of time, in order to maximise the energy reaching the receiver. In our numerical illustration, this program was presented for a schedule of 16 periods, with a route limit of 52 heliostats per period, where the results show an optimal energy profile, but a sub-optimal routing solution for each period.

The initial solution is then refined with a local search heuristic, which pairwise swaps groups of heliostats between consecutive days in the schedule. Each move amounts to solving a linear integer problem, where operational costs are reduced in the routing problems, at a cost of total energy gained during the schedule.

The optimisation procedure developed in this work can be utilised by current SPT plant operators in order to optimise their cleaning routes. It can also be utilised in the planning phase of a new SPT plant, where pattern-free heliostat fields will require more complex cleaning routes, which need to be optimised to ensure maximum energy generation.

The application of Operations Research techniques to SPT plant design and operation has many possibilities, where this work could be extended to include; time dependency if cleaning operations are conducted during the day, routing problems with depots due to water carrying capacity of cleaning vehicles, stochastic processes for weather events which have varying effects on the soiling of heliostats, and large scale problems with multiple towers and vehicles.

The length of the schedule optimised in Section 2.3 was 16 periods, which was chosen in order to present a study of an interesting length. This choice will affect the result of the optimisation procedure, due to variable local weather conditions, and further research of interest is to optimise the schedule length chosen, as well as the schedule itself.

The example route shown in Figure 2.9 does not follow the rows formed during the construction of the SPT plant, and assumes that the cleaning vehicle can navigate between heliostats. In the case of the PS10 SPT plant, the application of this route

is possible due to spacing between heliostats and the ground topology. However, some SPT plants have obstructions, both natural and man-made, within their fields. These obstructions will limit the paths that the cleaning vehicle can take, and must be taken into account when optimising the cleaning schedule. This can be implemented in the method developed in this study with additional constraints on the feasible region.

This investigation could be used to influence future design of SPT plants, in order to maximise their energy generation and reduce overall costs, by aiding in the design of cleaning schedules whilst adapting the layout of the heliostat field using techniques as in Carrizosa et al. [2015a]. The results presented use a novel swapping approach for pairs of periods in the schedule. However this is directly extendible for any number of periods at a time.

Another extension to this work could be the investigation into the effects of optimal cleaning schedules, where we look to maximise optical efficiency of the heliostats, against optimal aiming strategies as developed in Ashley et al. [2017].

In the presented work, the resulting cleaning schedule consists of a set of heliostats to be cleaned during each period. The routing problem for each period has been solved utilising a greedy algorithm, however an improvement to this study could consider a different approach.

The degradation of heliostat efficiency over time with respect to soiling can have large impacts on overall SPT plant performance [Sarver et al., 2013]. Many factors influence the exact degradation curve, including geographical location of the SPT plant and proximity of heliostats to one another. The effect of realistic degradation information on heliostat efficiency when combined with an optimisation procedure would allow plant operators to make the best decisions when approaching cleaning operations. For the purposes of this study, a linear degradation curve has been assumed, although a stochastic case with weather events was also investigated and should be implemented in future work.

Finally, as technology advances, more potential cleaning techniques become available, such as robots. Autonomous robots are being developed to clean heliostat fields, and the optimisation of their operations could further extend the model considered in this work.

Chapter 3

A first approach to the optimisation of aiming strategies

A first approach to the optimisation of aiming strategies

3.1 Introduction

The aiming strategy commonly used in research into the optimisation of SPTs assumes that all heliostats in the field aim at the centre of the receiver, see for example Carrizosa et al. [2015a], and a summary of various recent SPT optimisation techniques by Barberena et al. [2016]. This assumption allows for easier computation of the flux distribution across the receiver surface and reduces complexity of the adjustment of the heliostats.

Using a central aim point for all heliostats leads to a large heat flux at the centre of the receiver and large flux gradients towards the edge of the receiver, which can cause strong heat loads and potentially lead to damage over time and costly repairs [Lopez-Martinez and Rubio, 2002; Relloso and García, 2015; Salomé et al., 2013; Sánchez-González et al., 2015; Yu et al., 2014].

An uneven flux distribution across the receiver surface also lowers the efficiency of the energy transfer to the thermal fluid within the receiver [Fend et al., 2004; Yu et al., 2014]. Therefore, maintaining an even distribution will increase the efficiency and allow for greater energy production.

Some research has been conducted where more complex aiming strategies are considered for different receiver types [Astolfi et al., 2016; Belhomme et al., 2013], as well as closed-loop feedback mechanisms to provoke changes in aiming strategy [Berenguel et al., 2004; Kribus et al., 2004]. Applications of alternate optimisation algorithms for the aiming strategy have also been exhibited [Salomé et al., 2013; Sánchez-González et al., 2015; Yu et al., 2014; Cruz et al., 2016] and a summary of optimisation techniques collected [Baños et al., 2011].

The distribution of reflected energy from the heliostats onto the receiver is assumed to be a Gaussian, as detailed in Section 1.7. The distribution can be written in the form:

$$f_1(x,y)exp\Big(\frac{-f_2(u,v,x,y)}{2f_3^2(x,y)}\Big), \tag{3.1.1}$$

In order to reduce damage to receiver components and to optimise the energy reaching the receiver, multiple aim points across the receiver surface in a grid can be considered, as depicted in Figure 3.1: a set of possible points within the receiver is given, and the solver must choose, for each heliostat and time instant, the most appropriate aiming point.

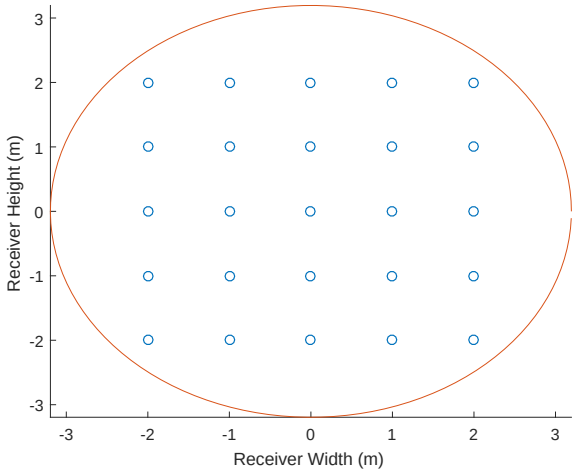

Figure 3.1: Aim Point Grid

The field of heliostats would then be split, so that a proportion of them aim at each point. The result of this would be to smooth the flux gradient across the receiver surface and to reduce the peak heat flux at the centre.

Another effect of this strategy would be to increase the amount of energy that is being lost due to spillage, where aiming towards the edge of the receiver causes some of the energy to miss completely.

The goal of the study in this chapter is to design an aiming strategy that minimises the flux gradient across the surface of the receiver, whilst minimising the spillage and maintaining a minimum amount of energy.

3.2 Changing Aim Point

The spillage efficiency f_{sp} for a particular heliostat is calculated as the integral of the distribution given in (3.2.1) across the receiver surface, as detailed in Section 1.7.4.

$$f_{sp}(x,y) = f_1(x,y) \int_0^{2\pi} \int_0^r exp\Big(\frac{-\tilde{f}_2(\rho,\phi,x,y)}{2f_3^2(x,y)}\Big)\rho\, d\rho\, d\phi\ , \tag{3.2.1}$$

where r is the radius of the circular receiver and $\tilde{f}_2(\rho,\phi,x,y) \equiv f_2(\rho\cos\phi, \rho\sin\phi, x, y)$.

In order to model the distribution of energy across the receiver surface when we consider an aiming point offset from the centre, the bounds of integration in (3.1.1)

need to be altered, as shown below.

Consider the Gaussian distribution of the reflected energy as centered at the origin, and that the receiver is offset by the aim point offset.

$$f_{sp}(t,x,y) = f_1(t,x,y)\int_0^{2\pi}\int_0^{\hat{r}(\phi)} \exp\Big(\frac{-\tilde{f}_2(\rho,\phi,x,y)}{2f_3^2(t,x,y)}\Big)\rho\, d\rho\, d\phi \ , \tag{3.2.2}$$

where $\hat{r}(\phi)$ is given by the solution of the equation $R^2 = \hat{r}^2 + r_0^2 - 2\hat{r}r_0 cos(\theta - \phi)$

We shall assume that the heliostat is always pointing within the receiver boundaries, if it is to be included in calculations (i.e. unless it is turned away for safety or other reasons and is then not producing output).

The spillage efficiency in (3.2.2) then becomes:

$$f_{sp}(t,x,y) \approx \frac{2\pi}{10} f_1(t,x,y) f_3^2(t,x,y) \sum_{i=1}^{10} \frac{1}{f_5(\phi_i,x,y)}\Big(1 - exp\Big(-\frac{\hat{r}(\phi_i)^2 f_5(\phi_i,x,y)}{2f_3^2(t,x,y)}\Big)\Big) \ , \tag{3.2.3}$$

where,

$$f_5(\phi_i,x,y) = \frac{(1+f_4^2(x,y)) + \cos\phi(1-f_4^2(x,y))}{2\,||\vec{w}||^2}. \tag{3.2.4}$$

Multiplying the spillage efficiency, $f_{sp}(t,x,y)$, by the solar radiation at a specific time point and by other losses inherent in the system (as detailed in Section 1.7) gives us the total energy that reaches the receiver at time t. This value is for one heliostat, aiming at a specific aimpoint.

3.3 Optimisation

In this section our goal is to develop an optimisation model for the selection of aiming points for the heliostats in a fixed field, in order to maximise the energy produced under some homogeneity constraints on radiation.

There are various optimisation techniques that could be applied to solve this problem, including heuristic methods such as *Ant Colony* or *Genetic Algorithm* techniques, however the BILP technique was implemented in this case. BILP techniques lead to the optimal solution within a finite time period, whereas this is not guaranteed with purely heuristic methods and is therefore not the best choice for this problem. Applying the BILP technique with a heuristic time limit allows a solution to be obtained quickly, whilst the gap between the obtained solution and the optimal solution will be between a defined upper bound.

Changing the aim point of a heliostat from the centre of the receiver to another point affects the amount of energy reaching the receiver by changing the slant range

(that is, the modulus of $\vec{w}$), the spillage efficiency, the cosine efficiency and the light distribution across the surface.

Let A_p be the set of aiming points on the receiver surface, where $A_p \in \mathbb{R}^2$ and let H be the set of heliostats aiming at the points in A_p. Let us define an optimisation procedure for any fixed time instant, t.

For $h \in H$, $a \in A_p$, set z_{ha} to the boolean variable defined as:

$$z_{ha} = \begin{cases} 1, & \text{if heliostat } h \text{ is allocated to aiming point } a \\ 0, & \text{otherwise.} \end{cases} \tag{3.3.1}$$

The reflected radiation pattern $F_b(h, a)$ is the radiation point value at aiming point b received from heliostat h aiming at aiming point a. The total integrated radiation, $f(h, a)$, is the total radiation received across the receiver from heliostat h aiming at aiming point a.

We therefore look to maximise the total incident energy on the receiver:

$$\text{Maximise} \sum_{a,h} f(h, a) z_{ha}. \tag{3.3.2}$$

We constrain this objective function by requiring that no heliostat may be looking at more than one aiming point on the receiver, but may be stowed in case of high winds or potential damage to the receiver or mirror.

This gives the constraint:

$$\sum_{h \in H} z_{ha} \leq 1 \quad \forall a \in A_p. \tag{3.3.3}$$

We also constrain the received energy at the aiming points:

$$C_* \leq \sum_{\substack{h \in H \\ a \in A_p}} F_b(h, a) z_{ha} \leq C^* \quad \forall b \in A_p, \tag{3.3.4}$$

where C^* is a fixed maximum energy and C_* is a fixed minimum energy. These constraints prevent the receiver being subject to excessive temperatures (which could cause permanent damage) and also ensure that a minimum amount of energy is being collected at each aiming point.

In order to approximate a uniform distribution of energy across the receiver, we will look to also constrain the range of energy received between any two aiming points by imposing

$$\max_a (\sum_{h,a} F_i(h, a) z_{ha}) - \min_a (\sum_{h,a} F_j(h, a) z_{ha}) \leq \tau \ , \tag{3.3.5}$$

where τ is a given constant.

This can also be written in the form

$$\max_a(\sum_{\substack{h\in H\\ a\in A_p}} F_i(h,a)z_{ha}) \leq \tau + \min_a(\sum_{\substack{h\in H\\ a\in A_p}} F_j(h,a)z_{ha}) \ , \tag{3.3.6}$$

which is equivalent to the following set of linear constraints:

$$\sum_{\substack{h\in H\\ a\in A_p}} F_i(h,a)z_{ha} \leq \tau + \sum_{\substack{h\in H\\ a\in A_p}} F_j(h,a)z_{ha} \qquad \forall i,j \in A_p, \ with \ i \neq j \tag{3.3.7}$$

The optimisation problem to be solved at each time instant t can then be summarised as follows:

$$\text{Maximise} \sum_{\substack{h\in H\\ a\in A_p}} f(h,a)z_{ha}$$

Subject to:

$$\sum_h z_{ha} \leq 1 \ \ \forall a \in A_p,$$

$$C_* \leq \sum_{\substack{h\in H\\ a\in A_p}} F_i(h,a)z_{ha} \leq C^* \qquad \forall i \in A_p,$$

$$\sum_{\substack{h\in H\\ a\in A_p}} F_i(h,a)z_{ha} \leq \tau + \sum_{\substack{h\in H\\ a\in A_p}} F_j(h,a)z_{ha} \qquad \forall i,j \in A_p \ with \ i \neq j$$

$$z_{ha} \in \{0,1\} \ \ \forall h \in H, \ \forall a \in A_p$$

The optimal aiming strategy for an SPT plant is dependent on the time of day, as well as the day of the year. For an optimal aiming strategy to be achieved, it must be optimised at a rate that will capture the changing radiation pattern over time.

In terms of the optimisation problem, both the objective function and the constraints will change as functions of time, caused by the variable incident radiation and physical constraints on the SPT plant. A rapid change in incident radiation at one point on the receiver surface, for instance caused by passing clouds, could potentially cause damage, indicating that frequent updates to the aiming strategy are needed.

As there is no guarantee that the optimal aiming pattern will remain optimal, or even feasible, over time, the optimisation procedure must be repeated frequently, using knowledge of local weather to constrain the problem in real-time.

The next part of this chapter applies this optimisation method to an SPT plant and demonstrates its efficiency with near real-time updates to the optimal aiming strategy during operation of the plant.

3.4 Results

For comparison against other research, we apply the aforementioned optimisation procedure with a grid of 25 aiming points to the PS10 plant in Sanlúcar la Mayor, Seville [Abengoa, 2019], as described in Section 1.6.6. Observe that in this field all heliostats are identical and arranged in a pattern, but the presented approach works for pattern-free fields and with heliostats of different sizes, such as the pattern-free fields considered in Carrizosa et al. [2017].

The aiming points allocated to the heliostats are colour coded according to the colours shown in Figure 3.3 and the location of the heliostats within the SPT field are shown in Figure 3.2, where the x-axis goes from East to West.

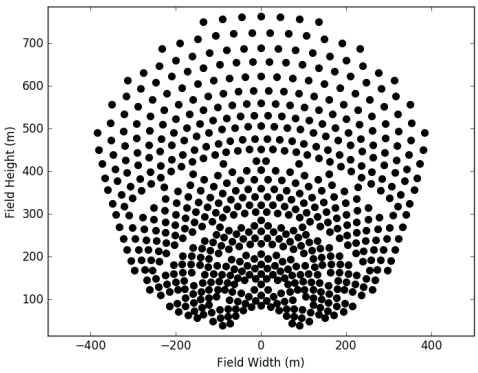

Figure 3.2: PS10 Layout

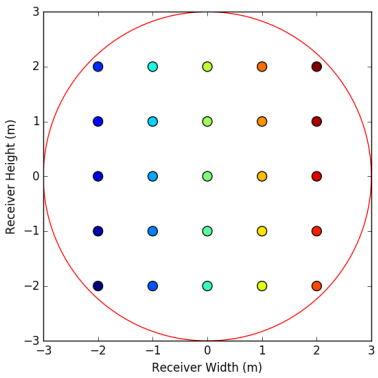

Figure 3.3: Aiming Points

The optimisation procedure is coded in Python, using the Gurobi optimisation package [Gurobi Optimization Solver, 2019]. The optimisation problems to be solved are difficult in short time scales, due to the large number of boolean variables. However, running an integer programming solver with a short time limit of 30 seconds was found to approximate the optimal solution closely and leads to near real-time satisfactory updates to the aiming strategy.

The values for the maximum, minimum and range constraints used in the analysis for this model were calculated in order to reflect working values that an SPT plant would define, based upon physical limits of the components. For this purpose, the problem is solved to optimality, without considering any constraints, to find the maximum energy across all aiming points. The problem is then constrained to 25% of this maximum and optimised in 30s, with the resulting range then constrained to 15% of its value and used

to find the constrained result.

The results in Figures 3.4 to 3.9 show the computed optimal aiming strategy and energy distribution, for three different times across a day. During the first solar hour of the day, shown in Figure 3.4, the heliostats located on the West side of the field have the smallest cosine angle, and are therefore aiming at the receiver edges. The heliostats on the East side have a larger cosine angle, and are therefore aimed at the centre of the receiver.

This result concurs with the distribution detailed in Section 1.7, where having a smaller cosine efficiency causes the distribution of energy on the receiver surface to be larger. The heliostats aiming at the center have the worst efficiency, and are aiming there to not lose as much energy to spillage. The heliostats with better efficiencies are therefore aiming elsewhere, as they dont lose as much energy by looking towards the edges.

To demonstrate the use of near real-time updates, we can look at the evolution of the aiming strategy over smaller timesteps. This will utilise SPT plant operators knowledge of local weather conditions and predictive technology to recalculate the optimal solution and react to changing weather conditions.

Passing clouds over a large heliostat field cause groups of heliostats to become less efficient, which will therefore change the optimal aiming strategy. The effect of clouds on CSP technology is of importance in the efficiency of an SPT plant, and has prompted the development of technology to predict the quantity and location of clouds, see Alonso et al. [2014]; Lopez-Martinez and Rubio [2002]; Alonso-Montesinos and Batlles [2015]. Standard procedure in order to prevent thermal shock to the receiver when a cloud passes by, is to aim heliostats away [Lopez-Martinez and Rubio, 2002], which will reduce overall energy collected.

Using the location and size of a cloud in the optimisation procedure outlined in this chapter allows an SPT plant to further optimise aiming strategies in near real-time, by re-optimising the strategy whilst taking into account constraints such as cloud passage. The size, shape, and location of a cloud may be changed within the code, where the heliostats that are covered are assumed to suffer a 70% drop in efficiency. An example of cloud implementation is furnished in Figure 3.10. Figures 3.11 and 3.12 show a comparison of the optimal results for 12pm, with and without a cloud, where it can be seen that the presence of a cloud alters the optimal aiming strategy.

The presented approach consists of solving an Integer Linear Programming problem, which makes no assumption on the heliostat field layout. Therefore, it is also applicable to irregularly distributed heliostats, such as those generated with the Greedy Algorithm developed in Carrizosa et al. [2015a]. This is demonstrated in Figures 3.13 and 3.14 for the irregular field presented in Carrizosa et al. [2015a].

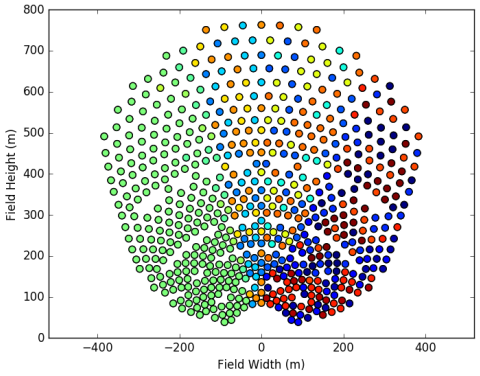

Figure 3.4: 6am Allocation

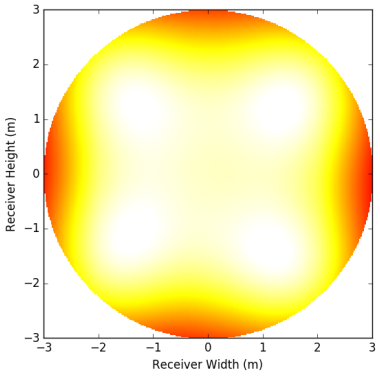

Figure 3.5: 6am Distribution

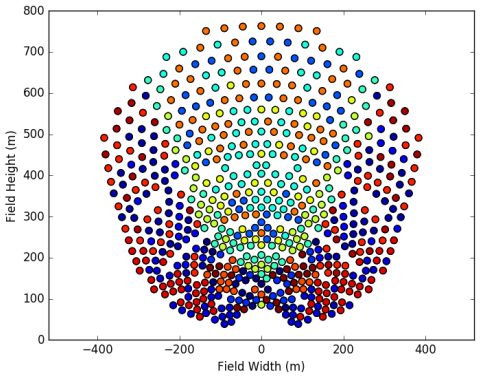

Figure 3.6: 12pm Allocation

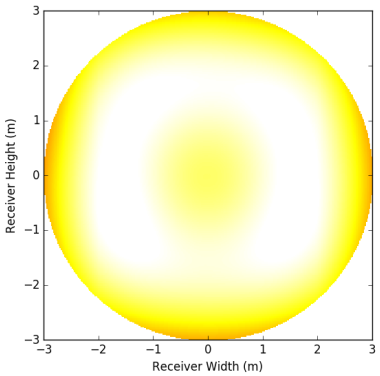

Figure 3.7: 12pm Distribution

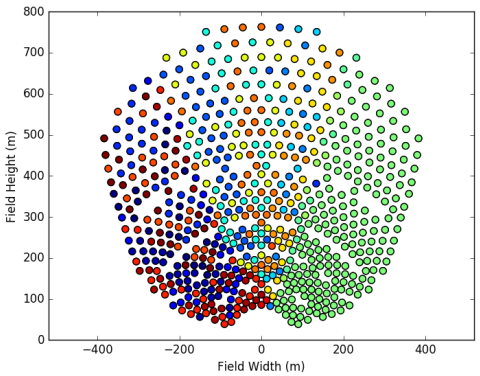

Figure 3.8: 6pm Allocation

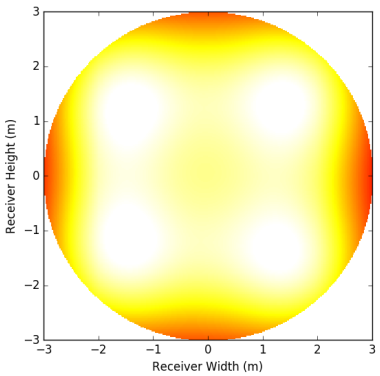

Figure 3.9: 6pm Distribution

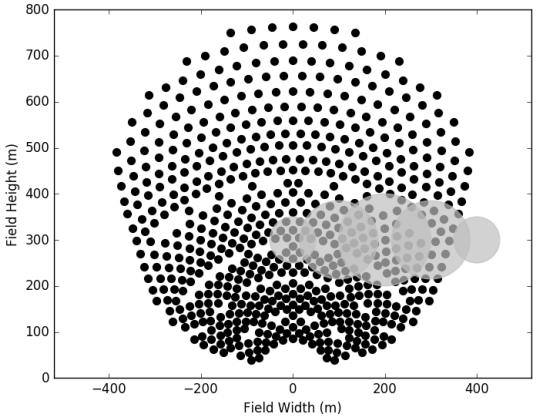

Figure 3.10: Cloud example

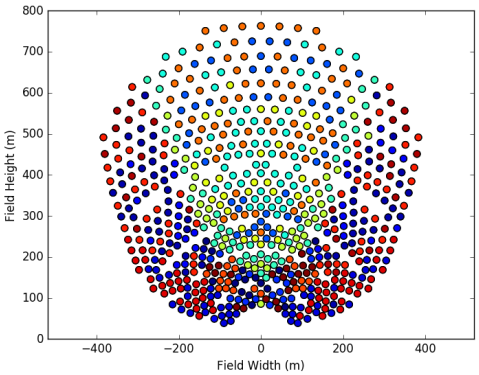

Figure 3.11: 12pm Allocation

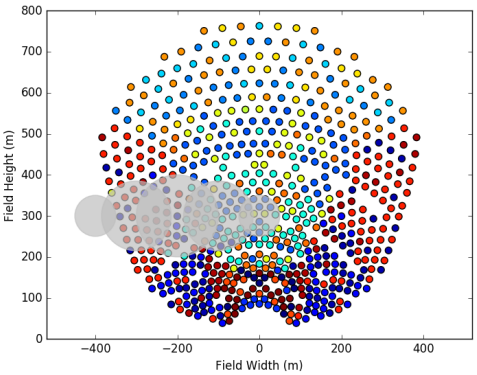

Figure 3.12: 12pm Allocation with cloud

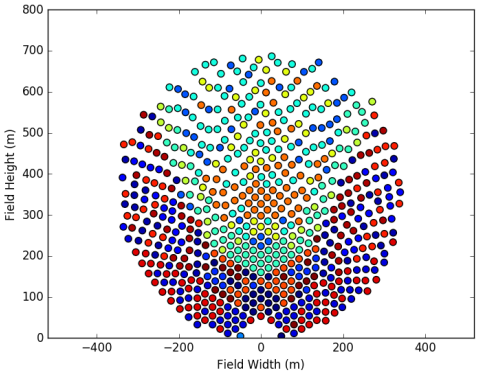

Figure 3.13: 12pm Allocation (Greedy field)

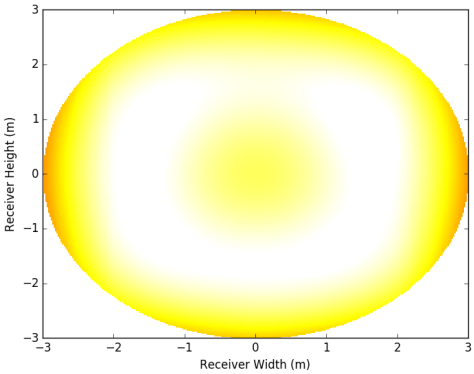

Figure 3.14: 12pm Distribution (Greedy field)

3.5 Conclusions

An aiming strategy has been developed to optimise the energy collected by an SPT plant at a near real-time scale, considering multiple constraints based upon physical requirements. This procedure has been demonstrated at multiple time points across a day and considered cloud effects and changing the shape of the heliostat field, showing that the procedure may be applied to any plant design and can be used to react to inclement weather whilst maintaining optimal energy production.

A linear integer problem with a short time limit was solved using an integer programming solver, without the use of additional preprocessing. It is expected that better results may be obtained if the solver is given a reasonably good starting solution, obtained by an *ad hoc* procedure which exploits the problem structure.

The energy distribution and aiming strategies presented are a theoretical representation of SPT performance, and should be validated against practical results from experiments with an SPT plant. This validation should be completed with the cooperation of an SPT plant operator and investigate the effects of implementing different aiming strategies and compare them with theoretical results.

The effect of inclement weather on the optimal aiming strategy employed has been demonstrated here to show capability of the model developed, and further research is given in Chapter 6.

Changing the location and quantity of aiming points on the receiver surface will affect the optimal solution. Increasing the number of aiming points may lead to a solution which provides a smoother distribution and higher energy generation, but it will increase the computational time considerably. Further research into the optimisation of aiming strategy and fixed aiming point locations at the same time should be considered, where a variety of optimisation techniques could be compared.

An interesting extension of the present work is the case in which there are multiple receivers [Carrizosa et al., 2015b; Schmitz et al., 2006], where the aiming strategy must be optimised using aiming points distributed across multiple locations. If the plant design is already given, the model considered in this chapter extends in a straightforward manner to this problem. If, on the contrary, the plant is to be designed, an alternating approach can be considered to optimise both the aiming strategy and the heliostat locations within the field.

Chapter 4

Continuous aiming strategies (I): the stationary case

Continuous aiming strategies (I): the stationary case

4.1 Introduction

In this chapter, as in Chapter 3, we develop an optimisation model for the aiming strategy of an SPT plant. In Chapter 3, a discrete approximation of the receiver surface Ω into a set of potential aiming points is used, thereby reducing problem dimensionality and allowing a BILP technique to be applied.

A more accurate approach is to allow the aiming point variables to take any value and be continuously differentiable across the receiver surface. This is equivalent to defining a separate aiming point for each heliostat in the field, within the set created by the boundaries of the receiver dimensions. This allows the simulation of SPT plant operations to better reflect real-life conditions, where aiming points for heliostats will not be limited to pre-set locations. This will be the viewpoint (and the main contribution) in this chapter.

Whilst the first objective is the maximisation of total radiation reaching the receiver surface, operational limitations of the SPT plant must be taken into consideration. As previously noted, these include inhomogeneous heating of the receiver surface, where large thermal fluxes can cause non-optimal energy generation, or even permanent damage to the receiver components. Hence, the objective in this chapter is to maximise the radiation captured by the SPT plant receiver, whilst taking into account the deviance from a desired radiation distribution across the receiver using continuous optimisation models. The two objectives will be combined into one single non-convex, non-linear criterion via additive weighting. By varying the weights, an approximation to the corresponding Pareto Front will be obtained. Some related heuristic methods can be found in Wagner and Wendelin [2018].

The structure of this chapter is as follows: Section 4.2 details the problem formulation; Section 4.3 describes how to numerically formulate the problem; Section 4.4 provides an illustrative example of the construction of the Pareto frontier of the bi-objective problem, and Section 4.5 presents concluding remarks.

4.2 Model

The first component of the criterion in our aiming strategy optimisation model is the radiation generated by the heliostats on the receiver surface.

As in Ashley et al. [2017], the radiation passing through the system is modelled using a Gaussian distribution on the receiver, a non-empty bounded open convex set $\Omega \subset \mathbb{R}^2$. We will denote by $|\Omega|$ (resp. $\bar{\Omega}$) the measure (resp. the closure) of Ω. In this work, any heliostat $h \in H$ will be required to aim at point $p_h \in \bar{\Omega}$. The value of this distribution evaluated at a cartesian point $(u, v) \in \Omega$ is denoted by $F_{u,v}(h, p)$, where the total radiation at any point (u, v) is the sum of contributions from all heliostats.

The total radiation captured over the whole receiver surface associated to heliostat h aiming at point $p_h \in \bar{\Omega}$ can be written as $f(h, p_h) = \int F_{u,v}(h, p_h) d\Omega$. Therefore the total radiation corresponding to all heliostats in H can be expressed in the form:

$$\sum_{h \in H} f(h, p_h). \tag{4.2.1}$$

The second criterion in this problem considers the difference between the radiation reaching the receiver and a desired target distribution $E^{tar}_{u,v}$. This distribution will in practise be decided by the SPT plant operators, depending on weather conditions and the thermal status of the receiver. This second objective can be expressed as the integral of the square of the calculated radiation $F_{u,v}(h, p_h)$ minus the target distribution $E^{tar}_{u,v}$:

$$\int \left[\sum_{h \in H} F_{u,v}(h, p_h) - E^{tar}_{u,v} \right]^2 d\Omega. \tag{4.2.2}$$

Other criteria, such as the overall radiation excess with respect to a target distribution, may be considered instead. The reason to choose (4.2.2) in this formulation is that, as seen below, it leads to a continuously differentiable objective function, which allows us to consider gradient based algorithms for the problem resolution.

Combining (4.2.1) and (4.2.2), we arrive at a suitable objective function, where we consider a parameter $A \in (0, 1)$ that controls the relative importance between maximising energy and minimising deviation from the target distribution:

$$A \sum_{h \in H} f(h, p_h) - (1 - A) \int \left[\sum_{h \in H} F_{u,v}(h, p_h) - E^{tar}_{u,v} \right]^2 d\Omega. \tag{4.2.3}$$

which is to be maximised.

Optimising the objective function in (4.2.3) over a range of values of A produces an approximation to the Pareto frontier of the bi-objective problem of simultaneous optimisation of energy generated and deviation with respect to the target distribution.

The following section devises a numerical method for the solution of the continuous

optimisation model proposed.

4.3 Numerical Methods

The continuous optimisation model proposed in Section 4.2 involves calculating integrals over the receiver surface Ω. For numerical purposes, these integrals must be replaced by summations over a finite set of equally spaced test points $(u_i, v_i) \in \Omega$ with $i = 1, ..., I$. The size of I directly affects the precision to which the problem in Equation (4.2.3) is approximated and, also, affects the numerical complexity of the problem solution. The deviation from the desired flux distribution $E^{tar}_{u,v}$ is then calculated and furnished only for the test points (u_i, v_i). It is important to note that we 'discretise' the receiver Ω only at the numerical integration level (remember that p_h can take any value in Ω).

The resulting objective function is the following:

$$g(\mathbf{P}) \coloneqq A \sum_{h \in H} f_{sp}(h, p_h) - (1 - A)\frac{|\Omega|}{I} \sum_{i=1}^{I} \left[\sum_{h \in H} F_{u_i,v_i}(h, p_h) - E^{tar}_{u_i,v_i} \right]^2, \qquad (4.3.1)$$

where $\mathbf{P} = (p_h) \quad h \in H$, $|\Omega|$ denotes the measure of Ω and $|I|$ is the cardinality of I.

The coefficient $\frac{|\Omega|}{I}$ stems from the numerical approximation of the integral in (4.2.3).

Thus, we want to solve a non-linear non-convex optimisation problem with continuous variables of large dimension (twice the number of heliostats in the field), subject to the convex constraints $p_h \in \bar{\Omega}$.

Function g in Equation (4.3.1) can then be maximised using a gradient ascent algorithm with projection, see Le Floch et al. [2015]; Ranganathan et al. [2011]. We start with an initial solution $\mathbf{P}_0$ and then, at each iteration of the algorithm, update the components of $\mathbf{P}$ in the direction of steepest ascent of the objective function g by step size γ. The final step in each iteration of the algorithm utilises a projection method to correct any values of $\mathbf{P}$ to ensure heliostats aim at Ω.

The selection of the stepsize γ taken at each update to the gradient ascent algorithm is an important factor in the convergence and much research has focused on this choice, for example Liu and Liu [2018]. If the stepsize is too large, the algorithm may diverge, and if it is too small, it will take too long to converge. A method to find the optimal stepsize at each iteration can be found using *Armijo's Rule* [McCormick, 1977], where a constant value $\epsilon \in (0, 1)$ is used to iteratively reduce the stepsize until an improvement on the objective function is no longer given.

This is tested at the k-th iteration of the algorithm against the $(k-1)$-th iteration as follows:

$$g(\mathbf{P}_k) > g(\mathbf{P}_{k-1}) \qquad (4.3.2)$$

Traditionally, the value of γ is fixed for all elements of the system. However, in this work the algorithm is adapted to allow different γ for each heliostat h:

$$\gamma_{k,h} = \gamma_{k-1,h} \cdot \epsilon. \tag{4.3.3}$$

This permits heliostats to take the greatest stepsize independently of each other, thereby potentially increasing the speed of the algorithm. However, it is also important to note that this procedure may in fact increase running times, so careful selection of ϵ is required.

Therefore, the gradient ascent algorithm reads:

$$\tilde{\mathbf{P}}_{k+1} = \mathbf{P}_k + \gamma_{k,h} \nabla g(\mathbf{P}_k), \quad \mathbf{P}_{k+1} = \mathcal{P}(\tilde{\mathbf{P}}_{k+1}), \tag{4.3.4}$$

where, for each $\mathbf{P}$, $\mathcal{P}(\mathbf{P})$ denotes the component-wise projection of $\mathbf{P}$ onto Ω.

The considered objective function and its gradient are complex. It is therefore important to customise related effective numerical techniques leading to reasonable computational effort.

The function being modelled in this chapter is highly multi-modal and, consequently, convergence to the global optimum is significantly dependent on the starting $\mathbf{P}_0$ given to the algorithm. We therefore apply a multistart procedure where the algorithm is run multiple times, utilising a different random allocation of starting heliostat aiming points. Applying this method for each value of A, it is possible to approximate the Pareto Front of the model.

It will be accepted that the aforementioned algorithm converges to a local optimum when the Euclidean norm of the gradient of the energy function is below a selected precision value c. The selection of this value determines how close to the local optimum the algorithm must finish, whilst also heavily influencing the computation time required.

Summarising, the convergence test used in the algorithm can be written in the form

$$\| \nabla g(\mathbf{P}) \| \leq c,$$

where

$$\begin{aligned} \nabla g(\mathbf{P}) = A \sum_{h \in H} \nabla f^{sp}(h, p_h) \\ - \frac{2(1-A)|\Omega|}{I} \sum_{i=1}^{I} \left[\left(\sum_{h \in H} F_{u_i,v_i}(h, p_h) - E^{tar}_{u_i,v_i} \right) \sum_{h \in H} \nabla F_{u_i,v_i}(h, p_h) \right]. \end{aligned} \tag{4.3.5}$$

Note that this approach can serve to consider many prescribed flux distributions $F_{u,v}$ (not necessarily Gaussian).

In the following section we apply the numerical discretisation of the continuous optimisation model developed in this chapter to a real SPT plant and we present an illustrative example.

4.4 Illustrative Example

The developed optimisation procedure is illustrated using the PS10 SPT plant in Sanlúcar la Mayor, Seville [Abengoa, 2019], as detailed in Section 1.6.6. This SPT plant has a field of 624 heliostats in a South facing field, arranged as shown in Figure 4.1.

The receiver Ω is a disk and the grid points (u_i, v_i) have been fixed equally spaced and of equal number in both dimensions.

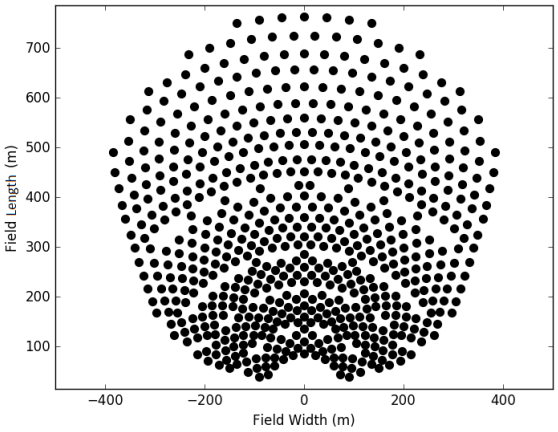

Figure 4.1: PS10 Heliostat Locations

The algorithm developed in Section 4.3 is implemented in Python on a standard specification desktop computer, for a chosen time point of midday.

The *Armijo's Rule* parameter ϵ is set to a value of 0.8, as the suggested value in McCormick [1977], and the initial value for γ is set to 0.01. A lower limit of γ equal to 10^{-8} is set, in order to prevent unnecessary computations occurring in the algorithm.

As mentioned in Section 4.3, since the problem is highly multi-modal, a multistart procedure has been implemented, where the best solution across 30 runs is selected for each variation of the parameter A.

Figure 4.2 shows the peak of the objective function for one value of A across 100 multistart runs, where the multi-modality of the problem can be clearly seen. The variance in solutions found over the 100 multistart runs is also affected by the stop criterion and step size used in each application of the algorithm, meaning that whilst only a few solutions may be found, the level of convergence may not be the same. This can be seen in Figure 4.2 by the number of peaks and troughs at similar, but

slightly different, values. These possibly represent the same solution, reached at different levels of convergence. Therefore, when utilising an adequate selection of step size and convergence test, it is found that a multistart operation with 30 runs suffices in practise to find a solution. The convergence of the gradient to zero and the objective function to the solution can be seen in Figures 4.3-4.4 for one particular simulation.

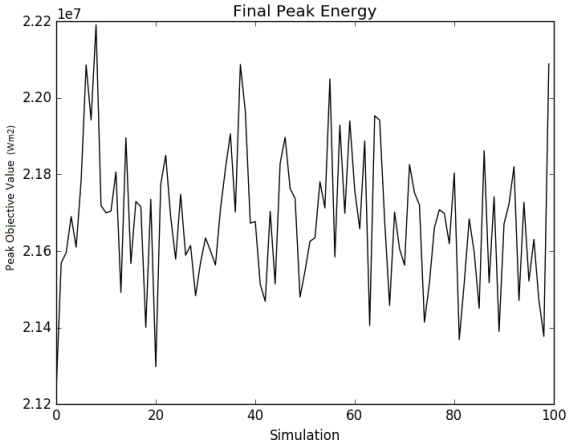

Figure 4.2: Multistart analysis

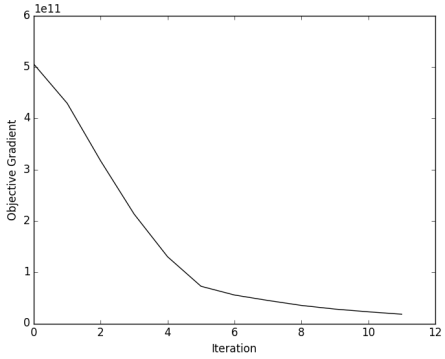

Figure 4.3: Gradient convergence

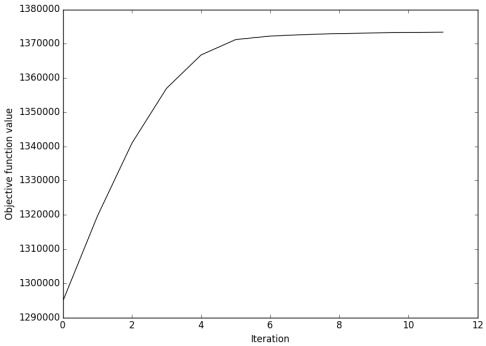

Figure 4.4: Objective function convergence

The parameter A in the objective function in Equation (4.3.1) has been tested between 0 and 1 in steps of 0.01. A value of 0 indicates that the deviation from the target distribution objective is the most important contribution. Contrarily, a value of 1 indicates that the total radiation objective is the most relevant. The target distribution has been assumed constant across the receiver surface. It is important to note that the chosen target distribution must be tailored to the SPT plants current conditions, and a constant distribution has been implemented here as an example.

The values of both objectives for each value of A are shown in Figure 4.5, where

the *Pareto Front* has also been marked. The set of Pareto equilibria identifies those solutions which cannot be improved in terms of both objectives, and therefore give the best optima in terms of minimising target distribution deviation and maximising total radiation capture.

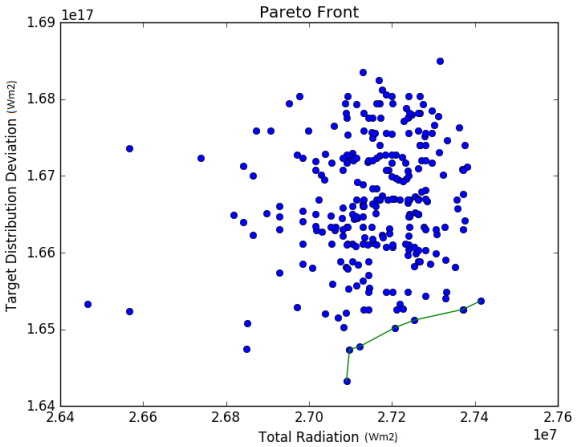

Figure 4.5: Objective values with *Pareto Front*

The results shown in Figure 4.5 indicate that the choice of A can produce highly differing results in the objective function, and this can generate quite different aiming strategies trading off energy maximisation and minimisation of deviation from the target radiation distribution. This is illustrated in Figures 4.6a-4.7b.

Figure 4.6a shows the resultant aiming strategy when the value of A is set to 0.9, causing the captured radiation to be significantly more important than adhering to the target distribution. The aiming strategy will capture more radiation, as shown in Figure 4.6b, but will fail to yield a homogeneous flux distribution, due to the centrally focused heliostats.

Figure 4.7a shows the resultant aiming strategy when A is set to 0.3, which creates a much more homogeneous flux distribution, as shown in Figure 4.7b. These Figures demonstrate the importance of the value of making a judicious choice of A, since improvement in both objectives is highly dependent on its choice.

The results illustrated in this section are for one particular time point, and two examples of the weighting variable A. Each run of this simulation takes less than 10 seconds, which is then multiplied by the number of multistarts performed. With advance knowledge of local weather conditions, the optimal aiming strategy can be calculated without conditions on time. However, to account for rapid changes in weather, it may be useful to re-calculate the optimal aiming strategy in short time scales. Therefore, the rapid computation of this algorithm is advantageous, and also lends itself to applications in SPT plants with larger heliostat field sizes.

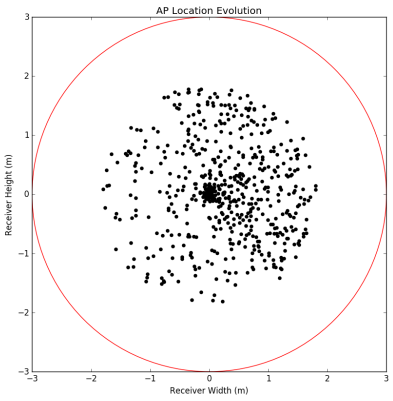

(a) Optimised aiming strategy

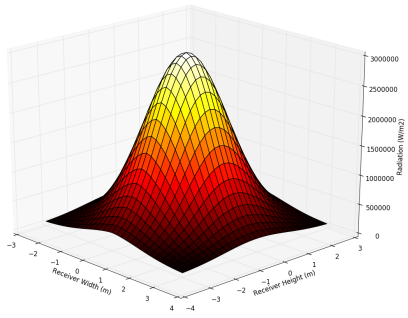

(b) Optimised flux distribution with maximum flux 2.8e6

Figure 4.6: Optimised result with $A = 0.9$

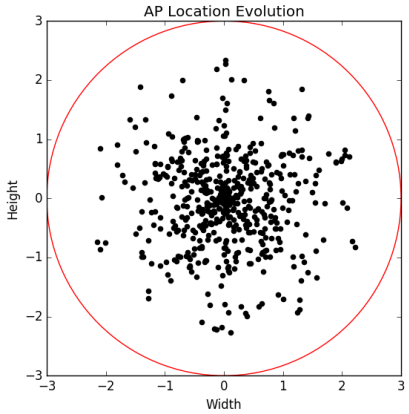

(a) Optimised aiming strategy

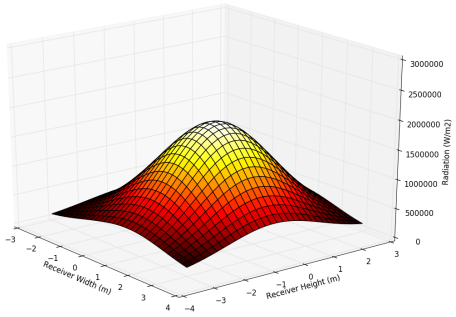

(b) Optimised flux distribution with maximum flux 2e6

Figure 4.7: Optimised result with $A = 0.3$

The next section draws conclusions from the method and numerical illustration developed in this work, and also discusses possible extensions and current research.

4.5 Conclusions

In this work, a bi-objective optimisation model has been implemented to find the optimal aiming strategy for an SPT plant of any size or shape, and a numerical illustration for a real SPT plant is presented.

For the PS10 SPT plant with a field of 624 heliostats, the optimal aiming strategy has been found using the objective function given in (4.3.1), that must be viewed as

a numerical approximation to (4.2.3). In this illustrative example, we have solved the optimisation problem with a multistart procedure for multiple values of the parameter A in $(0, 1)$.

Utilising the optimisation model and numerical method developed in this work, it is possible for the operators of an SPT plant to identify the optimal aiming strategy, considering current weather and plant requirements. Depending on the choice of the weighting parameter A in the objective function, it is possible to seek a desired balance between maximising overall radiation captured and minimising deviation from a desired distribution across the receiver.

The method developed in this work significantly improves upon the method presented in Chapter 3, as here the problem space is not constrained by pre-set aiming points, and allows for realistic representation of SPT plant operations, where it is possible to monitor relative performance of each objective.

The numerical method developed for this work made use of Armijo's rule to iterate the step-size in the algorithm, with independent step-sizes for all components in the set space. This modification can cause longer run times for the simulation. However, a careful application of the algorithm in this case allows it to improve performance and converge to the optimal solution. This performance increase over other methods is of critical importance when simulations in an SPT plant will be re-run during the course of a day for changing local weather conditions.

For the PS10 SPT plant, the optimal aiming strategy can be easily found using the method outlined in this work. For larger SPT plants with more heliostats in the field, the same arguments and techniques can be applied. However, if the number of heliostats is large, and the associated computational cost becomes untenable, an amendment can be made to reduce the problem dimensionality. A possible modification could be the use of a clustering algorithm, such as in Ashley et al. [2017]; Carrizosa et al. [2013]. In such research, the heliostats in the field are clustered using an optimisation procedure which takes into account potential radiation generation as well as physical location and, then, the same aiming strategy is chosen for all heliostats within the same cluster.

Another extension to this work that could assist in reducing computational cost is the application of stochastic techniques [Fonseca et al., 2017; Schmidt et al., 2013; Wang, 2017] where, at each step, the gradient is calculated for just a random sample of heliostats and then used to update the general population. Such methods reduce the calculation time required for each iteration of the algorithm at the cost of utilising several (or many) potentially erroneous components of the gradients.

Chapter 5

Continuous aiming strategies (II): the dynamic case

Continuous aiming strategies (II): the dynamic case

5.1 Introduction

The mathematical complexity of constrained optimisation problems is enlarged when the system being considered is dynamic in nature, that is to say, when the decision variables are functions of time. For example in Schmid [2012], the authors utilise approximate dynamic programming to optimise problems within ambulance management and present a numerical illustration utilising real-world data; in Pillac et al. [2013], the authors present a review of dynamic optimisation vehicle routing problems and discuss various solution methods. Such problems more closely model many realistic situations and posses interesting theoretical formulations.

Chapters 3 and 4 considered a stationary constrained optimisation problem applied to an SPT plant. The purpose of that work was to determine aiming strategies that maximise the radiation energy reaching the target (receiver), considering physical constraints on the system.

The work presented in this chapter looks to extend the optimisation model considered in Chapter 4 to the dynamic case, where additional time-dependent constraints are considered.

The theoretical properties of the dynamic case are developed below, where, as usual, for any Euclidean space S, we denote by $|\cdot|$ (and sometimes $||\cdot||$) the corresponding Euclidean norm. On the other hand, $H^1(0,T;S)$ stands for the Sobolev space of continuous functions $\mathbf{p}:[0,T]\mapsto S$ such that $\dot{\mathbf{p}}(t)$ exists *a.e.* and

$$\int_0^T |\dot{\mathbf{p}}(t)|^2\,dt < +\infty.$$

Also, $\langle\cdot\,,\cdot\rangle$ will stand for the duality product usually associated to the Hilbert space $H^1(0,T;S)$ and the symbol C will denote a generic positive constant.

In this work, we consider the general dynamic optimisation problem:

$$\begin{cases} \text{Maximise } J(\mathbf{p}) = \int_0^T G(t, \mathbf{p}(t))\, dt \\ \text{Subject to } \mathbf{p} \in \mathbf{P}_{ad} \end{cases} \tag{5.1.1}$$

where $\mathbf{P}_{ad}$ is a subset of a Hilbert space $\mathbf{P}$ of functions $\mathbf{p} = \mathbf{p}(t)$ that take values in an Euclidean space $\mathbf{F}$ and we assume that

$$\begin{cases} G : [0,T] \times \mathbf{F} \mapsto \mathbb{R} \text{ is a continuous function,} \\ G \text{ is differentiable with respect to } \mathbf{p} \text{ at any } (t, \mathbf{p}) \text{ and} \\ \dfrac{\partial G}{\partial \mathbf{p}} : [0,T] \times \mathbf{F} \mapsto \mathbb{R} \text{ is continuous.} \end{cases} \tag{5.1.2}$$

More precisely, in this work $\mathbf{P}$ and $\mathbf{P}_{ad}$ will be given by

$$\mathbf{P} = H^1(0,T;\mathbf{F}), \tag{5.1.3}$$

$$\mathbf{P}_{ad} = \{\mathbf{p} \in \mathbf{P} : \mathbf{p}(t) \in \Omega \quad \forall t \in [0,T], \quad M(\mathbf{p}) \leq \sigma\}, \tag{5.1.4}$$

where

$$\Omega \text{ is a nonempty convex compact set in } \mathbf{F} \tag{5.1.5}$$

and

$$M : H^1(0,T;\mathbf{F}) \mapsto \mathbf{E} \text{ is a } C^1 \text{ mapping.} \tag{5.1.6}$$

Here, $\mathbf{E}$ is another Euclidean space and $\sigma \in \mathbf{E}$. In (5.1.4) and henceforth, the inequality $M(\mathbf{p}) \leq \sigma$ must be understood component-wise.

We will also consider the set $\mathbf{P}_0 = \{\mathbf{p} \in \mathbf{P} : \mathbf{p}(t) \in \Omega \quad \forall t \in [0,T]\}$. It will be assumed that

$$M \text{ is } \textit{sequentially weakly lower semicontinuous} \text{ in } H^1(0,T;\mathbf{F}), \tag{5.1.7}$$

in the sense that $\mathbf{p}^n \to \mathbf{p}$ weakly in $H^1(0,T;\mathbf{F})$ implies $\liminf_{n\to+\infty} M(\mathbf{p}^n) \geq M(\mathbf{p})$ and

$$M \text{ is } \textit{coercive} \text{ in } \mathbf{P}_0, \tag{5.1.8}$$

in the sense that the set of functions $\mathbf{p} \in \mathbf{P}_0$ satisfying $M(\mathbf{p}) \leq \sigma$ is bounded in $H^1(0,T;\mathbf{F})$.

The previous "general" problem can be used to model the optimisation of an aiming strategy for an SPT plant if we assume that

- $\mathbf{p} = \mathbf{p}(t)$ defines the set of points aimed by the heliostats on the receiver at times $t \in [0,T]$,
- Ω is the receiver surface,

- $G = A \cdot G_1 + (1 - A) \cdot G_2$ is a balanced combination of the objective functions G_1 and G_2 (radiation and deviation from a target aiming strategy),
- $J(\mathbf{p})$ is, accordingly, a quantification of the payoff produced by the aiming strategy determined by $\mathbf{p}$ and
- $M(\mathbf{p})$ is a measure of the change over time of the aiming strategy, corresponding to $\mathbf{p}$ and the associated energy reaching the receiver.

This chapter is devoted to solving the previous optimisation problem (5.1.1), paying special attention to the SPT plant application, where more details will be given in Sections 5.4 and 5.5.

The plan of this chapter is the following. In Section 5.2, we first prove the existence of a solution to (5.1.1) and subsequently characterise the solutions by an appropriate optimality system. We then formulate two iterative algorithms in Section 5.3, the first one relying on a penalty method and the second one using Augmented Lagrangian techniques. Section 5.4 is devoted to particularise (5.1.1) in the context of an SPT plant; there, the existence and characterisation of optimal aiming strategies are established. The algorithms are illustrated with numerical experiments for a real SPT plant in Section 5.5. Finally, Section 5.6 contains some conclusions and the description of future work.

5.2 Theoretical Properties: Existence and Optimality Results

This section deals with the theoretical analysis of (5.1.1). Our first result is the following:

Theorem 1. *Assume that the assumptions* (5.1.2)-(5.1.8) *are satisfied and the set* $\mathbf{P}_{ad}$*, given by* (5.1.4)*, is non-empty. Then there exists at least one solution to* (5.1.1).

PROOF: The proof is standard if we take into account the well known properties of the spaces involved in the formulation of the problem, see for instance Ekeland and Temam [1976].

Let $\{\mathbf{p}^n\}$ be a maximising sequence for (5.1.1), that is, a sequence in $\mathbf{P}_{ad}$ such that

$$J(\mathbf{p}^n) \to \sup_{\mathbf{p} \in \mathbf{P}_{ad}} J(\mathbf{p}) \quad \text{as } n \to +\infty.$$

Then the $\mathbf{p}^n$ are uniformly bounded in $H^1(0,T;\mathbf{F})$, since they all belong to $\mathbf{P}_{ad}$ and (5.1.8) holds. Consequently, at least for a subsequence (again indexed by n), one has

$$\mathbf{p}^n \to \hat{\mathbf{p}} \quad \text{weakly in } H^1(0,T;\mathbf{F}) \text{ and strongly in } C^0([0,T];\mathbf{F}).$$

The set $\mathbf{P}_{ad}$ is closed in $\mathbf{P}$, thanks to (5.1.5) and (5.1.7). Hence, $\hat{\mathbf{p}} \in \mathbf{P}_{ad}$. On the other hand, $\mathbf{p} \mapsto J(\mathbf{p})$ is continuous in $C^0([0,T];\mathbf{F})$, thanks to (5.1.2). Therefore, one has

$$J(\hat{\mathbf{p}}) = \max_{\mathbf{p}\in\mathbf{P}_{ad}} J(\mathbf{p}).$$

This ends the proof. □

Remark 1. In view of the possible non-convexity of J and M, uniqueness is out of scope in general. □

Recall that $\mathbf{P}_0$ is a non-empty closed convex set of $H^1(0,T;\mathbf{F})$. In our second result, we present suitable necessary optimality conditions that must be satisfied by the solutions to (5.1.1). For simplicity, we will assume from now on that $\mathbf{E} = \mathbb{R}^2$ and we will denote by M_1 and M_2 (resp. σ_1 and σ_2) the components of M (resp. σ).

Theorem 2. *Let $\hat{\mathbf{p}}$ be a solution to* (5.1.1). *Assume that the constraints associated to M are qualified at $\hat{\mathbf{p}}$, that is:*

- $\exists \mathbf{q}^1, \mathbf{q}^2 \in H^1(0,T;\mathbf{F})$ *such that* $\langle M_i'(\hat{\mathbf{p}}), \mathbf{q}^i\rangle < 0$ *for* $i = 1,2$

Then, there exist $\lambda_1, \lambda_2 \geq 0$ such that the triplet $(\hat{\mathbf{p}}, \lambda_1, \lambda_2)$ satisfies

$$\begin{cases} \langle J'(\hat{\mathbf{p}}), \mathbf{p}-\hat{\mathbf{p}}\rangle - \lambda_1\langle M_1'(\hat{\mathbf{p}}), \mathbf{p}-\hat{\mathbf{p}}\rangle - \lambda_2\langle M_2'(\hat{\mathbf{p}}), \mathbf{p}-\hat{\mathbf{p}}\rangle \leq 0 \quad \forall \mathbf{p} \in \mathbf{P}_0, \\ \lambda_i(M_i(\hat{\mathbf{p}}) - \sigma_i) = 0, \quad i = 1,2. \end{cases} \tag{5.2.1}$$

For the proof, it suffices to apply directly the Karush-Kuhn-Tucker principle; see for instance Theorem 9-2.3 in Nocedal et al. [1999].

5.3 Some Iterative Algorithms

5.3.1 Penalisation

In this section, we introduce an iterative method for the solution of the dynamic optimisation problem (5.1.1) based on penalisation techniques. The advantage of this approach is that it reduces the task to the solution of another optimisation problem whose constraints are very easy to handle. The drawback is that a (small) parameter must be introduced and this can have a significant (undesired) influence in the results.

Thus, let us fix $\mu > 0$ and let us set

$$J_\mu(\mathbf{p}) := J(\mathbf{p}) - \frac{1}{2\mu}|(M(\mathbf{p}) - \sigma)_+|^2, \tag{5.3.1}$$

Here, $z_+ = (M(\mathbf{p}) - \sigma)_+$ stands for the positive part of z (understood in the component-wise sense) and, as before, $|\cdot|$ denotes the Euclidean norm in $\mathbf{E}$.

Then, the aforementioned approximation of (5.1.1) is the following:

$$\begin{cases} \text{Maximise } J_\mu(\mathbf{p}) \\ \text{Subject to } \mathbf{p} \in \mathbf{P}_0. \end{cases} \tag{5.3.2}$$

It is reasonable to expect that, for small $\mu > 0$, any solution to the penalized problem (5.3.2) solves approximately (5.1.1).

In the remainder of this section, we will be concerned with the numerical solution of (5.3.2). To this purpose, we will first introduce a time discretisation and then an iterative algorithm of the gradient ascent kind.

Thus, let us begin by replacing $H^1(0,T;\mathbf{F})$ by a finite dimensional subspace.

The easiest and most natural way is to introduce a large integer N, set $\tau := T/N$, consider a uniform partition $\{t^0 = 0 < t^1 < t^2 < ... < t^N = T\}$ with $t^n = n\tau$ for all n and then work in the corresponding space of functions $\mathbf{p}_N : [0,T] \mapsto \mathbf{F}$ which are continuous and piecewise linear.

This space will be denoted by $\mathbf{X}_N$. We will also consider the closed convex set $\mathbf{P}_{0,N} := \mathbf{X}_N \cap \mathbf{P}_0$ and the orthogonal projector $\mathcal{P}_{0,N} : \mathbf{X}_N \mapsto \mathbf{P}_{0,N}$. Observe that $\mathcal{P}_{0,N}(\mathbf{p}_N)(t)$ is, for each t, the projection of each component of $\mathbf{p}_N(t)$ onto Ω. The N-th approximated problem is then

$$\begin{cases} \text{Maximise } J_\mu(\mathbf{p}_N) \\ \text{Subject to } \mathbf{p}_N \in \mathbf{P}_{0,N}. \end{cases} \tag{5.3.3}$$

In order to solve this problem, we can apply a gradient ascent algorithm with variable step size and projection. Accordingly, in the n-th iterate we compute the function $\mathbf{p}_N^{n+1}$, with

$$\mathbf{p}_N^{n+1} = \mathcal{P}_{0,N}(\tilde{\mathbf{p}}_N^{n+1}), \quad \tilde{\mathbf{p}}_N^{n+1} = \mathbf{p}_N^n + \gamma_n \nabla J_\mu(\mathbf{p}_N^n). \tag{5.3.4}$$

Here, γ_n is a conveniently chosen positive number and $\nabla J_\mu(\mathbf{p}_N^n)$ denotes the gradient of the objective function in (5.3.3), that is,

$$\nabla J_\mu(\mathbf{p}_N) = \nabla J(\mathbf{p}_N) - \frac{1}{\mu}\left(M(\mathbf{p}_N) - \sigma\right)_+ \cdot \nabla M(\mathbf{p}_N). \tag{5.3.5}$$

Therefore, the gradient ascent algorithm requires, at each step, the calculation of the derivative of the objective function and a projection of each component of $\mathbf{p}_N(t)$ for each nodal time $t = t_j$. Obviously, the complexity of this computation depends on the properties of the particular function $G = G(t,\mathbf{p})$ and the mapping $M : H^1(0,T;\mathbf{F}) \mapsto \mathbf{E}$ and the sizes of $\dim \mathbf{F}$ and N.

The described penalisation algorithm, denoted Algorithm 1 in this chapter, is outlined in the pseudocode shown below.

Algorithm 1 Penalisation

$\mu \leftarrow$ Set penalisation parameter (small) *float*
$\gamma_0 \leftarrow$ Set initial step size *float*
Tol $\leftarrow$ Simulation tolerance *float*
$\mathbf{p}_0 \leftarrow$ Initial variable set *float*
for $N = 1$ *to* T **do**
  while *ObjDiff* $>$ *Tol* **do**
    while *StepDiff* ≤ 0 **do**
      $J(\mathbf{p}) \leftarrow$ Calculate objective function *float*
      $M(\mathbf{p}) \leftarrow$ Calculate constraint set *float*
      $\nabla J_\mu(\mathbf{p}_N) = \nabla J(\mathbf{p}_N) - \frac{1}{\mu}\left(M(\mathbf{p}_N) - \sigma\right)_+ \cdot \nabla M(\mathbf{p}_N)$.
      $\tilde{\mathbf{p}}_N^{n+1} = \mathbf{p}_N^n + \gamma_n \nabla J_\mu(\mathbf{p}_N^n)$.
      $\mathbf{p}_N^{n+1} = \mathcal{P}_{0,N}(\tilde{\mathbf{p}}_N^{n+1})$
      $J(\tilde{\mathbf{p}}_N^{n+1}) \leftarrow$ Calculate updated objective function *float*
      StepDiff $= |J_\mu(\mathbf{p}_N^{n+1}) - J_\mu(\mathbf{p}_N^n)|$
      $\gamma_{n+1} = \gamma_n \cdot \epsilon$
      Next;
    end while
    ObjDiff $= |J_\mu(\mathbf{p}_N^{n+1}) - J_\mu(\mathbf{p}_{N-1}^{n+1})|$
    Next;
  end while
end for
end;

5.3.2 Augmented Lagrangian

The optimisation problem (5.1.1) can also be solved using the information furnished by Theorem 2. This is indicated in this section, again after time discretisation, through the so called *Augmented Lagrangian* techniques. Recall that $\mathbf{E} = \mathbb{R}^2$ and M_1 and M_2 denote the components of M.

Thus, let us first introduce the so called Augmented Lagrangian $\mathcal{L}_\mu : H^1(0,T;\mathbf{F}) \times \mathbf{E} \mapsto \mathbb{R}$, with

$$\mathcal{L}_\mu(\mathbf{p};\lambda) := J(\mathbf{p}) - \sum_{i=1}^{2} \psi(M_i(\mathbf{p}) - \sigma_i, \lambda_i; \mu), \tag{5.3.6}$$

where we have introduced

$$\psi(z,\beta;\mu) := \begin{cases} z\cdot\beta + \dfrac{1}{2\mu}|z|^2 & \text{if} \quad z + \mu\beta \geq 0 \\ -\dfrac{\mu}{2}|\beta|^2 & \text{otherwise,} \end{cases} \tag{5.3.7}$$

and, again, $\mu > 0$.

Then, it can be proved that the optimisation problem (5.1.1) is equivalent to the following

$$\begin{cases} \text{Minimise} \ \sup_{\mathbf{p}\in\mathbf{P}_0} \mathcal{L}_\mu(\mathbf{p};\lambda) \\ \text{Subject to: } \lambda \in \mathbf{E},\ \lambda \geq 0. \end{cases} \tag{5.3.8}$$

An explanation of this equivalence can be given arguing as follows. The inequality constraint $M(\mathbf{p}) \leq \sigma$ is equivalent to the equality $M(\mathbf{p}) + s = \sigma$, with the so called *slack variable* s belonging to $\mathbf{E}$ and $s \geq 0$. In view of the Karush-Kuhn-Tucker optimality condition (5.2.1), it makes sense to consider the "Modified Lagrangian"

$$\hat{\mathcal{L}}(\mathbf{p}, s; \lambda) := J(\mathbf{p}) - \lambda \cdot (M(\mathbf{p}) + s - \sigma) \tag{5.3.9}$$

and its penalised version

$$\hat{\mathcal{L}}_\mu(\mathbf{p}, s; \lambda) := J(\mathbf{p}) - \lambda \cdot (M(\mathbf{p}) + s - \sigma) - \frac{1}{2\mu}|M(\mathbf{p}) + s - \sigma|^2. \tag{5.3.10}$$

Then, recalling (5.3.6)-(5.3.7), it is easy to check that

$$\sup_{s\in\mathbf{E},\ s\geq 0} \hat{\mathcal{L}}_\mu(\mathbf{p}, s; \lambda) = \mathcal{L}_\mu(\mathbf{p}; \lambda),$$

whence we see that (5.3.8) is an appropriate reformulation of (5.1.1).

As in the previous section, in practice, in order to solve (5.3.8) we must provide a finite dimensional approximation. With the notation used in Section 5.3.1, a suitable choice is the following:

$$\begin{cases} \text{Minimise} \ \sup_{\mathbf{P}_{0,N}} \mathcal{L}_\mu(\mathbf{p}_N;\lambda) \\ \text{Subject to: } \lambda \in \mathbf{E},\ \lambda \geq 0. \end{cases} \tag{5.3.11}$$

This problem can be solved with a duality-penalty algorithm that, at the n-th step, furnishes the multiplier λ^{n+1} according to the following:

- Compute a solution $\mathbf{p}_N^n$ to the problem

$$\begin{cases} \text{Maximise } \mathcal{L}_\mu(\mathbf{p}_N;\lambda^n) \\ \text{Subject to } \mathbf{p}_N \in \mathbf{P}_{0,N} \end{cases} \tag{5.3.12}$$

- Then, take

$$\lambda^{n+1} = (\lambda^n + \frac{1}{\mu}(M_i(\mathbf{p}_N^n) - \sigma))_+. \tag{5.3.12$'$}$$

This will be denoted Algorithm 2 in this work, and is given in the pseudocode given

below.

As in Section 5.3.1, the solution of (5.3.12) can be obtained through a variable step gradient ascent method with projection. Thus, at the k-th step, we compute $\mathbf{p}_N^{n,k+1}$, with

$$\mathbf{p}_N^{n,k+1} = \mathcal{P}_{0,N}(\tilde{\mathbf{p}}_N^{n,k+1}), \quad \tilde{\mathbf{p}}_N^{n,k+1} = \mathbf{p}_N^{n,k} + \gamma_k \nabla \mathcal{L}_\mu(\mathbf{p}_N^{n,k}; \lambda^n). \tag{5.3.13}$$

Algorithm 2 Augmented Lagrangian

$\lambda \leftarrow$ Lagrangian multiplier *float*
$\sigma \leftarrow$ Constraint constant*float*
$\mu \leftarrow$ Penalty constant*float*
Tol $\leftarrow$ Simulation tolerance *float*
$\mathbf{p} \leftarrow$ Variable set *float*
$J \leftarrow$ Objective function *float*
$M \leftarrow$ Constraint set *float*
for $t = 1$ *to* T **do**
  while *ObjDiff* $>$ *Tol* **do**
    while *StepDiff* ≤ 0 **do**
      $J(\mathbf{p}) \leftarrow$ Calculate objective function *float*
      $M(\mathbf{p}) \leftarrow$ Calculate constraint set *float*
      $\nabla J_\mu(\mathbf{p}_N) = \nabla J(\mathbf{p}_N) - \frac{1}{\mu}\left(M(\mathbf{p}_N) - \sigma\right)_+ \cdot \nabla M(\mathbf{p}_N)$.
      Maximise $\hat{\mathcal{L}}_\mu(\mathbf{p}, s; \lambda)$
      Fix s
      Maximise $\mathcal{L}_\mu(\mathbf{p}_N; \lambda^n)$
      $\tilde{\mathbf{p}}_N^{n,k+1} = \mathbf{p}_N^{n,k} + \gamma_k \nabla \mathcal{L}_\mu(\mathbf{p}_N^{n,k}; \lambda^n)$
      $\mathbf{p}_N^{n,k+1} = \mathcal{P}_{0,N}(\tilde{\mathbf{p}}_N^{n,k+1})$
      $J_\mu(\tilde{\mathbf{p}}_N^{n+1}) \leftarrow$ Calculate updated objective function *float*
      StepDiff $= |J_\mu(\mathbf{p}_N^{n+1}) - J_\mu(\mathbf{p}_N^n)|$
      $\gamma_{k+1} = \gamma_k \cdot \epsilon$
      Next;
    end while
    ObjDiff $= |\hat{\mathcal{L}}_\mu(\mathbf{p}_N^{n,k+1}; \lambda^n) - \hat{\mathcal{L}}_\mu(\mathbf{p}_N^{n,k}; \lambda^n)|$
    $\lambda^{n+1} = (\lambda^n + \frac{1}{\mu}(M_i(\mathbf{p}_N^n) - \sigma))_+$
    Next;
  end while
end for
end;

In the following section, we detail the model for an SPT plant and verify that all assumptions made in the formulation of the general problem in Section 5.1 remain valid.

5.4 The Model for an SPT Plant

As considered in Chapters 3-4, the aiming point of each heliostat in the field on the receiver surface directly affects the energy generation. In particular, it has been shown that, although maximising incident radiation is important, it is also beneficial to maintain a desired flux distribution to aid thermal transfer [Relloso and García, 2015; Yu et al., 2014].

In this chapter we extend the models previously discussed to the dynamic case, considering time dependent variables and constraints. These constraints, as introduced in Sections 5.1-5.2, concern physical aspects of the SPT. One of them must be viewed as a limitation on the rotational speed of the heliostat and is obviously justified by operational reasons. On the other hand, the radiation at any point of the receiver surface should not vary drastically over short time periods, in order to prevent flash heating and this is considered in the second constraint.

The radiation passing through the system is modelled using a Gaussian distribution, as presented in Section 1.7.

We assume that there are H heliostats in the field and we denote by $p_h(t)$ the point aimed at by the h-th heliostat at time t. We have $p_h(t) \in \bar{\Omega}_R$ for all h and t; $\Omega_R \subset \mathbb{R}^2$ is bounded, open and convex with $0 \in \Omega_R$ and we take $\Omega = \bar{\Omega}_R$. Accordingly, the Euclidean space $\mathbf{F}$ will have dimension $2H$:

$$\mathbf{F} = \mathbb{R}^{2H}. \tag{5.4.1}$$

The usual Euclidean norm in $\mathbf{F}$ will be denoted by $\|\cdot\|$.

At time t, the radiation measured at a point $(u, v) \in \Omega$ and furnished by the h-th heliostat is given by $F_{u,v}(h, p_h(t), t)$. For each h, the real-valued function $(u, v, p_h, t) \mapsto F_{u,v}(h, p_h, t)$ is smooth. The associated total radiation captured over the receiver surface Ω for a given heliostat h is thus given by

$$F_0(h, p_h(t), t) := \iint_\Omega F_{u,v}(h, p_h(t), t)\, du\, dv.$$

Therefore, the total radiation supplied by all heliostats at time t can be written in the form

$$f(\mathbf{p}(t), t) := \sum_{h=1}^{H} F_0(h, p_h(t), t) = \iint_\Omega \Big(\sum_{h=1}^{H} F_{u,v}(h, p_h(t), t) \Big)\, du\, dv, \tag{5.4.2}$$

where we have used the notation $\mathbf{p} := (p_1, \ldots, p_H)$.

In order to limit the motion of heliostats, so that they do not move faster than their velocity limits, we introduce the velocity $\dot{p}_h = \dot{p}_h(t)$ of each heliostat h, the velocity vector $\dot{\mathbf{p}} = \dot{\mathbf{p}}(t)$ and a target velocity vector $\mathbf{V}_p \in \mathbf{F}$ with $\mathbf{V}_p \geq 0$ and we impose the

collective velocities to be approximately below $\mathbf{V}_p$ in the sense that

$$\int_0^T \|(\dot{\mathbf{p}}(t) - \mathbf{V}_p)_+\|^2 \, dt \leq \sigma_1$$

for some $\sigma_1 \geq 0$.

The change in time in radiation at each point of the receiver must also be limited and kept below a fixed value σ_2. This will be witten in the form

$$\int_0^T \left(\iint_\Omega \Big| \sum_{h=1}^H \frac{d}{dt} F_{u,v}(h, p_h(t), t) \Big|^2 \, du \, dv \right) dt \leq \sigma_2.$$

Our objective is to maximise the radiation captured by the receiver, whilst maintaining a target energy profile which maximises absorption. Thus, we deal with the constrained optimisation problem (5.1.1), where

$$\begin{cases} G(t, \mathbf{p}) := A \iint_\Omega \Big(\sum_{h=1}^H F_{u,v}(h, p_h, t) \Big) \, du \, dv \\ \qquad\qquad - (1 - A) \iint_\Omega \Big| \sum_{h=1}^H F_{u,v}(h, p_h, t) - E_{u,v}^{tar}(t) \Big|^2 \, du \, dv \end{cases} \tag{5.4.3}$$

($A \in [0, 1]$ is a weighting parameter),

$$M_1(\mathbf{p}) := \int_0^T \|(\dot{\mathbf{p}}(t) - \mathbf{V}_p)_+\|^2 \, dt, \tag{5.4.4}$$

$$M_2(\mathbf{p}) := \int_0^T \Big(\iint_\Omega \Big| \sum_{h=1}^H \frac{d}{dt} F_{u,v}(h, p_h(t), t) \Big|^2 \, du \, dv \Big) \, dt, \tag{5.4.5}$$

the σ_i are prescribed non-negative constants and $E_{u,v}^{tar} = E_{u,v}^{tar}(t)$ is the desired target distribution at time t.

For convenience, we will assume that

$$\sigma_2 > M_2(0) = \int_0^T \Big(\iint_\Omega \Big| \sum_{h=1}^H \frac{d}{dt} F_{u,v}(h, 0, t) \Big|^2 \, du \, dv \Big) \, dt. \tag{5.4.6}$$

This is sufficient to guarantee that the zero function in $H^1(0, T; \mathbf{F})$ belongs to $\mathbf{P}_{ad}$ and, consequently, $\mathbf{P}_{ad}$ is non-empty.

In the following sections, we will check that the theoretical analysis in Section 5.2 and the proposed iterative algorithms in Section 5.3 are valid in this framework. In particular, we consider the existence of optimal aiming strategies, their characterisation through optimality conditions and finite dimensional approximations and penalty and duality-penalty solution methods are described.

5.4.1 Existence and Optimality

The following result holds:

Proposition 1. *Let* $\mathbf{F}$, G *and* M *be given by* (5.4.1) *and* (5.4.3)–(5.4.5) *and let* $\mathbf{P}$ *and* $\mathbf{P}_{ad}$ *be given by* (5.1.3)–(5.1.4). *Then, the assumptions* (5.1.2) *and* (5.1.5)–(5.1.8) *are satisfied.*

PROOF: It is clear that (5.1.2), (5.1.5) and (5.1.6) are satisfied. For convenience, let us introduce $a_h(t,p_h;u,v) \coloneqq \frac{\partial}{\partial p_h}F_{u,v}(h,p_h,t)$, $b_h(t,\mathbf{p};u,v) \coloneqq \sum_{h=1}^{H} F_{u,v}(h,p_h,t) - E^{tar}_{u,v}(t)$ and $c(t,\mathbf{p},\mathbf{q};u,v) \coloneqq \sum_{h=1}^{H} \frac{d}{dt}\frac{\partial}{\partial p_h}F_{u,v}(h,p_h,t)q_h$.

Then one has

$$\frac{\partial G}{\partial p_h}(t,\mathbf{p}) = A\iint_\Omega a_h(t,p_h;u,v)\,du\,dv - 2(1-A)\iint_\Omega b_h(t,\mathbf{p};u,v)a_h(t,p_h;u,v)\,du\,dv,$$

for all h and $(t,\mathbf{p})$ and

$$\langle M_1'(\mathbf{p}),\mathbf{q}\rangle = 2\int_0^T (\dot{\mathbf{p}}(t)-\mathbf{V}_p)_+\cdot\dot{\mathbf{q}}(t)\,dt \tag{5.4.7}$$

and

$$\langle M_2'(\mathbf{p}),\mathbf{q}\rangle = 2\int_0^T \Big[\iint_\Omega \Big(\sum_{h=1}^{H}\frac{d}{dt}F_{u,v}(h,p_h(t),t)\Big)c(t,\mathbf{p}(t),\mathbf{q}(t);u,v)\,du\,dv\Big]\,dt \tag{5.4.8}$$

for all $\mathbf{p},\mathbf{q}\in H^1(0,T;\mathbf{F})$.

Let us now check that (5.1.7) holds. Assume that $\mathbf{p}_n \to \mathbf{p}$ weakly in $H^1(0,T;\mathbf{F})$. Since this implies the uniform convergence of the $\mathbf{p}_n$ in $[0,T]$, we have

$$\lim_{n\to+\infty} M_2(\mathbf{p}_n) = M_2(\mathbf{p}) \tag{5.4.9}$$

On the other hand, since the function $\mathbf{p}\mapsto M_1(\mathbf{p})$ is convex and continuous in $H^1(0,T;\mathbf{F})$, we also have

$$\liminf_{n\to+\infty} M_2(\mathbf{p}_n) \geq M_2(\mathbf{p}). \tag{5.4.10}$$

From (5.4.9) and (5.4.10), we get (5.1.7).

Finally, it is clear that (5.1.8) is satisfied. Indeed, if $\mathbf{p}\in\mathbf{P}_0$ and $M(\mathbf{p})\leq\sigma$, we have in particular that

$$\|p(t)\| \leq C \quad \forall t\in[0,T] \tag{5.4.11}$$

and

$$\int_0^T ||\dot{\mathbf{p}}(t)||^2\,dt \le 2\int_0^T ||(\dot{\mathbf{p}}(t)^2 - \mathbf{V}_p)_+||^2\,dt + C \le C, \tag{5.4.12}$$

whence $\mathbf{p}$ belongs to a bounded set in $H^1(0,T;\mathbf{F})$.

This ends the proof.

□

From Proposition 1, we get the following consequences:

- Theorem 1 can be applied and there exists at least one optimal aiming strategy for the modelled SPT plant.
- Theorem 2 can also be applied and, assuming that at an optimal $\hat{\mathbf{p}}$ the constraints associated to the M_i are qualified, we get the necessary conditions (5.2.1) for some multipliers $\lambda_1, \lambda_2 \ge 0$.

5.4.2 Finite Dimensional Approximation and Iterative Algorithms

In practice, as in Sections 5.3.1 and 5.3.2, we must approximate the infinite dimensional problem (5.1.1) corresponding to (5.4.3)-(5.4.5) and replace $H^1(0,T;\mathbf{F})$ by $\mathbf{X}_N$ and $\mathbf{P}_0$ by $\mathbf{P}_{0,N}$. The resulting tasks are thus to solve (5.3.3) and/or (5.3.11).

Note that, in both cases, the computations of $\nabla J(\mathbf{p}_N)$, $\nabla M_1(\mathbf{p}_N)$ and $\nabla M_2(\mathbf{p}_N)$ are needed and this requires integrals on Ω, with respect to (u,v) of several functions. For this reason, it is convenient to fix a set of test points (u_i,v_i), $1 \le i \le I$ and replace these integrals by appropriate finite sums.

The total radiation reaching the receiver at time t is therefore approximated by:

$$\int_0^T \iint_\Omega \Big(\sum_{h=1}^H F_{u,v}(h,p_h(t),t)\Big)\,du\,dv\,dt \;\approx\; \sum_{n=1}^N \sum_{i=1}^I \sum_{h=1}^H F_{u_i,v_i}(h,p_h(t^n),t^n) \tag{5.4.13}$$

Similarly, the deviation from the target distribution is approximated by:

$$\int_0^T \iint_\Omega b(t,\mathbf{p}(t);u,v)^2\,du\,dv\,dt \;\approx\; \sum_{n=1}^N \sum_{i=1}^I b(t^n,\mathbf{p}(t^n);u^i,v^i)^2. \tag{5.4.14}$$

Finally, the constraint mappings M_1 and M_2 given by (5.4.4)-(5.4.5) are approximated as follows:

$$M_1(\mathbf{p}) = \int_0^T \|(\dot{\mathbf{p}}(t) - \mathbf{V}_p)_+\|^2\,dt \;\approx\; M_1^N(\mathbf{p}_N) := \sum_{n=1}^N (\frac{1}{2}|\mathbf{p}(t^n) - \mathbf{p}(t^{n-1})| - V_p)_+^2, \tag{5.4.15}$$

$$\begin{aligned} M_2(\mathbf{p}) &= \int_0^T \left(\iint_\Omega \Big(\sum_{h=1}^{H} \frac{d}{dt} F_{u,v}(h, p_h^n(t), t) \Big)^2 du\, dv \right) dt \\ &\approx M_2^N(\mathbf{p}_N) := \sum_{n=1}^{N} \sum_{i=1}^{I} \Big| \sum_{h=1}^{H} F_{u_i,v_i}(h, p_h(t^n), t^n) - F_{u_i,v_i}(h, p_h(t^{n-1}), t^{n-1}) \Big|^2. \end{aligned} \tag{5.4.16}$$

Penalisation Algorithm

After these approximations, we see that, in the case of the SPT model, the objective function in (5.3.3) is given by:

$$\begin{aligned} J_\mu^N(\mathbf{p}_N) = A \sum_{n=1}^{N} \sum_{i=1}^{I} \sum_{h=1}^{H} F_{u_i,v_i}(h, p_h(t^n), t^n) - (1-A) \sum_{n=1}^{N} \sum_{i=1}^{I} b(t^n, \mathbf{p}(t^n); u^i, v^i)^2 \\ - \frac{1}{2\mu} \Big[\Big(\sum_{n=1}^{N} (\frac{1}{2} |\mathbf{p}(t^n) - \mathbf{p}(t^{n-1})| - V_p)_+^2 - \sigma_1 \Big)_+^2 \\ + \Big(\sum_{n=1}^{N} \sum_{i=1}^{I} \Big| \sum_{h=1}^{H} F_{u_i,v_i}(h, p_h(t^n), t^n) - F_{u_i,v_i}(h, p_h(t^{n-1}), t^{n-1}) \Big|^2 - \sigma_2 \Big)_+^2 \Big], \end{aligned} \tag{5.4.17}$$

It is not difficult to compute from this identity the partial derivatives of J_μ^N and, accordingly, its gradient ∇J_μ. This makes it possible to apply the gradient ascent algorithm in the present context.

The choice of step size parameters γ^k used for the gradient ascent algorithm have a large impact on the speed of convergence. In the SPT plant context, the objective function is non-linear, non-convex and of large dimensions, indicating that step size choice will also factor heavily into likelihood of convergence of the algorithm.

As in Chapter 4, we apply a variant to the *Armijo's Rule*, whereby the parameter γ^k is different for each component, that is, for each heliostat $h \in H$. Consequently, the γ_h^k are computed according to the rules

$$\gamma_h^k = \gamma_h^{k-1} \cdot \epsilon_h, \quad h = 1, \ldots, H. \tag{5.4.18}$$

The gradient ascent method with projection is then:

$$\mathbf{p}_N^{n+1} = \mathcal{P}_{0,N}(\tilde{\mathbf{p}}_N^{n+1}), \quad \tilde{\mathbf{p}}_N^{n+1} = \mathbf{p}_N^n + \Gamma^k \nabla J_\mu(\mathbf{p}_N^n), \tag{5.4.19}$$

where $\Gamma^k = \mathrm{diag}(\gamma_1^k, \ldots, \gamma_N^k)$.

The gradient ascent method applied to the penalisation algorithm, as described in the pseudocode given in Algorithm 1, is applied at each step of the discretised time period. The computed optimal result at a given time is then used as the initial guess

for the next time step. In this way, the overall optimal schedule can be found by considering each discretised time point individually.

Augmented Lagrangian Algorithm

Following the finite dimensional reduction method outlined in Section 5.4.2, the Augmented Lagrangian given in equation (5.3.6) can be approximated as follows:

$$\begin{aligned}\mathcal{L}_\mu(\mathbf{p}_N,\lambda) \simeq \mathcal{L}_\mu^N(\mathbf{p}_N,\lambda) \coloneqq A\sum_{n=1}^{N}\sum_{i=1}^{I}\sum_{h=1}^{H} F_{u_i,v_i}(h,p_h(t^n),t^n)\\ -(1-A)\sum_{n=1}^{N}\sum_{i=1}^{I}\sum_{h=1}^{H} b(t^n,\mathbf{p}(t^n);u^i,v^i)^2 - \sum_{i=1}^{2}\psi(M_i^N(\mathbf{p}_N)-\sigma_i,\lambda_i;\mu),\end{aligned} \tag{5.4.20}$$

where ψ is defined in (5.3.7) and M_1^N and M_2^N are respectively given in (5.4.15) and (5.4.16).

The gradient of this function can be calculated as before and the gradient ascent method can be applied to the intermediate problems (5.3.12).

The Augmented Lagrangian algorithm, as summarised in the pseudocode in Algorithm 2, follows a similar procedure to that of the penalisation algorithm, with extra stages to update the Lagrangian multipliers. Recall that, after the computation of the solution to (5.3.12), the Lagrange multipliers must be updated, according to the formula (5.3.12′). Then, a new optimisation problem must be solved using the last computed solution as an initial iterate and so on.

In the following section, we present an illustrative example that demonstrates, in the framework of the optimisation of SPT plants, the usefulness of the formulation (5.1.1), the theoretical results in Section 5.2 and the functionality of the presented algorithms.

5.5 A Numerical Experiment

The behavior of the previous algorithms is illustrated for the PS10 SPT plant, whose details are found in Section 1.6.6. The field of this SPT plant has 624 heliostats arranged in a radial pattern around a centrally located tower. The layout of the heliostats can be seen in Figure 5.1, where the receiver is mounted atop a North facing tower.

In Figure 5.2, the reflected solar radiation at midday is shown, where the heliostats are colour coded according to the energy they would provide to the system if they aimed at the centre of the receiver. From this figure, it can be clearly seen that an adequate aiming strategy is important, as there are large differences in the energy contributions provided by the heliostats in the field. It is completely natural to fix a dynamic aiming strategy, as the incident radiation on the heliostat field changes over time.

Utilising the algorithms developed in Section 5.3 and the SPT plant model described in Section 5.4, we present a numerical illustration that finds the optimal aiming strategy for the PS10 SPT plant across a single day.

We consider 10 equally spaced time points, where input to the model includes incident solar radiation on the field and solar angle.

We look to optimise the general dynamic optimisation problem (5.1.1), by considering the two forms given by the algorithms: penalisation (5.3.3) and Augmented Lagrangian (5.3.12). As already mentioned, the objective is to maximise radiation reaching the receiver surface across the day, whilst restricting the movement speed of heliostat aim points and also limiting the change in radiation over time at any point on the receiver.

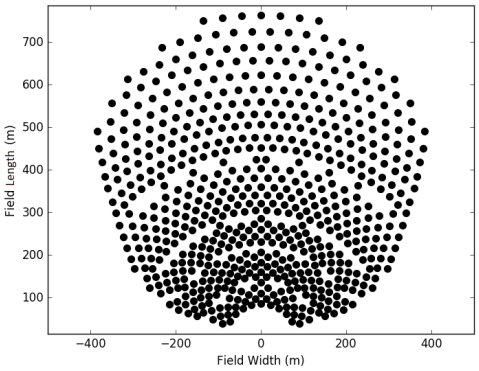

Figure 5.1: Heliostat Layout

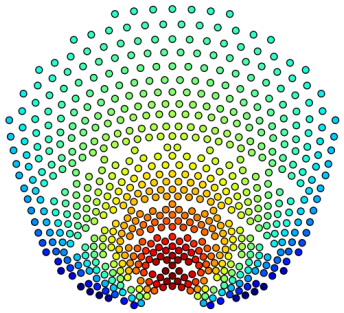

Figure 5.2: Reflected radiation for midday

5.5.1 Penalisation Algorithm

The penalisation algorithm is applied to the 10 point optimisation problem, with the parameter values given in Table 5.1. We set a uniform target distribution and fix limits on the aiming point velocities and global change in radiation along the receiver. Considering the constraints derived in Section 5.3.1, we then look to maximise the objective function at each time point utilising the gradient ascent method.

To start the algorithm, we define an initial set of aiming points on the receiver, randomly spread, as shown in Figure 5.3. This choice is ideal for early morning, as it allows for a slow warm-up of the entire receiver surface.

Parameter	Value	Summary
T	10	Number of time points
σ_1	0	M_1 constraint threshold
σ_2	1e4	M_2 constraint threshold
H	624	Number of heliostats in field.
μ	1e5	Penalisation constant
V_p	0.5	Velocity constraint constant
E^{tar}	2.2e6	Target uniform distribution value (Wm^2)
A	0.7	Weighting parameter
γ_0	0.01	Initial step size

Table 5.1: Penalisation algorithm parameter values

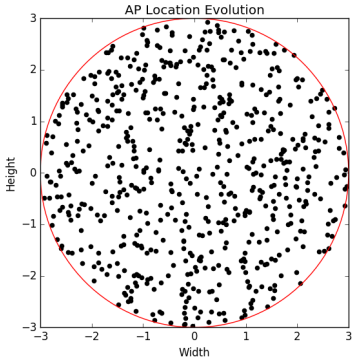

Figure 5.3: Initial aiming point distribution

The resultant set of aiming points and the radiation distribution on the receiver are then used as the initial solution to the first time problem. Each subsequent time point is then considered, utilising the computed optimal solution from the previous one as its initial solution. The aiming strategies for all time points are given in Figures 5.4–5.13.

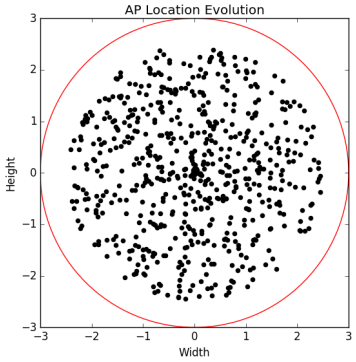

Figure 5.4: t=1 aiming distribution

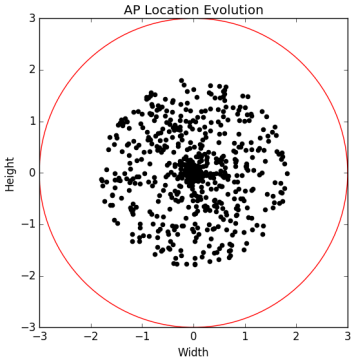

Figure 5.5: t=2 aiming distribution

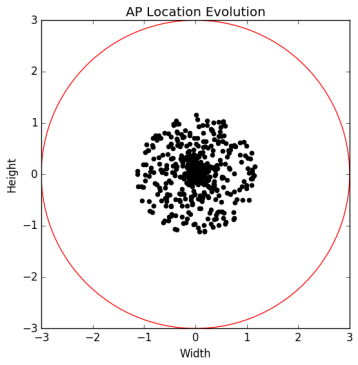

Figure 5.6: t=3 aiming distribution

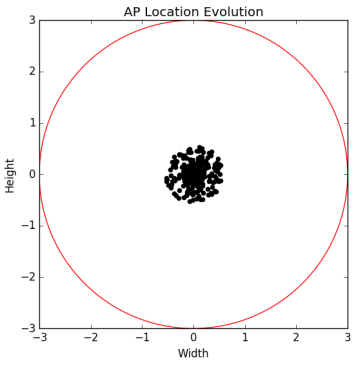

Figure 5.7: t=4 aiming distribution

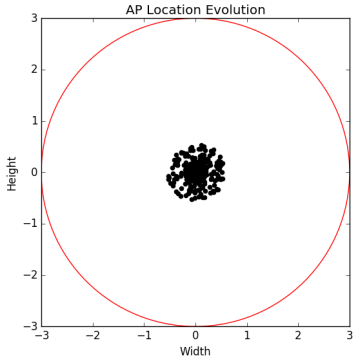

Figure 5.8: t=5 aiming distribution

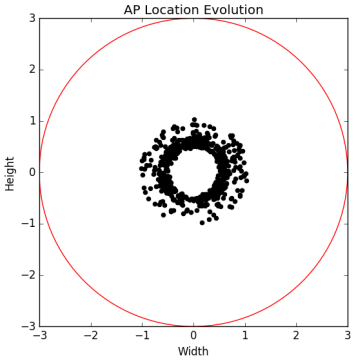

Figure 5.9: t=6 aiming distribution

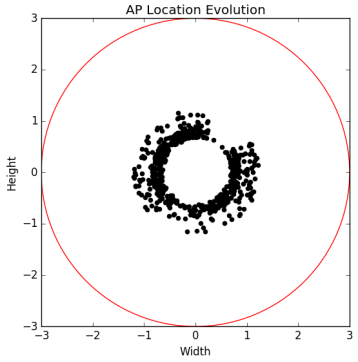

Figure 5.10: t=7 aiming distribution

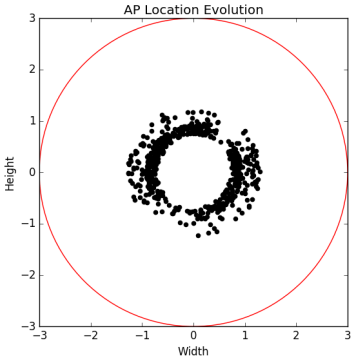

Figure 5.11: t=8 aiming distribution

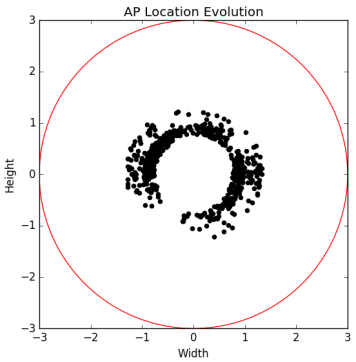

Figure 5.12: t=9 aiming distribution

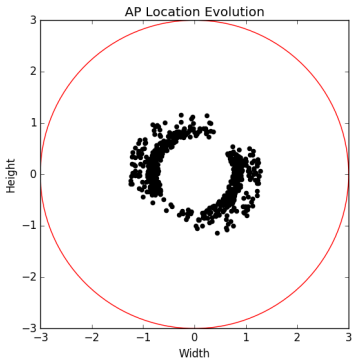

Figure 5.13: t=10 aiming distribution

From Figures 5.4–5.13, the evolution of the aiming strategy across the day can be seen. The effect of the dynamic constraints on aiming point velocity and change in radiation can be seen in the slow movement of aim points towards the center in Figures 5.4–5.8. During these early hours of low incident solar radiation, the maximum is captured when a heliostat aims at the center.

The change in aiming strategy from Figure 5.8 to 5.9 identifies a shift in behaviour, caused by the incident radiation on the heliostat field and the target distribution imposed in the constraints.

Figure 5.14 gives the level of incident radiation on the heliostat field for the considered time period, and Figure 5.15 gives the maximum radiation value detected on the receiver with the indicated aiming strategy. It can be seen that, as the level of incident radiation on the field increases (towards midday), the same happens to the maximum level of radiation on a particular point on the receiver. This is due to the centrally focused aiming strategy shown in Figure 5.7.

Once the level of radiation reaches the target distribution limit given in Table 5.1, at time $t = 5$, the aiming strategy must adjust in order to maintain a uniform distribution, as seen in Figure 5.9.

The computation time of the penalisation algorithm is dependent on the prescribed model parameters, such as step size, constraint limits, convergence tolerance, etc. However, with an adequate selection of these parameters, the previous numerical illustration can be achieved in 2.5 minutes utilising a computer with specifications: Intel®Core™ i7-7700HQ CPU @ 2.80 GHz.

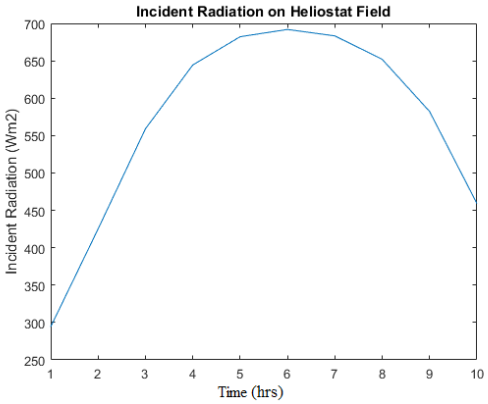

Figure 5.14: Incident radiation on SPT plant field

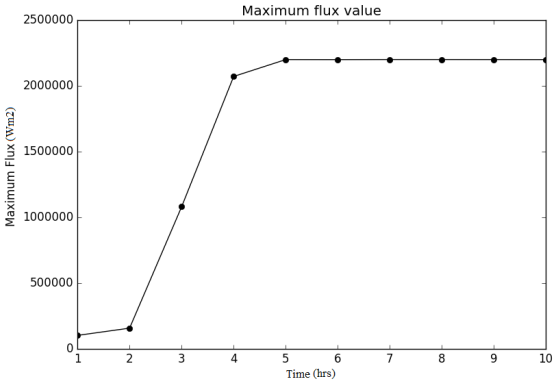

Figure 5.15: Maximum flux on receiver over time

5.5.2 Augmented Lagrangian Algorithm

The Augmented Lagrangian algorithm is also applied to the 10 point optimisation problem, with the parameter values given in Table 5.2. We set a uniform target distribution and fix limits on the aiming point velocities and change in radiation along the receiver. Considering the constraints in Section 5.3.2, we then look to maximise the objective function across each time point utilising the gradient ascent method.

Parameter	Value	Summary
T	10	Number of time points
σ_1	0	M_1 constraint threshold
σ_2	1e4	M_2 constraint threshold
H	624	Number of heliostats in field.
μ	2e-5	Penalisation constant
λ_0	1e6	Initial Lagrange multiplier
V_p	0.5	Velocity constraint constant
E^{tar}	2.2e6	Target uniform distribution value (Wm^2)
A	0.7	Weighting parameter
γ_0	0.01	Initial step size

Table 5.2: Augmented Lagrangian algorithm parameter values

To start the algorithm, we define an initial set of aiming points on the receiver as in the case of the penalisation algorithm, shown in Figure 5.16.

For each time point considered, the algorithm takes the initial solution from the previous time step, and optimises using the gradient ascent method described in Section 5.3.2. Once a solution has been found for a particular time point, the Lagrangian multipliers are updated, and the solution is used to re-optimise the same time point.

This is repeated until no improvement on the solution can be found. The resultant solution is then used as the initial solution to the next time point.

The computed aiming strategies using the augmented lagrangian algorithm are then given in Figures 5.17-5.41.

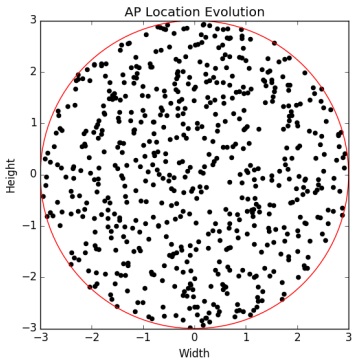

Figure 5.16: t=0 aiming distribution

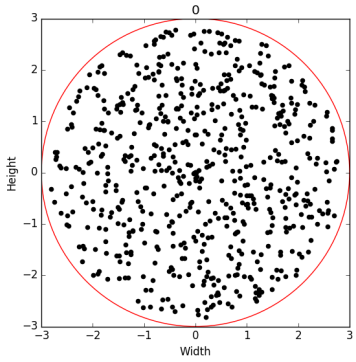

Figure 5.17: t=1, λ_0 aiming distribution

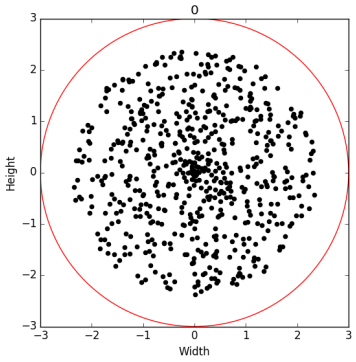

Figure 5.18: t=1, λ_1 aiming distribution

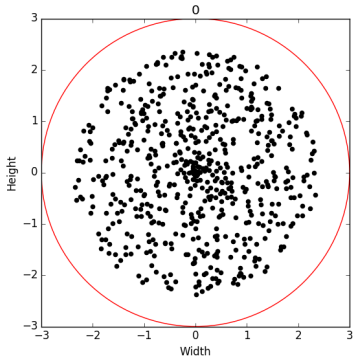

Figure 5.19: t=1, λ_2 aiming distribution

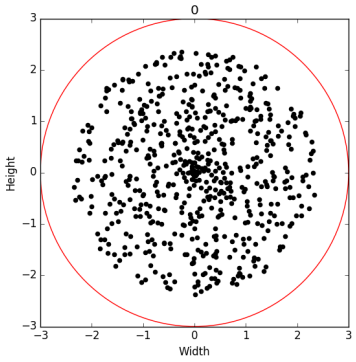

Figure 5.20: t=1, λ_3 aiming distribution

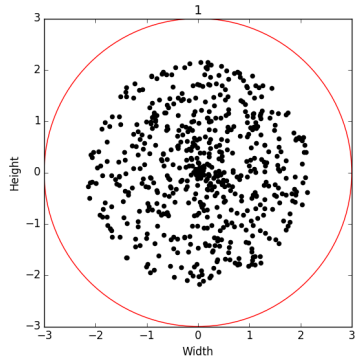

Figure 5.21: t=2, λ_0 aiming distribution

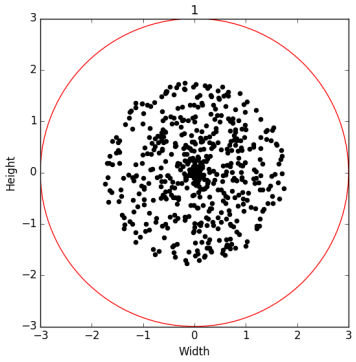

Figure 5.22: t=2, λ_1 aiming distribution

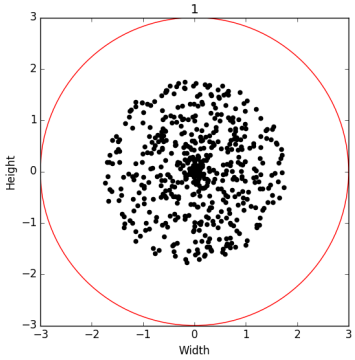

Figure 5.23: t=2, λ_2 aiming distribution

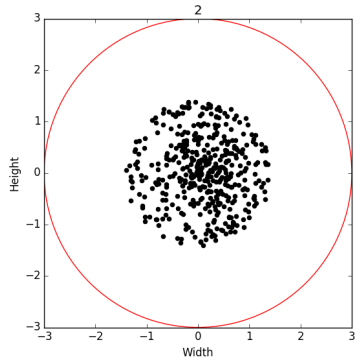

Figure 5.24: t=3, λ_0 aiming distribution

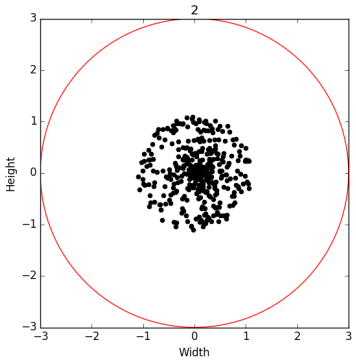

Figure 5.25: t=3, λ_1 aiming distribution

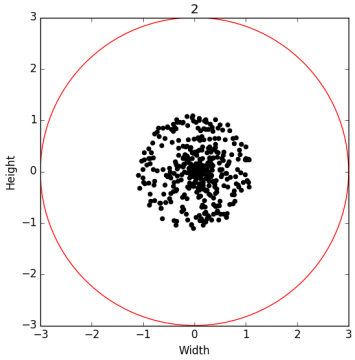

Figure 5.26: t=3, λ_2 aiming distribution

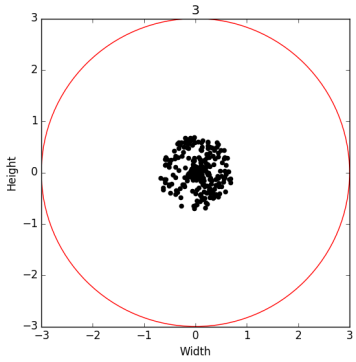

Figure 5.27: t=4, λ_0 aiming distribution

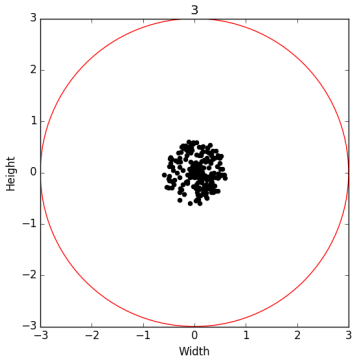

Figure 5.28: t=4, λ_1 aiming distribution

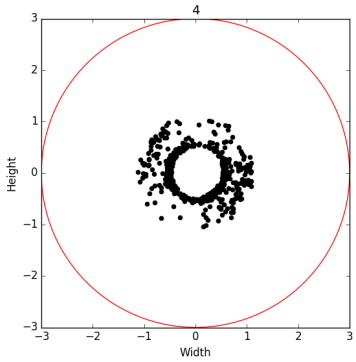

Figure 5.29: t=5, λ_0 aiming distribution

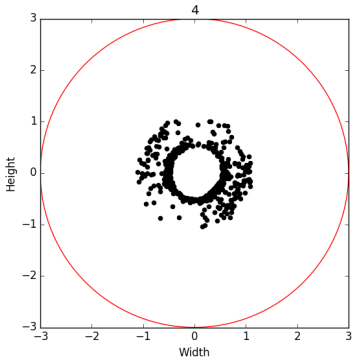

Figure 5.30: t=5, λ_1 aiming distribution

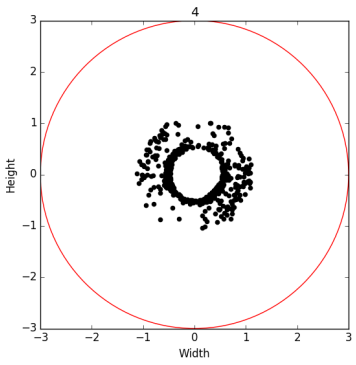

Figure 5.31: t=5, λ_2 aiming distribution

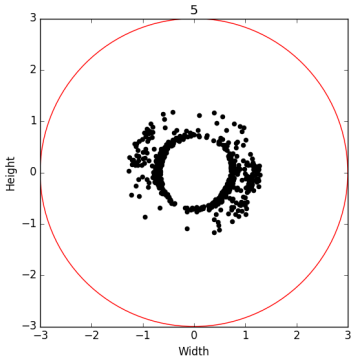

Figure 5.32: t=6, λ_0 aiming distribution

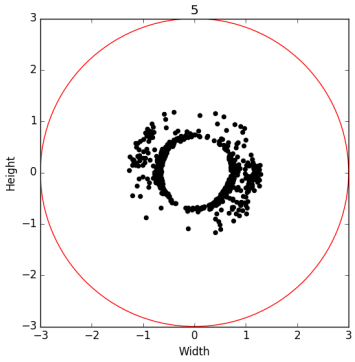

Figure 5.33: t=6, λ_1 aiming distribution

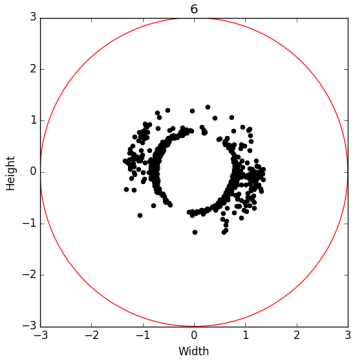

Figure 5.34: t=7, λ_0 aiming distribution

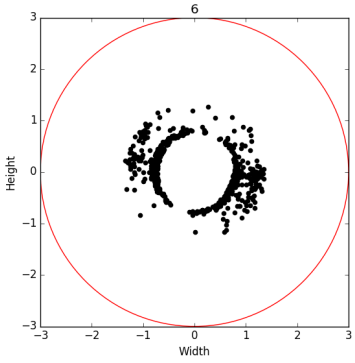

Figure 5.35: t=7, λ_1 aiming distribution

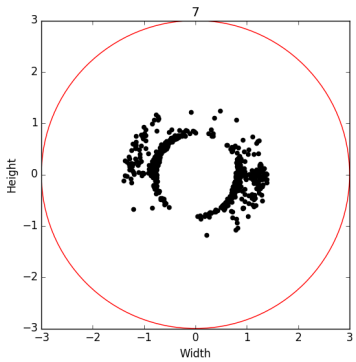

Figure 5.36: t=8, λ_0 aiming distribution

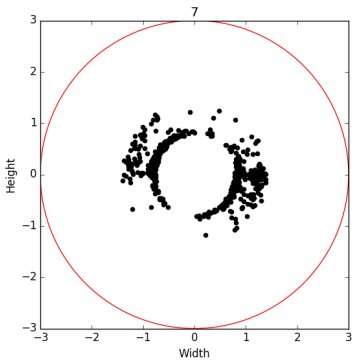

Figure 5.37: t=8, λ_1 aiming distribution

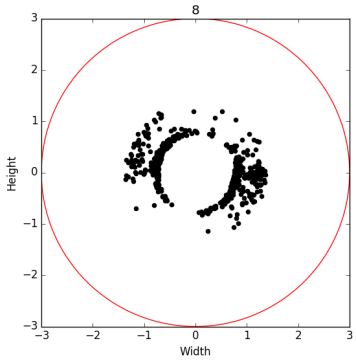

Figure 5.38: t=9, λ_0 aiming distribution

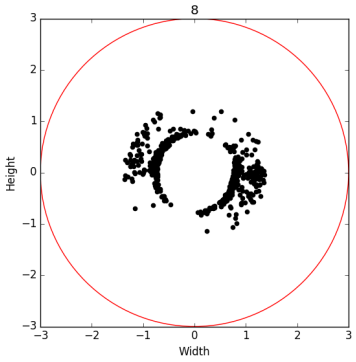

Figure 5.39: t=9, λ_1 aiming distribution

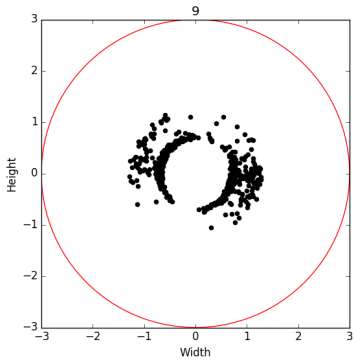

Figure 5.40: t=10, λ_0 aiming distribution

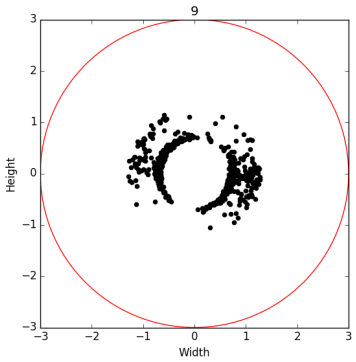

Figure 5.41: t=10, λ_1 aiming distribution

The maximum flux on the receiver surface and the incident radiation level on the heliostat field are given in Figure 5.42.

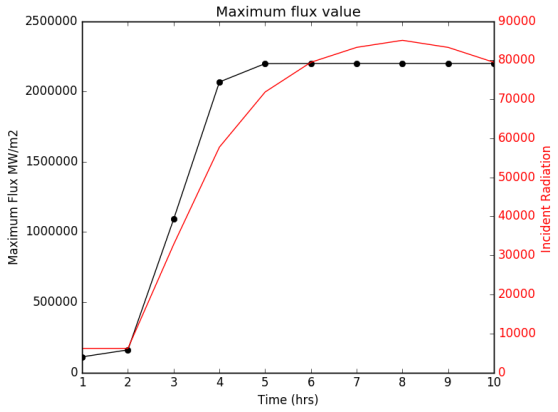

Figure 5.42: Maximum flux on receiver (black) and incident solar radiation (red)

The results furnished by the Augmented Lagrangian algorithm agree with those provided by the penalisation algorithm.

5.5.3 Numerical Considerations

The PS10 plant field contains 624 heliostats, however there exist other larger SPT plants (with potentially thousands of heliostats) which greatly increases the dimensionality of the problem. The aiming points are described on the receiver surface in polar coordinates, necessitating $2H$ variables for the gradient ascent technique. Within each step of the algorithm, the gradients must be calculated, and aiming points updated, before the radiation calculations are performed. For larger values of H, the application of the algorithms presented in this chapter may become infeasible, due to computation times.

For the numerical approximations presented in this work, the heliostat field size will have an effect on performance.

5.6 Conclusions

In this chapter, a general dynamic optimisation problem has been investigated. Theoretical properties of the problem have been discussed, including the demonstration of solution existence and optimality. Furthermore, a real-world example for an SPT plant has been considered, where a mathematical model that describes transfer of energy within the system is developed. The theoretical properties of the general optimisation problem are shown applicable to the real world problem, and dynamic constraints that describe SPT plant limitations are given. The goal of this work was the dynamic optimisation of aiming strategies in an SPT plant, where the objective function was non-linear, non-convex and of large dimension. Two algorithms have been considered to find the optimal solution, and a numerical illustration is given using real data.

The numerical illustration finds the optimal aiming strategy for an SPT plant over the period of one day, considering the change in incident radiation from the Sun as input. The physical limitations of the plant have been introduced as dynamic constraints, in terms of heliostat rotation speed and flux homogeneity on the receiver surface over time.

The two algorithms presented (Penalisation and Augmented Lagrangian) provide similar results in the numerical experiment, in similar computational times. The Augmented Lagrangian algorithm is a modification of a penalty technique, which should provide better numerical stability in some cases. With larger size problems, and adequately chosen parameters, this model could increase the reliability of the algorithm.

The dynamic optimisation problem considered in this work must be viewed as an improvement of other research concerning the optimisation of aiming strategies in SPT plants, for example Astolfi et al. [2017b]; Wang [2017], due to the inclusion of dynamic constraints. Instead of optimising the aiming strategy at certain fixed times, the method presented in this work looks to optimise across a time period. This approach can arrive to a solution that more closely reflects the true optimum when considering problems in dynamic systems.

The methods presented in this chapter can be adapted to all types of SPT plants, and even other forms of concentrating solar power technology. The inclusion of more heliostats, or multiple receivers, has been carried out in several real-world plants and the work presented here can be directly extended to consider these cases.

The use of a modified *Armijos' Rule* for the step size in the gradient ascent method can lead to faster convergence. However, with a poor parameter selection, this may actually reduce the convergence speed. Further adaptation to the algorithms presented here should consider carefully the effects of such techniques, in conjunction with a highly multi-modal objective function.

Considering the problem dimensionality when increasing the number of variables, specifically the number of heliostats in our example, one method that could be used to extend the presented approach could be to use a clustering algorithm. Thus, the heliostats could be clustered into groups, considering a weighted objective of difference in location and energy, as detailed in Chapter 2.

As remarked in Section 5.5.3, as the dimensionality of the problem increases, the performance of the proposed algorithms deteriorates. An extension to this work could consider a stochastic gradient method, which would reduce the required calculations at each step of the algorithm, thereby allowing larger problems to be tackled with the proposed method.

Finally, the integration of dynamic aiming strategy optimisation with a three dimensional thermal transfer model of the receiver is considered as the next step in this work. Thermal transfer from the incident radiation on the receiver surface, through to the HTF in the interior, is a three dimensional dynamic process that is highly depen-

dent on both solar input and current temperature distribution in the receiver materials. Varying factors such as the aiming strategy and the flow rate of the HTF will affect this process, and should be included in the dynamic coupled model.

Chapter 6

Inclement Weather Effects on Optimal Aiming Strategies in Solar Power Tower plants

Inclement weather effects on optimal aiming strategies

6.1 Introduction

Optimisation strategies for SPT plants are typically performed using normal weather conditions, however inclement weather has been shown to have an effect on the productivity of an SPT plant, as well as on the lifespan of the receiver components, due to thermal fluctuations [Martínez-Chico et al., 2011]. Research into weather and its affects on SPTs [Breitkreuz et al., 2007; Dürr, 2004; Augsburger and Favrat, 2013] has also been conducted, with a review of articles given in Tapakis and Charalambides [2013].

In this chapter we will utilise the optical model methodology from Section 1.7 to model the passage of clouds across an SPT, and optimise the aiming strategy implemented in order to protect the receiver from damage and to maximise energy produced.

The effect of a cloud on the production of an SPT plant can be described in terms of efficiency curves for the heliostats within the field. The efficiency of a heliostat field changes across time due to solar conditions, and the introduction of a cloud will produce a localised effect of efficiency loss. The characteristics of a cloud, such as size, location and density, determine the scale of efficiency loss and are naturally uncertain across time. Therefore we apply the methodology from Chapter 3, whilst considering uncertain cloud characteristics, represented by the efficiency curves of the heliostats within the field.

6.2 Optimisation

A linear integer programming technique is applied in order to optimise the aiming strategy of the heliostat field.

Let A_p be the set of aiming points on the receiver surface and let H be the set of heliostats aiming at the points in A_p. Let us define an optimisation procedure for any fixed time instant, t.

For $h \in H$, $a \in A_p$, set z_{ha} to the boolean variable defined as:

$$z_{ha} = \begin{cases} 1, & \text{if heliostat } h \text{ is allocated to aiming point } a \\ 0, & \text{otherwise.} \end{cases} \tag{6.2.1}$$

The reflected radiation pattern r_{ha}^{b} is the radiation point value at aiming point b received from heliostat h aiming at aiming point a. The total integrated radiation, R_{ha}, is the total radiation received across the receiver from heliostat h aiming at aiming point a.

We therefore look to maximise the total incident energy on the receiver:

$$\text{Maximise } \sum_{a,h} R_{ha} z_{ha}. \tag{6.2.2}$$

We constrain this objective function by requiring that no heliostat may be looking at more than one aiming point on the receiver, but may be stowed in case of high winds or potential damage to the receiver or mirror.

This gives the constraint:

$$\sum_{h \in H} z_{ha} \leq 1 \quad \forall a \in A_p. \tag{6.2.3}$$

We also constrain the received energy at the aiming points:

$$C_* \leq \sum_{\substack{h \in H \\ a \in A_p}} r_{ha}^{b} z_{ha} \leq C^* \quad \forall b \in A_p, \tag{6.2.4}$$

where C^* is a fixed maximum energy and C_* is a fixed minimum energy. These constraints prevent the receiver being subject to excessive temperatures (which could cause permanent damage) and also ensure that a minimum amount of energy is being collected at each aiming point.

In order to approximate a uniform distribution of energy across the receiver, we will look to also constrain the range of energy received between any two aiming points by imposing

$$\max_a (\sum_{h,a} r_{ha}^{i} z_{ha}) - \min_a (\sum_{h,a} r_{ha}^{j} z_{ha}) \leq \tau \ , \tag{6.2.5}$$

where τ is a given constant.

This can also be written in the form

$$\max_a (\sum_{\substack{h \in H \\ a \in A_p}} r_{ha}^{i} z_{ha}) \leq \tau + \min_a (\sum_{\substack{h \in H \\ a \in A_p}} r_{ha}^{j} z_{ha}) \ , \tag{6.2.6}$$

which is equivalent to the following set of linear constraints:

$$\sum_{\substack{h\in H\\ a\in A_p}} r_{ha}^{i} z_{ha} \leq \tau + \sum_{\substack{h\in H\\ a\in A_p}} r_{ha}^{j} z_{ha} \qquad \forall i,j \in A_p,\ with\ i \neq j \tag{6.2.7}$$

The optimisation problem to be solved at each time instant t can then be summarised as follows:

$$\text{Maximise} \sum_{\substack{h\in H\\ a\in A_p}} R_{ha} z_{ha}$$

Subject to:

$$\sum_{h} z_{ha} \leq 1 \quad \forall a \in A_p,$$

$$C_* \leq \sum_{\substack{h\in H\\ a\in A_p}} r_{ha}^{i} z_{ha} \leq C^* \qquad \forall i \in A_p,$$

$$\sum_{\substack{h\in H\\ a\in A_p}} r_{ha}^{i} z_{ha} \leq \tau + \sum_{\substack{h\in H\\ a\in A_p}} r_{ha}^{j} z_{ha} \qquad \forall i,j \in A_p\ with\ i \neq j$$

$$z_{ha} \in \{0,1\} \quad \forall h \in H,\ \forall a \in A_p$$

The uncertainty of the cloud location in the heliostat field can be considered as a stochastic programming problem, where we will assume a set of possible scenarios S_c, where each scenario represents a possible set of characteristics for the cloud.

This method implies that we have knowledge of the clouds characteristics in terms of a probability distribution. The probability for each scenario could be generated from historical data for the geographical location of the SPT or from weather tracking technology, but for demonstration purposes a uniform distribution will be applied here.

The optimisation problem can then be considered as:

$$Max \sum_{s\in S_c} p(s) \sum_{\substack{h\in H\\ a\in A_p}} R_{ha}^{s} Z_{ha} \tag{6.2.8}$$

where p(s) is the probability distribution of each scenario.

The constraints then become:

$$\sum_{h} z_{ha} \leq 1 \quad \forall a \in A_p,$$

$$C_* \leq \sum_{\substack{h\in H\\ a\in_p}} p(s) r_{ha}^{is} z_{ha} \leq C^* \qquad \forall i \in A_p, \forall s \in S_c,$$

$$\sum_{\substack{h\in H\\ a\in_p}} p(s) r_{ha}^{is} z_{ha} \leq \tau + \sum_{\substack{h\in H\\ a\in A_p}} p(s) r_{ha}^{js} z_{ha} \qquad \forall i,j \in A_p, \forall s \in S_c \; with \; i \neq j$$

$$z_{ha} \in \{0,1\} \;\; \forall h \in H, \; \forall a \in A_p$$

Optimising this problem then gives us the aiming strategy that is best when considering the uncertainty of cloud characteristics.

6.3 Results

The presented optimisation problem is applied to the PS10 SPT whose technical details are given in Section 1.6.6, where a grid of aim points on the receiver surface is defined, as shown in Figure 6.1, and the locations of the heliostats within the field are shown in Figure 6.2.

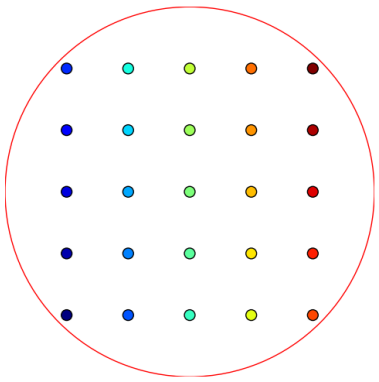

Figure 6.1: Aiming point layout on receiver

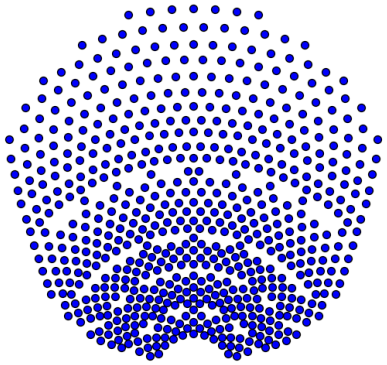

Figure 6.2: PS10 Heliostat field layout

A cloud is modelled, as shown in Figure 6.3, over a portion of the heliostat field. The location, size and density of the cloud is uncertain, and this uncertainty is considered as a uniform distribution, where each variable can differ by 10% of a known value, which would be taken from current weather condition knowledge in practise but is demonstrated here with set values.

Figure 6.4 shows the optimal aiming strategy and Figure 6.5 the energy distribution on the receiver surface for the first solar hour of a day, with clear skies. The heliostats are colour coded depending on their aiming point allocation, in accordance with Figure 6.1.

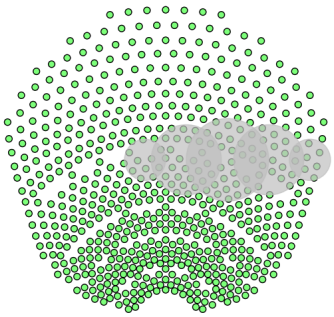

Figure 6.3: Example of cloud implementation

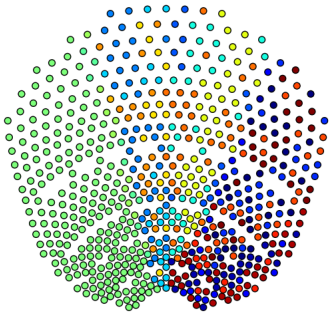

Figure 6.4: Optimal aiming strategy

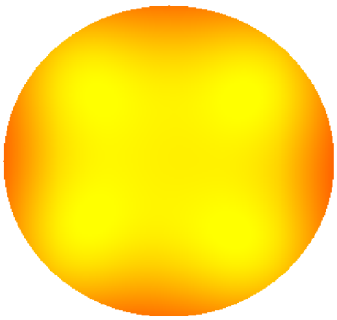

Figure 6.5: Energy distribution on receiver surface

Figure 6.6 shows the optimal aiming strategy and Figure 6.7 the energy distribution on the receiver surface for the same time point, with uncertain cloud characteristics based upon the cloud shown in Figure 6.3.

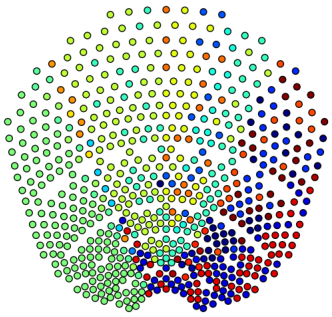

Figure 6.6: Optimal aiming strategy with cloud uncertainty

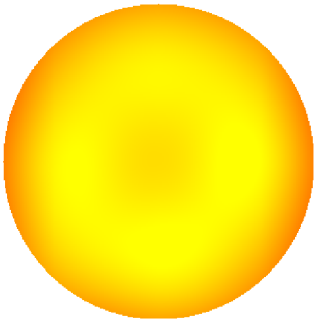

Figure 6.7: Energy distribution on receiver surface with cloud uncertainty

The optimal aiming strategy for the heliostat field changes with a cloud implemented, but does not exhibit a specific pattern based upon the cloud location. This is expected, as the allocation of aiming points is primarily affected by the cosine angle of the incident radiation, and less by the magnitude of radiation. Therefore the results show that to maintain the constraints of homogeneity on the receiver surface, the overall aiming strategy must change, not only the heliostats covered by the cloud.

6.4 Conclusions

The effect of uncertainty in cloud location, size and density on the optimal aiming strategy for an SPT plant heliostat field has been investigated. The method has been demonstrated for a time point at the PS10 SPT plant and shows how the efficiency of the plant can be maximised when there is local inclement weather.

A stochastic linear integer programming technique has been applied with short time limits, which provide near-optimal solutions in near real-time. It is expected that increasing computational power and providing the solver with an initial heuristic solution could further increase the speed of the program.

The uncertainty of the cloud parameters has been modelled in this chapter using a uniform distribution, considering 5 possible scenarios. This method is directly extendible to include more scenario possibilities and a different probability distribution for their occurrence. These factors can be determined by considering historical weather data for the region of interest, as well as the inclusion of weather predicting technology such as satellite data and cloud detecting cameras.

The optimisation method used in this research intends to find a near-optimal solution, that is solved within short timescales. It was found that solutions sufficiently close to the optimal solution can be found with a simulation time of 30s, allowing this method to be implemented in real time with local weather predictions for an SPT plant.

Depending on the location of the SPT plant, other types of inclement weather may be typical, such as rain, snow and sand storms. The method implemented in this article may be extended to account for such weather conditions, and demonstrate their effect on the efficiency of an SPT plant.

The next step in this work is the inclusion of stochastic inclement weather in the dynamic aiming strategy optimisation presented in Chapter 5. In this case, not only will the objective of maximising energy (or reaching a target distribution) be reached when considering inclement weather, but additional dynamic constraints can be added to prevent flash heating on the receiver due to cloud passage over the heliostat field.

List of Figures

List of Tables

Bibliography

Glenn A. Jones and Kevin J. Warner. The 21st century population-energy-climate nexus. Energy Policy, 93:206–212, 2016. ISSN 03014215. doi: 10.1016/j.enpol.2016.02.044. URL http://dx.doi.org/10.1016/j.enpol.2016.02.044.

Steve Sorrell. Reducing energy demand: A review of issues, challenges and approaches. Renewable and Sustainable Energy Reviews, 47:74–82, 2015. ISSN 18790690. doi: 10.1016/j.rser.2015.03.002. URL http://dx.doi.org/10.1016/j.rser.2015.03.002.

Florinda Martins, Carlos Felgueiras, and Miroslava Smitková. Fossil fuel energy consumption in European countries. Energy Procedia, 153:107–111, 2018. ISSN 18766102. doi: 10.1016/j.egypro.2018.10.050. URL https://doi.org/10.1016/j.egypro.2018.10.050.

Steve Sorrell, Jamie Speirs, Roger Bentley, Adam Brandt, and Richard Miller. Global oil depletion: A review of the evidence. Energy Policy, 38(9):5290–5295, 2010. ISSN 03014215. doi: 10.1016/j.enpol.2010.04.046. URL http://dx.doi.org/10.1016/j.enpol.2010.04.046.

Ian Chapman. The end of Peak Oil? Why this topic is still relevant despite recent denials. Energy Policy, 64:93–101, 2014. ISSN 03014215. doi: 10.1016/j.enpol.2013.05.010. URL http://dx.doi.org/10.1016/j.enpol.2013.05.010.

Daniel J. Soeder. The successful development of gas and oil resources from shales in North America. Journal of Petroleum Science and Engineering, 163(December 2017):399–420, 2018. ISSN 09204105. doi: 10.1016/j.petrol.2017.12.084. URL https://doi.org/10.1016/j.petrol.2017.12.084.

Dieter Helm. The future of fossil fuels-is it the end? Oxford Review of Economic Policy, 32(2):191–205, 2016. ISSN 14602121. doi: 10.1093/oxrep/grw015.

Richard G. Williams, Vassil Roussenov, Philip Goodwin, Laure Resplandy, and Laurent Bopp. Sensitivity of global warming to carbon emissions: Effects of heat and carbon uptake in a suite of earth system models. Journal of Climate, 30(23):9343–9363, 2017. ISSN 08948755. doi: 10.1175/JCLI-D-16-0468.1.

David C. Mowery, Richard R. Nelson, and Ben R. Martin. Technology policy and global warming: Why new policy models are needed (or why putting new wine in old bottles won't work). Research Policy, 39(8):1011–1023, 2010. ISSN 00487333. doi: 10.1016/j.respol.2010.05.008.

Payam Nejat, Fatemeh Jomehzadeh, Mohammad Mahdi Taheri, Mohammad Gohari, and Muhd Zaimi Muhd. A global review of energy consumption, CO2 emissions and policy in the residential sector (with an overview of the top ten CO2 emitting countries). Renewable and Sustainable Energy Reviews, 43:843–862, 2015. ISSN 13640321. doi: 10.1016/j.rser.2014.11.066. URL http://dx.doi.org/10.1016/j.rser.2014.11.066.

Peter Christoff. The promissory note: COP 21 and the Paris Climate Agreement. Environmental Politics, 25(5):765–787, 2016. ISSN 17438934. doi: 10.1080/09644016.2016.1191818. URL http://dx.doi.org/10.1080/09644016.2016.1191818.

Kevin J. Warner and Glenn A. Jones. A population-induced renewable energy timeline in nine world regions. Energy Policy, 101(August 2016):65–76, 2017. ISSN 03014215. doi: 10.1016/j.enpol.2016.11.031. URL http://dx.doi.org/10.1016/j.enpol.2016.11.031.

Patrick Moriarty and Damon Honnery. Can renewable energy power the future? Energy Policy, 93:3–7, 2016. ISSN 03014215. doi: 10.1016/j.enpol.2016.02.051. URL http://dx.doi.org/10.1016/j.enpol.2016.02.051.

Ehsanul Kabir, Pawan Kumar, Sandeep Kumar, Adedeji A. Adelodun, and Ki Hyun Kim. Solar energy: Potential and future prospects. Renewable and Sustainable Energy Reviews, 82(August 2017):894–900, 2018. ISSN 18790690. doi: 10.1016/j.rser.2017.09.094.

Ted Trainer. Some problems in storing renewable energy. Energy Policy, 110(July):386–393, 2017. ISSN 03014215. doi: 10.1016/j.enpol.2017.07.061. URL https://doi.org/10.1016/j.enpol.2017.07.061.

Eric Viardot. The role of cooperatives in overcoming the barriers to adoption of renewable energy. Energy Policy, 63:756–764, 2013. ISSN 03014215. doi: 10.1016/j.enpol.2013.08.034. URL http://dx.doi.org/10.1016/j.enpol.2013.08.034.

Ken Willis, Riccardo Scarpa, Rose Gilroy, and Neveen Hamza. Renewable energy adoption in an ageing population: Heterogeneity in preferences for micro-generation technology adoption. Energy Policy, 39(10):6021–6029, 2011. ISSN 03014215. doi: 10.1016/j.enpol.2011.06.066. URL http://dx.doi.org/10.1016/j.enpol.2011.06.066.

Staffan Jacobsson and Anna Johnson. The diffusion of renewable energy technology: An analytical framework and key issues for research. Energy Policy, 28(9):625–640, 2000. ISSN 03014215. doi: 10.1016/S0301-4215(00)00041-0.

John K. Kaldellis and D. Zafirakis. The wind energy (r)evolution: A short review of a long history. Renewable Energy, 36(7):1887–1901, 2011. ISSN 09601481. doi: 10.1016/j.renene.2011.01.002.

Bent Sørensen. A history of renewable energy technology. Energy Policy, 19(1):8–12, 1991. ISSN 03014215. doi: 10.1016/0301-4215(91)90072-V.

Christiane Zarfl, Alexander E. Lumsdon, Jürgen Berlekamp, Laura Tydecks, and Klement Tockner. A global boom in hydropower dam construction. Aquatic Sciences, 77(1):161–170, 2014. ISSN 14209055. doi: 10.1007/s00027-014-0377-0.

Akhtar Hussain, Syed Muhammad Arif, and Muhammad Aslam. Emerging renewable and sustainable energy technologies: State of the art. Renewable and Sustainable Energy Reviews, 71(December 2016):12–28, 2017. ISSN 18790690. doi: 10.1016/j.rser.2016.12.033. URL http://dx.doi.org/10.1016/j.rser.2016.12.033.

Yogesh Kumar, Jordan Ringenberg, Soma Shekara Depuru, Vijay K. Devabhaktuni, Jin Woo Lee, Efstratios Nikolaidis, Brett Andersen, and Abdollah Afjeh. Wind energy: Trends and enabling technologies. Renewable and Sustainable Energy Reviews, 53:209–224, 2016. ISSN 18790690. doi: 10.1016/j.rser.2015.07.200.

Bhubaneswari Parida, S. Iniyan, and Ranko Goic. A review of solar photovoltaic technologies. Renewable and Sustainable Energy Reviews, 15(3):1625–1636, 2011. ISSN 13640321. doi: 10.1016/j.rser.2010.11.032. URL http://dx.doi.org/10.1016/j.rser.2010.11.032.

Christian Breyer, Dmitrii Bogdanov, Arman Aghahosseini, Ashish Gulagi, Michael Child, Ayobami Solomon Oyewo, Javier Farfan, Kristina Sadovskaia, and Pasi Vainikka. Solar photovoltaics demand for the global energy transition in the power sector. Progress in Photovoltaics: Research and Applications, 26(8):505–523, 2018. ISSN 1099159X. doi: 10.1002/pip.2950.

Ze Dong Cheng, Xue Ru Zhao, Ya Ling He, and Yu Qiu. A novel optical optimization model for linear Fresnel reflector concentrators. Renewable Energy, 129:486–499, 2018. ISSN 18790682. doi: 10.1016/j.renene.2018.06.019. URL https://doi.org/10.1016/j.renene.2018.06.019.

Evangelos Bellos, Emmanouil Mathioulakis, Elias Papanicolaou, and Vassilis Belessiotis. Experimental investigation of the daily performance of an integrated linear Fresnel

reflector system. Solar Energy, 167(April):220–230, 2018. ISSN 0038092X. doi: 10.1016/j.solener.2018.04.019. URL https://doi.org/10.1016/j.solener.2018.04.019.

Md Tasbirul Islam, Nazmul Huda, A. B. Abdullah, and R. Saidur. A comprehensive review of state-of-the-art concentrating solar power (CSP) technologies: Current status and research trends. Renewable and Sustainable Energy Reviews, 91 (November 2017):987–1018, 2018. ISSN 18790690. doi: 10.1016/j.rser.2018.04.097. URL https://doi.org/10.1016/j.rser.2018.04.097.

Craig S. Turchi, Judith Vidal, and Matthew Bauer. Molten salt power towers operating at 600−650°C: Salt selection and cost benefits. Solar Energy, 164(November 2017): 38–46, 2018. ISSN 0038092X. doi: 10.1016/j.solener.2018.01.063. URL https://doi.org/10.1016/j.solener.2018.01.063.

Alexander Bonk, Salvatore Sau, Nerea Uranga, Marta Hernaiz, and Thomas Bauer. Advanced heat transfer fluids for direct molten salt line-focusing CSP plants. Progress in Energy and Combustion Science, 67:69–87, 2018. ISSN 03601285. doi: 10.1016/j.pecs.2018.02.002. URL https://doi.org/10.1016/j.pecs.2018.02.002.

Alejandro Calderón, Anabel Palacios, Camila Barreneche, Mercè Segarra, Cristina Prieto, Alfonso Rodriguez-Sanchez, and A. Inés Fernández. High temperature systems using solid particles as TES and HTF material: A review. Applied Energy, 213(June 2017):100–111, 2018. ISSN 03062619. doi: 10.1016/j.apenergy.2017.12.107. URL https://doi.org/10.1016/j.apenergy.2017.12.107.

Abdelrahman El-Leathy, Sheldon Jeter, Hany Al-Ansary, Syed Noman Danish, Rageh Saeed, Said Abdel-Khalik, Matthew Golob, Eldwin Djajadiwinata, and Zeyad Al-Suhaibani. Thermal performance evaluation of lining materials used in thermal energy storage for a falling particle receiver based CSP system. Solar Energy, 178 (December 2018):268–277, 2019. ISSN 0038092X. doi: 10.1016/j.solener.2018.12.047. URL https://doi.org/10.1016/j.solener.2018.12.047.

Simone Polimeni, Marco Binotti, Luca Moretti, and Giampaolo Manzolini. Comparison of sodium and KCl-MgCl2 as heat transfer fluids in CSP solar tower with sCO2 power cycles. Solar Energy, 162(September 2017):510–524, 2018. ISSN 0038092X. doi: 10.1016/j.solener.2018.01.046.

M. R. Rodríguez-Sánchez, A. Sánchez-González, and D. Santana. Feasibility study of a new concept of solar external receiver: Variable velocity receiver. Applied Thermal Engineering, 128:335–344, 2018. ISSN 13594311. doi: 10.1016/j.applthermaleng.2017.08.173.

Erminia Leonardi, Lorenzo Pisani, Iñigo Les, Amaia Mutuberria Larrayoz, Shahab Rohani, and Peter Schöttl. Techno-economic heliostat field optimization: Comparative analysis of different layouts. Solar Energy, 180(December 2018):601–607, 2019. ISSN 0038092X. doi: 10.1016/j.solener.2019.01.053. URL https://doi.org/10.1016/j.solener.2019.01.053.

N. C. Cruz, S. Salhi, J. L. Redondo, J. D. Álvarez, M. Berenguel, and P. M. Ortigosa. Design of a parallel genetic algorithm for continuous and pattern-free heliostat field optimization. Journal of Supercomputing, 75(3):1–16, 2018a. ISSN 15730484. doi: 10.1007/s11227-018-2404-8. URL https://doi.org/10.1007/s11227-018-2404-8.

Marc Chesney, Pierre Lasserre, and Bruno Troja. Mitigating global warming: a real options approach. Annals of Operations Research, 255(1-2):465–506, 2017. ISSN 15729338. doi: 10.1007/s10479-016-2258-5.

E. Carrizosa, C. Domínguez-Bravo, E. Fernández-Cara, and M. Quero. A heuristic method for simultaneous tower and pattern-free field optimization on solar power systems. Computers & Operations Research, 57:109–122, 2015a. ISSN 03050548. doi: 10.1016/j.cor.2014.11.017. URL http://www.sciencedirect.com/science/article/pii/S0305054814003219.

Tim Conroy, Maurice N. Collins, James Fisher, and Ronan Grimes. Thermohydraulic analysis of single phase heat transfer fluids in CSP solar receivers. Renewable Energy, 129:150–167, 2018. ISSN 18790682. doi: 10.1016/j.renene.2018.05.101. URL https://doi.org/10.1016/j.renene.2018.05.101.

Michael J. Wagner and Tim Wendelin. SolarPILOT: A power tower solar field layout and characterization tool. Solar Energy, 171(August 2016):185–196, 2018. ISSN 0038092X. doi: 10.1016/j.solener.2018.06.063.

Pascal Richter, Gregor Heiming, Nils Lukas, and Martin Frank. SunFlower: A new solar tower simulation method for use in field layout optimization. AIP Conference Proceedings, 2033(November), 2018. ISSN 15517616. doi: 10.1063/1.5067217.

Cianan A. Sims, Clifford K. Ho, Luke Horstman, Timothy Wendelin, and Julius E. Yellowhair. Tower illuminance model (TIM): Interactive real-time flyover simulation tool to evaluate glare and avian-flux hazards. AIP Conference Proceedings, 2033 (November), 2018. ISSN 15517616. doi: 10.1063/1.5067219.

Reine Reoyo-Prats, Alex Carling Plaza, Olivier Faugeroux, Bernard Claudet, Audrey Soum-Glaude, Christina Hildebrandt, Yaniv Binyamin, Alina Agüero, and Tobias Meißner. Accelerated aging of absorber coatings for CSP receivers under real high solar flux. Evolution of their optical properties. Solar Energy Materials and Solar

Cells, 193(January):92–100, 2019. ISSN 09270248. doi: 10.1016/j.solmat.2018.12.030. URL https://doi.org/10.1016/j.solmat.2018.12.030.

Yasmine Lalau, Olivier Faugeroux, Bernard Claudet, Emmanuel Guillot, Damien Andre, Marc Huger, Alain Proust, and Thierry Chotard. A method for experimental thermo-mechanical aging of materials submitted to concentrated solar irradiation. Solar Energy Materials and Solar Cells, 192(November 2018):161–169, 2019. ISSN 09270248. doi: 10.1016/j.solmat.2018.12.017. URL https://doi.org/10.1016/j.solmat.2018.12.017.

María López-Herraiz, Azucena Bello Fernández, Noelia Martinez, and Manuel Gallas. Effect of the optical properties of the coating of a concentrated solar power central receiver on its thermal efficiency. Solar Energy Materials and Solar Cells, 159:66–72, 2017. ISSN 09270248. doi: 10.1016/j.solmat.2016.08.031. URL http://dx.doi.org/10.1016/j.solmat.2016.08.031.

Florent Larrouturou, Cyril Caliot, and Gilles Flamant. Influence of receiver surface spectral selectivity on the solar-to-electric efficiency of a solar tower power plant. Solar Energy, 130:60–73, 2016. ISSN 0038092X. doi: 10.1016/j.solener.2016.02.008. URL http://dx.doi.org/10.1016/j.solener.2016.02.008.

Saeb M. Besarati, D. Yogi Goswami, and Elias K. Stefanakos. Optimal heliostat aiming strategy for uniform distribution of heat flux on the receiver of a solar power tower plant. Energy Conversion and Management, 84:234–243, 2014. ISSN 01968904. doi: 10.1016/j.enconman.2014.04.030. URL http://dx.doi.org/10.1016/j.enconman.2014.04.030.

Marco Binotti, Paolo De Giorgi, David Sanchez, and Giampaolo Manzolini. Comparison of Different Strategies for Heliostats Aiming Point in Cavity and External Tower Receivers. Journal of Solar Energy Engineering, 138(2):021008, 2016. ISSN 0199-6231. doi: 10.1115/1.4032450. URL http://solarenergyengineering.asmedigitalcollection.asme.org/article.aspx?doi=10.1115/1.4032450.

Francesco Crespi, Andrea Toscani, Paolo Zani, David Sánchez, and Giampaolo Manzolini. Effect of passing clouds on the dynamic performance of a CSP tower receiver with molten salt heat storage. Applied Energy, 229(August):224–235, 2018. ISSN 03062619. doi: 10.1016/j.apenergy.2018.07.094. URL https://doi.org/10.1016/j.apenergy.2018.07.094.

Adrien Salomé, Fabien Chhel, Gilles Flamant, Alain Ferrière, and Frederik Thiery. Control of the flux distribution on a solar tower receiver using an optimized aiming point strategy: Application to THEMIS solar tower. Solar Energy, 94:352–366, 2013. ISSN 0038092X. doi: 10.1016/j.solener.2013.02.025.

E.P. Roth and R.B. Pettit. The effect of soiling on solar mirrors and techniques used to maintain high relfectivity. Solar Materials Science, pages 199–227, 1980. doi: 10.1016/B978-0-12-511160-7.50013-2. URL http://linkinghub.elsevier.com/retrieve/pii/B9780125111607500132.

A. Fernández-García, L. Álvarez-Rodrigo, L. Martínez-Arcos, R. Aguiar, and J. M. Márquez-Payés. Study of different cleaning methods for solar reflectors used in CSP plants. Energy Procedia, 49:80–89, 2013. ISSN 18766102. doi: 10.1016/j.egypro.2014.03.009. URL http://dx.doi.org/10.1016/j.egypro.2014.03.009.

Abengoa. Abengoa PS10 SPT Plant. http://www.abengoasolar.com/web/en/plantas_solares/plantas_para_terceros/espana/index.htm, 2019. Accessed: 22/02/2017.

BrightSource Energy, 2019. BrightSource Energy. http://www.brightsourceenergy.com/ivanpah-update#.XMLUB6TRZPZ. Accessed: 26/04/2019.

Andreas Pfahl, Joe Coventry, Marc Röger, Fabian Wolfertstetter, Juan Felipe Vásquez-Arango, Fabian Gross, Maziar Arjomandi, Peter Schwarzbözl, Mark Geiger, and Phillip Liedke. Progress in heliostat development. Solar Energy, 152:3–37, 2017. ISSN 0038092X. doi: 10.1016/j.solener.2017.03.029. URL http://dx.doi.org/10.1016/j.solener.2017.03.029.

Michael Hardt, Daniel Martínez, Antonio González, Candido Garrido, Sergio Aladren, José Ramón Villa, and Jaime Saenz. HECTOR - heliostat cleaning team-oriented robot. SolarPaces Conference, 2011.

Thomas Ashley, Emilio Carrizosa, and Enrique Fernández-Cara. Heliostat field cleaning scheduling for Solar Power Tower plants: A heuristic approach. Applied Energy, 235 (November 2018):653–660, 2019a. ISSN 03062619. doi: 10.1016/j.apenergy.2018.11.004.

Diego Gabriel Rossit, Universidad Nacional, Daniele Vigo, and Fernando Tohm. Improving Visual Attractiveness in Capacitated Vehicle Routing Problems : a Heuristic Algorithm. pages 748–755, 2016.

Thomas Ashley, Emilio Carrizosa, and Enrique Fernández-Cara. Optimisation of aiming strategies in Solar Power Tower plants. Energy, 2017. ISSN 03605442. doi: 10.1016/j.energy.2017.06.163. URL http://linkinghub.elsevier.com/retrieve/pii/S0360544217311581.

S. Relloso and E. García. Tower Technology Cost Reduction Approach after Gemasolar Experience. Energy Procedia, 69:1660–1666, 2015. ISSN 18766102. doi: 10.1016/j.egypro.2015.03.125. URL http://dx.doi.org/10.1016/j.egypro.2015.03.125.

M. Berenguel, P.M. Ortigosa, J.D. Álvarez, J.L. Redondo, and N.C. Cruz. A two-layered solution for automatic heliostat aiming. Engineering Applications of Artificial Intelligence, 72(October 2016):253–266, 2018. ISSN 09521976. doi: 10.1016/j.engappai.2018.04.014. URL https://doi.org/10.1016/j.engappai.2018.04.014.

Marco Astolfi, Marco Binotti, Simone Mazzola, Luca Zanellato, and Giampaolo Manzolini. Heliostat aiming point optimization for external tower receiver. Solar Energy, 157:1114–1129, 2017a. ISSN 0038092X. doi: 10.1016/j.solener.2016.03.042. URL https://doi.org/10.1016/j.solener.2016.03.042.

E. A. Igel and R. L. Hughes. Optical analysis of solar facility heliostats. Solar Energy, 22(3):283–295, 1979. ISSN 0038092X. doi: 10.1016/0038-092X(79)90143-9.

F. J. Collado, A. Gómez, and J. A. Turégano. An analytic function for the flux density due to sunlight reflected from a heliostat. Solar Energy, 37(3):215–234, 1986. ISSN 0038092X. doi: 10.1016/0038-092X(86)90078-2.

Qiang Yu, Zhifeng Wang, and Ershu Xu. Analysis and improvement of solar flux distribution inside a cavity receiver based on multi-focal points of heliostat field. Applied Energy, 136:417–430, 2014. ISSN 03062619. doi: 10.1016/j.apenergy.2014.09.008. URL http://dx.doi.org/10.1016/j.apenergy.2014.09.008.

Gurobi Optimization Solver, 2019. Gurobi Optimization Solver. http://www.gurobi.com/. Accessed: 22/02/2017.

Thomas Ashley, Emilio Carrizosa, and Enrique Fernández-Cara. Continuous Optimisation Techniques for Optimal Aiming Strategies in Solar Power Tower Plants (Submitted). 2018.

Thomas Ashley, Emilio Carrizosa, and Enrique Fernández-Cara. Dynamic Continuous Optimisation Applied to Renewable Energy (Submitted). 2019b.

M. Martínez-Chico, F. J. Batlles, and J. L. Bosch. Cloud classification in a mediterranean location using radiation data and sky images. Energy, 36(7):4055–4062, 2011. ISSN 03605442. doi: 10.1016/j.energy.2011.04.043. URL http://dx.doi.org/10.1016/j.energy.2011.04.043.

M. Lopez-Martinez and F.R. Rubio. Cloud detection system for a solar power tower plant. IEEE 2002 28th Annual Conference of the Industrial Electronics Society. IECON 02, 3:2560–2565, 2002. doi: 10.1109/IECON.2002.1185377. URL http://ieeexplore.ieee.org/lpdocs/epic03/wrapper.htm?arnumber=1185377.

Alberto Sánchez-González, María Reyes Rodríguez-Sánchez, and Domingo Santana. Aiming strategy model based on allowable flux densities for molten salt central receivers. Solar Energy, 2015. ISSN 0038092X. doi: 10.1016/j.solener.2015.12.055.

A Mutuberria, J Pascual, M V Guisado, and F Mallor. Comparison of heliostat field layout design methodologies and impact on power plant efficiency. Energy Procedia, 69:1360–1370, 2015. ISSN 1876-6102. doi: 10.1016/j.egypro.2015.03.135. URL http://dx.doi.org/10.1016/j.egypro.2015.03.135.

Carmen Ana Domínguez-Bravo, Sebastian James Bode, Gregor Heiming, Pascal Richter, Emilio Carrizosa, Enrique Fernández-Cara, Martin Frank, and Paul Gauché. Field-design optimization with triangular heliostat pods. AIP Conference Proceedings, 1734(May 2016), 2016. ISSN 15517616. doi: 10.1063/1.4949153.

E. Carrizosa, Carmen-Ana Domínguez-Bravo, E. Fernández-Cara, and M. Quero. An optimization tool to design the field of a solar power tower plant allowing heliostats of different sizes. International Journal of Energy Research, 2017. ISSN 12310956. doi: 10.1002/er.

Manuel Blanco-Muriel, Diego C. Alarcón-Padilla, Teodoro López-Moratalla, and Martín Lara-Coira. Computing the solar vector. Solar Energy, 70(5):431–441, 2001. ISSN 0038092X. doi: 10.1016/S0038-092X(00)00156-0.

F. Biggs and C. N. Vittitoe. Helios model for the optical behavior of reflecting solar concentrators. NASA STI/Recon Technical Report N, 79:31806, 1979. URL http://adsabs.harvard.edu/abs/1979STIN...7931806B.

F. J. Collado and J. A. Turégano. Calculation of the annual thermal energy supplied by a defined heliostat field. Solar Energy, 42(2):149–165, 1989. ISSN 0038092X. doi: 10.1016/0038-092X(89)90142-4.

Francisco J. Collado and Jesús Guallar. Campo: Generation of regular heliostat fields. Renewable Energy, 46(October):49–59, 2012. ISSN 09601481. doi: 10.1016/j.renene.2012.03.011.

J.G. Barberena, A. Mutuberria Larrayoz, M. Sánchez, and A. Bernardos. State-of-the-art of Heliostat Field Layout Algorithms and their Comparison. Energy Procedia, 93(March):31–38, 2016. ISSN 18766102. doi: 10.1016/j.egypro.2016.07.146. URL http://linkinghub.elsevier.com/retrieve/pii/S1876610216305732.

Francisco J. Collado. Quick evaluation of the annual heliostat field efficiency. Solar Energy, 82(4):379–384, 2008. ISSN 0038092X. doi: 10.1016/j.solener.2007.10.007.

Marcelino Sánchez and Manuel Romero. Methodology for generation of heliostat field layout in central receiver systems based on yearly normalized energy surfaces. Solar Energy, 80(7):861–874, 2006. ISSN 0038092X. doi: 10.1016/j.solener.2005.05.014.

N C Cruz, S Salhi, J L Redondo, J D Álvarez, M Berenguel, and P M Ortigosa. Hector, a new methodology for continuous and pattern-free heliostat field optimization. Applied Energy, 225(May):1123–1131, 2018b. ISSN 0306-2619. doi: 10.1016/j.apenergy.2018.05.072. URL https://doi.org/10.1016/j.apenergy.2018.05.072.

Travis Sarver, Ali Al-Qaraghuli, and Lawrence L. Kazmerski. A comprehensive review of the impact of dust on the use of solar energy: History, investigations, results, literature, and mitigation approaches. Renewable and Sustainable Energy Reviews, 22:698–733, 2013. ISSN 13640321. doi: 10.1016/j.rser.2012.12.065. URL http://dx.doi.org/10.1016/j.rser.2012.12.065.

G. Singh, D. Saini, N. Yadav, R. Sarma, L. Chandra, and R. Shekhar. Dust Deposition Mechanism and Cleaning Strategy for Open Volumetric Air Receiver Based Solar Tower Sub-systems. Energy Procedia, 69:2081–2089, 2015. ISSN 18766102. doi: 10.1016/j.egypro.2015.03.222. URL http://dx.doi.org/10.1016/j.egypro.2015.03.222.

M. Grotschel and Y. Wakabayashi. A cutting plane algorithm for a clustering problem. Mathematical Programming, 45:59–96, 1989.

Pierre Hansen and Brigitte Jaumard. Cluster analysis and mathematical programming. Mathematical Programming, 79(1-3):191–215, 1997. ISSN 0025-5610. doi: 10.1007/BF02614317. URL http://link.springer.com/10.1007/BF02614317.

Pasquale Avella, Antonio Sassano, and Igor Vasil. Computational study of large-scale p -Median problems. Mathematical Programming, 109:89–114, 2007. ISSN 0025-5610. doi: 10.1007/s10107-005-0700-6.

Mark S Daskin and Kayse Lee Maass. The p-median problem. Location Science, 2015. doi: 10.1007/978-3-319-13111-5. URL http://link.springer.com/10.1007/978-3-319-13111-5.

Nenad Mladenović, Jack Brimberg, Pierre Hansen, and José A. Moreno-Pérez. The p-median problem: A survey of metaheuristic approaches. European Journal of Operational Research, 179(3):927–939, 2007. ISSN 03772217. doi: 10.1016/j.ejor.2005.05.034.

Sérgio Barreto, Carlos Ferreira, José Paixão, and Beatriz Sousa Santos. Using clustering analysis in a capacitated location-routing problem. European Journal of Operational Research, 179(3):968–977, 2007. ISSN 03772217. doi: 10.1016/j.ejor.2005.06.074.

Thibaut Vidal, Maria Battarra, Anand Subramanian, and Güneş Erdoğan. Hybrid metaheuristics for the Clustered Vehicle Routing Problem. Computers and Operations Research, 58:87–99, 2015. ISSN 03050548. doi: 10.1016/j.cor.2014.10.019.

Maaike Hoogeboom, Maria Battarra, Güneş Erdoğan, and Daniele Vigo. Erratum-Exact Algorithms for the Clustered Vehicle Routing Problem. Operations Research, 64(2):456–457, 2016. ISSN 0030-364X. doi: 10.1287/opre.2016.1491. URL http://pubsonline.informs.org/doi/10.1287/opre.2016.1491.

Caroline Prodhon and Christian Prins. A survey of recent research on location-routing problems. European Journal of Operational Research, 238(1):1–17, 2014. ISSN 03772217. doi: 10.1016/j.ejor.2014.01.005. URL http://dx.doi.org/10.1016/j.ejor.2014.01.005.

Thomas Fend, Bernhard Hoffschmidt, Robert Pitz-Paal, Oliver Reutter, and Peter Rietbrock. Porous materials as open volumetric solar receivers: Experimental determination of thermophysical and heat transfer properties. Energy, 29(5-6):823–833, 2004. ISSN 03605442. doi: 10.1016/S0360-5442(03)00188-9.

Marco Astolfi, Marco Binotti, Simone Mazzola, Luca Zanellato, and Giampaolo Manzolini. Heliostat aiming point optimization for external tower receiver. Solar Energy, pages 1–16, 2016. ISSN 0038-092X. doi: 10.1016/j.solener.2016.03.042. URL http://dx.doi.org/10.1016/j.solener.2016.03.042.

Boris Belhomme, Robert Pitz-Paal, and Peter Schwarzbözl. Optimization of Heliostat Aim Point Selection for Central Receiver Systems Based on the Ant Colony Optimization Metaheuristic. Journal of Solar Energy Engineering, 136(February 2014):011005, 2013. ISSN 0199-6231. doi: 10.1115/1.4024738. URL http://solarenergyengineering.asmedigitalcollection.asme.org/article.aspx?doi=10.1115/1.4024738.

M. Berenguel, F. R. Rubio, A. Valverde, P. J. Lara, M. R. Arahal, E. F. Camacho, and M. López. An artificial vision-based control system for automatic heliostat positioning offset correction in a central receiver solar power plant. Solar Energy, 76(5):563–575, 2004. ISSN 0038092X. doi: 10.1016/j.solener.2003.12.006.

Abraham Kribus, Irina Vishnevetsky, Amnon Yogev, and Tatiana Rubinov. Closed loop control of heliostats. Energy, 29(5-6):905–913, 2004. ISSN 03605442. doi: 10.1016/S0360-5442(03)00195-6.

N. C. Cruz, J. L. Redondo, J. D. Álvarez, M. Berenguel, and P. M. Ortigosa. A parallel Teaching-Learning-Based Optimization procedure for automatic heliostat aiming. The Journal of Supercomputing, 2016. ISSN 0920-8542. doi: 10.1007/s11227-016-1914-5. URL http://link.springer.com/10.1007/s11227-016-1914-5.

R. Baños, F. Manzano-Agugliaro, F. G. Montoya, C. Gil, A. Alcayde, and J. Gómez. Optimization methods applied to renewable and sustainable energy: A review. Renewable and Sustainable Energy Reviews, 15(4):1753–1766, 2011. ISSN 13640321. doi: 10.1016/j.rser.2010.12.008.

J. Alonso, F. J. Batlles, G. López, and A. Ternero. Sky camera imagery processing based on a sky classification using radiometric data. Energy, 68(May):599–608, 2014. ISSN 03605442. doi: 10.1016/j.energy.2014.02.035. URL http://dx.doi.org/10.1016/j.energy.2014.02.035.

J. Alonso-Montesinos and F. J. Batlles. Solar radiation forecasting in the short- and medium-term under all sky conditions. Energy, 83:387–393, 2015. ISSN 03605442. doi: 10.1016/j.energy.2015.02.036. URL http://dx.doi.org/10.1016/j.energy.2015.02.036.

E. Carrizosa, C. Domínguez-Bravo, E. Fernández-Cara, and M. Quero. Optimization of multiple receivers solar power tower systems. Energy, 90:2085–2093, 2015b. ISSN 03605442. doi: 10.1016/j.energy.2015.08.005.

Mark Schmitz, Peter Schwarzbözl, Reiner Buck, and Robert Pitz-Paal. Assessment of the potential improvement due to multiple apertures in central receiver systems with secondary concentrators. Solar Energy, 80(1):111–120, 2006. ISSN 0038092X. doi: 10.1016/j.solener.2005.02.012.

Caroline Le Floch, Francois Belletti, Samveg Saxena, Alexandre M. Bayen, and Scott Moura. Distributed optimal charging of electric vehicles for demand response and load shaping. Proceedings of the IEEE Conference on Decision and Control, 54rd IEEE(Cdc):6570–6576, 2015. ISSN 07431546. doi: 10.1109/CDC.2015.7403254.

Raghuram Ranganathan, Wasfy Mikhael, Nasser Kutkut, and Issa Batarseh. Adaptive sun tracking algorithm for incident energy maximization and efficiency improvement of PV panels. Renewable Energy, 36(10):2623–2626, 2011. ISSN 09601481. doi: 10.1016/j.renene.2010.06.011. URL http://dx.doi.org/10.1016/j.renene.2010.06.011.

Zexian Liu and Hongwei Liu. An efficient gradient method with approximate optimal stepsize for large-scale unconstrained optimization. Numerical Algorithms, 78(1):21–39, 2018. ISSN 15729265. doi: 10.1007/s11075-017-0365-2.

Garth P. McCormick. A Modification of Armijo ' S Step-Size Rule for Negative Curvature. Mathematical Programming, 13:111–115, 1977.

Emilio Carrizosa, Nenad Mladenović, and Raca Todosijević. Variable neighborhood search for minimum sum-of-squares clustering on networks. European Journal of

Operational Research, 230(2):356–363, 2013. ISSN 03772217. doi: 10.1016/j.ejor.2013.04.027.

Rahul Rahul Mark Fonseca, Bailian Chen, Jan Dirk Jansen, and Albert Reynolds. A Stochastic Simplex Approximate Gradient (StoSAG) for optimization under uncertainty. International Journal for Numerical Methods in Engineering, 109(13):1756–1776, 2017. ISSN 10970207. doi: 10.1002/nme.5342.

Mark Schmidt, Nicolas Le Roux, and Francis Bach. Minimizing Finite Sums with the Stochastic Average Gradient. pages 83–112, 2013. ISSN 14364646. doi: 10.1007/s10107-016-1030-6. URL http://arxiv.org/abs/1309.2388.

Honggang Wang. Multi-objective retrospective optimization using stochastic zigzag search. European Journal of Operational Research, 263(3):946–960, 2017. ISSN 03772217. doi: 10.1016/j.ejor.2017.06.039. URL http://dx.doi.org/10.1016/j.ejor.2017.06.039.

Verena Schmid. Solving the dynamic ambulance relocation and dispatching problem using approximate dynamic programming. European Journal of Operational Research, 219(3):611–621, 2012. ISSN 03772217. doi: 10.1016/j.ejor.2011.10.043. URL http://dx.doi.org/10.1016/j.ejor.2011.10.043.

Victor Pillac, Michel Gendreau, Christelle Guéret, and Andrés L. Medaglia. A review of dynamic vehicle routing problems. European Journal of Operational Research, 225(1):1–11, 2013. ISSN 03772217. doi: 10.1016/j.ejor.2012.08.015. URL http://dx.doi.org/10.1016/j.ejor.2012.08.015.

Ivar Ekeland and Roger Temam. Convex analysis and variational problems. Elsevier, 1976. ISBN 9780080875224.

Jorge Nocedal, Stephen J Wright, and Stephen M Robinson. Numerical Optimization. Springer, 1 edition, 1999. ISBN 0387987932. doi: 10.1007/b98874.

Marco Astolfi, Marco Binotti, Simone Mazzola, Luca Zanellato, and Giampaolo Manzolini. Heliostat aiming point optimization for external tower receiver. Solar Energy, 157:1114–1129, 2017b. ISSN 0038092X. doi: 10.1016/j.solener.2016.03.042. URL https://doi.org/10.1016/j.solener.2016.03.042.

H. Breitkreuz, M. Schroedter-Homscheidt, and T. Holzer-Popp. A case study to prepare for the utilization of aerosol forecasts in solar energy industries. Solar Energy, 81(11):1377–1385, 2007. ISSN 0038092X. doi: 10.1016/j.solener.2007.01.009.

Bruno Dürr. Automatic cloud amount detection by surface longwave downward radiation measurements. Journal of Geophysical Research, 109(D5):D05201, 2004. ISSN

0148-0227. doi: 10.1029/2003JD004182. URL http://doi.wiley.com/10.1029/2003JD004182.

Germain Augsburger and Daniel Favrat. Modelling of the receiver transient flux distribution due to cloud passages on a solar tower thermal power plant. Solar Energy, 87 (1):42–52, 2013. ISSN 0038092X. doi: 10.1016/j.solener.2012.10.010.

R. Tapakis and A. G. Charalambides. Equipment and methodologies for cloud detection and classification: A review. Solar Energy, 95:392–430, 2013. ISSN 0038092X. doi: 10.1016/j.solener.2012.11.015. URL http://dx.doi.org/10.1016/j.solener.2012.11.015.